What sets the pace of glacier change in a warming world? Examining the roles of climate, geometry, and dynamics

John Erich Christian

A dissertation
submitted in partial fulfillment of the
requirements for the degree of

Doctor of Philosophy

University of Washington

2020

Reading Committee:

Michelle Koutnik, Chair

Gerard Roe, Chair

Knut Christianson

Alexander Robel

Program Authorized to Offer Degree:
Earth and Space Sciences

University of Washington

Abstract

What sets the pace of glacier change in a warming world?
Examining the roles of climate, geometry, and dynamics

John Erich Christian

Co-Chairs of the Supervisory Committee:
Michelle Koutnik
Earth and Space Sciences

Gerard Roe
Earth and Space Sciences

Glaciers are fundamentally sensitive to climate. Following a perturbation in either precipitation or temperature, their extent on the landscape must change in order to re-balance accumulation and melt. This equilibrium response is fairly straightforward, but in the context of anthropogenic warming, contemporary glacier change is fundamentally a transient problem. This dissertation focuses on basic physical controls on this transient response.

First, I use a recently-developed statistical model to identify modes of climate variability that drive anomalies in glacier mass balance, and assess their effects on decadal trends. The remainder of the dissertation investigates glacier response times using a combination of numerical and analytical models. This work extends the theoretical basis of glacier response times into a framework for addressing practical questions about ongoing glacier change. These include the current disequilibrium of mountain glaciers, the relative impact of ocean vs. atmospheric forcing on marine-terminating glaciers, and the challenge of attributing glacier changes to natural or anthropogenic forcing.

In each case, the results depend on fundamental constraints related to the glacier's geometry and climate setting. While the particular parameters vary by glacier, these constraints arise from basic principles of ice flow, and are thus very robust. While there will always

be details specific to any particular glacier, these experiments clarify fundamental processes that will affect glacier change in any setting.

Table of Contents

ACKNOWLEDGMENTS

I wish to express sincere appreciation to many individuals who supported me in this work, and in my overall education. First and foremost, I am deeply grateful to my advisors Michelle Koutnik and Gerard Roe for being dedicated mentors, exemplary scientists, and trusted friends throughout my own development as a scientist. I also wish to thank my committee, Knut Christianson, Edwin Waddington, Alexander Robel, and Randall LeVeque for insights and guidance on this dissertation research, as well as many other aspects of Earth Science. Knut Christianson and Erin Whorton provided valuable opportunities to engage in field science, which gave breadth to my education and deepened my perspective on modeling. The glaciology group and Earth and Space Sciences department have been a wonderful group of colleagues and friends, whom I will dearly miss. I would also like to acknowledge the University of Washington and the National Science Foundation for supporting my research and the communities that allow knowledge to grow. Finally, my friends and family have sustained me with their support, patience, and curiosity over these years, and for this I am deeply grateful.

DEDICATION

To my parents, Elizabeth and David

Chapter 1
INTRODUCTION

1.1 Introduction

This dissertation investigates how glaciers evolve in time, in response to climate variations. I focus on the era of anthropogenic climate change, which commenced approximately in the late 19th century (IPCC, 2013). During this period, glaciers around the world have lost mass and retreated significantly (e.g., Leclercq et al., 2014). Glacier retreat is a very visible and tangible change to the natural world, often showcased in striking side-by-side photographs of historical and modern glacier extent. Accordingly, the rapid loss of ice around the world is prominent in public discourse on climate change. It has very direct societal impacts as well, from global sea level rise to changes in water supply for downstream environments and communities.

The global signal of glacier change is unambiguous. However, variations in retreat though time and between individual glaciers hint at complexity lying beneath the global picture of ice loss. For example, brief readvances have punctuated the retreat of some glaciers, while neighboring glaciers retreated monotonically. Understanding what controls these transient responses is important at a fundamental level. We need to understand the dynamics in order to interpret the link between observed retreat or mass loss and climate. Also, projections of future glacier behavior depend on our ability to accurately emulate these processes in models. Finally, given the rate of ice loss and its prominence in the public eye, the scientific community has an opportunity and obligation to provide clarity on these changes—and especially on what causes notable variations between glaciers.

In this dissertation, I use several recently-developed analytical tools to revisit two well-known premises that complicate efforts to understand transient glacier change. The first

premise is that any given glacier responds to climate over a characteristic "memory" timescale. The second is that temporal variability is intrinsic to the climate system, and obscures trends due to anthropogenic forcing. I continue this introductory chapter by providing background on these premises, and summarizing the four studies that comprise the bulk of the dissertation. The four studies then follow as separate chapters. A concluding chapter synthesizes a few key ideas, and discusses some possibilities for future work.

Premise one: Glaciers have a memory of past climate

The first major premise is that a glacier's response following a climate perturbation occurs over a characteristic timescale. In other words, glaciers retain a finite "memory" of past climate. Jóhannesson et al. (1989) proposed a simple metric for the response time of a mountain glacier, $-H/b_t$, where H is the characteristic ice thickness and b_t is the (negative) mass balance rate near the terminus. For most settings, this gives response times from 10^1 to 10^2 years. Other analytical metrics, as well as empirical fits to observations and model output, yield a similar range. Subsequent studies have offered refinements to the analytical expression (e.g., Harrison et al., 2001), and to the response function that ultimately describes the transient terminus response (Roe and Baker, 2014). Additionally, response times with a similar form have also been developed for marine-terminating glaciers, which are more complex systems than their alpine cousins, and also extend into millennial timescales (Robel et al., 2018). The basic premise of decadal or longer response times implies that understanding glacier change in era of anthropogenic forcing must take these transient ice dynamics into account.

The principles embedded in the response times are also an important conceptual guide in this dissertation, especially in Chapters 3–5, and so warrant some introduction here. The Jóhannesson et al. (1989) metric (and those following from it) can be interpreted as a reservoir timescale: the transient response of the glacier must depend on the volume associated with a given length change (H, assuming constant width), and the rate at which volume is exchanged where the change occurs (i.e., the terminus; b_t). However, it is also worth noting that H and

b_t implicitly capture the aggregate dynamics of a glacier in steady state. Many mediating parameters, such as the catchment shape, bed slope, ice rheology, and mass balance gradient, conspire to set H and b_t. But importantly, the resulting values of H and b_t contain enough of these details to describe transient terminus behavior (Jóhannesson et al., 1989), and more recent work has demonstrated that this holds over a wide range of parameters (Roe and Baker, 2014). The constraints of geometry (both of the glacier catchment, and ice thickness) and mass balance are recurrent themes used to interpret results throughout this work.

Premise two: Glaciers are sensitive to natural climate variability

The second premise is that glaciers are sensitive not only to long-term climate changes, but also the variability that is an intrinsic part of the climate system. The climate of a given location depends fundamentally on the transport of heat and moisture from other locations, via the circulation of the ocean and atmosphere. Variations in this circulation—for example, in the trajectories of air and water parcels—are fundamentally chaotic (Lorenz, 1963) and can be treated as stochastic in time for many purposes (Hasselmann, 1976). Short-term atmospheric variations are integrated by slower systems to produce lower-frequency variability (e.g., Deser et al., 2003). And so a wide range of variations exist even in the absence of any external changes, and together are referred to as "internal variability". Because much of this variability is related to the transport and storage of heat and moisture, temporal anomalies are most obvious locally, and tend to cancel out as climate is averaged over larger scales. However, a non-negligible amount of internal variability persists into global mean temperature, associated with short-term anomalies in the planet's energy balance.

Internal variability gives rise to very familiar statistical challenges when studying any variable that is sensitive to climate. However, advances in the last decade have provided new insights into the challenges that internal climate variability poses for correctly identifying the component of warming that is due to anthropogenic forcing. New statistical methods and large climate model ensembles show that unforced fluctuations in the coupled atmosphere-ocean system can significantly bias decadal warming trends in observations (e.g., Wallace

et al., 2012) and model projections (e.g. Deser et al., 2012), especially at local and regional scales (e.g., Hawkins and Sutton, 2009). Internal variability must be considered when characterizing the climate forcing affecting glaciers, especially in terms of the anthropogenic component. Additionally, because of their response times, glaciers integrate climate variability and produce slower length fluctuations (e.g., Oerlemans, 2001; Roe and Baker, 2014). The structure of the natural climate variability thus affects the natural glacier fluctuations as well.

1.2 Research approach

These premises have long been recognized, but there remain open questions as to how to account for them. Differing interpretations of natural climate variations, such as the Little Ice Age and decadal modes of variability, can lead to different interpretations of glacier observations, or may affect assumptions built into models. Additionally, metrics for response times and their mathematical implementation vary in the literature (e.g., Jóhannesson et al., 1989; Oerlemans, 2001; Harrison et al., 2001; Lüthi, 2009; Marzeion et al., 2012; Roe and Baker, 2014). These assumptions, too, can affect conclusions about past and future glacier change. Finally, the wide range of geometries and climate settings of individual glaciers poses a challenge for testing these competing assumptions. Individual records of terminus position or mass balance may reflect different glacier response characteristics and different realizations of climate variability at the same time. This makes disentangling different effects in the collection of observational records a complex task.

The primary goal of this dissertation is not to account for every detail and "close the book" on any particular glacier, or collection of glaciers. Instead, I use several recently-developed analytical tools to revisit fundamental questions raised by the above premises. These tools provide new ways to quantitatively investigate basic underlying mechanisms, related to climate variability or response times, that mediate glacier change. My goal is to contribute insights that are relevant across many settings, and could serve as robust starting points for future analyses, whether for a particular glacier or the global picture.

My primary approach for doing this is conducting model experiments targeting a range of idealized glaciers. This helps to isolate the most general principles. My experiments in Chapters 3–5 combine numerical ice-flow models with recently-developed analytical models. The latter are systems of differential equations for a reduced set of glacier variables (e.g, length). I view these different model types as complementary tools. By simulating a 1-D thickness profile, the numerical models capture a more detailed view of a glacier's dynamical and geometric response to forcing. They also help to benchmark the capabilities and limits of the simpler models. In turn, the reduced models highlight the basic constraints of large-scale geometry and mass conservation. Their formulation as linear dynamical systems also provides links to powerful concepts in timeseries analysis. This brings a useful formalism to the concept of response times, which allows me to better evaluate previous assumptions in the literature. Finally, I have found that the exercise of comparing results from models with different degrees of physical complexity is an effective way to develop intuition for the actual systems we are trying to understand. *What allows a simple model to emulate a more complex one? What essential physics is it capturing or ignoring? How might these principles be observed in the real world?* Such questions guide my analyses in the background of the more-specific research topics.

This dissertation also includes analyses of observations from glaciers in Western North America (Chapters 2 and 4). In Chapter 2, I apply a new statistical model rather than a dynamical glacier model, so this chapter is somewhat distinct. However, while these analyses lead to some basic conclusions for the target glaciers, they are also meant to explore broader lessons about climate variability. Similarly, in Chapter 4 I focus on glaciers in the Washington Cascades, but highlight principles that should be considered for any population of glaciers. Thus I invite the reader to approach these case studies with the dissertation's broader questions about transient glacier change in mind.

1.3 Summary of Chapters

Chapter 2: Identifying dynamically induced variability in glacier mass-balance records

This chapter starts from the premise of internal climate variability, and investigates the implications for the climate forcing that glaciers have experienced in recent decades. In other words, the focus is on changes in the glaciers inputs. Records of glacier mass balance (i.e., accumulation vs. melt) reveal a very direct relationship with glaciers and their local climate, and are a natural starting point for assessing the effects of anthropogenic warming. However, the large biases in multidecadal climate trends identified by recent studies (e.g. Wallace et al., 2012; Deser et al., 2012) raise a complicating question: *how well do observed trends in glacier mass balance reflect the external forcing?*

These recent advances have highlighted the challenges associated with internal variability, but also offer new tools to account for it. I applied one, known as "dynamical adjustment" (e.g., Wallace et al., 2012), to investigate mass balance trends for three glaciers in Washington and Alaska. This statistical method identifies the patterns of atmospheric circulation variability that project onto mass balance anomalies. Accounting for this leaves a clearer picture of any externally-forced trend.

I found that 50-year trends in mass balance have been minimally affected by internal variability. Increases in summer melt are thus consistent with an external forcing. The analysis also reveals coherent structures of climate variability that produce much of the variance on shorter timescales, and which can have opposing effects on glaciers in different regions. Thus the method is also useful for understanding geographic differences in decadal trends.

Chapter 3: Committed retreat: controls on glacier disequilibrium in a warming climate

For the remainder of the dissertation, I focus primarily on the glacier length response to climate forcing—in other words, the system's outputs. Chapter 3 focuses on a basic consequence of glacier response times: any system with memory will lag an applied forcing,

implying that glaciers are currently out of equilibrium. In the context of anthropogenic warming since the late 19th century, this raises the question: *how well does observed glacier retreat reflect the full response to anthropogenic warming?*

The disequilibrium of mountain glaciers has been previously documented in a number of studies. However, most have focused on particular glaciers and regions. Additionally, there is still inconsistency in the manner and degree to which disequilibrium is represented in modeling studies and projections. The goal of this chapter is to investigate this basic behavior in a general way. Key to this is considering an instantaneous equilibrium response, which for glaciers is largely dictated by the geometry of the landscape and the imposed climate. This allows me to define metrics for disequilibrium that highlight the essential transient glacier dynamics. I conduct idealized experiments with several models to compare factors that affect disequilibrium. The most important are the response time itself (or any factors that affect H/b_t), and the correct underlying model that implements the response time.

Chapter 4: Differences in the transient response of individual glaciers: a case study in the Washington Cascades

This chapter applies the lessons of Chapter 3 to the glaciers of the Cascade mountains in Washington State. Because of the strong geometric controls on the response time, a range of glacier sizes and slopes within a region implies a range of response times. Thus, the primary question is: *How much to the transient responses and current states of glaciers vary within a region?*

I estimated response times for 383 glaciers in the Cascades based on a simple geometric scaling relationships, finding a range of 10–60 years for most glaciers. While these are fairly typical response times, I show that the tails of this distribution yield significantly different conclusions about the current disequilibrium of individual glaciers. The fundamental lesson is that conclusions drawn about one glacier should not necessarily be extrapolated to neighboring glaciers without considering their individual response times.

Chapter 5: The contrasting response of outlet glaciers to interior and ocean forcing

The final chapter approaches the transient responses of large marine-terminating outlet glaciers that drain ice sheets. Floating termini make the dynamics and mass exchange of these systems more complex compared to their alpine counterparts. Recent work has demonstrated that this leads to two widely-separated characteristic response times: a "fast" multi-decadal response and a slow millennial response (Robel et al., 2018). Also, they are sensitive to climate via two distinct pathways: ocean forcing at the terminus, and atmospheric forcing over their large interior catchments. The main question guiding this chapter is: *How does the transient terminus response depend on whether perturbations come from the ocean or atmosphere?*

This work thus extends the premise of glacier response times into larger and more complex settings. I show how ocean and atmospheric forcing project differently onto the fast and slow responses, affecting the amount of advance or retreat that can occur on decadal to centennial timescales. The premise of natural climate variability also takes on a new element in this chapter, because the relative roles of ocean and atmospheric variability must also be considered. I show that the role of ocean variability is especially important because it typically exhibits more temporal persistence than atmospheric variability, which enhances natural glacier fluctuations. These analyses thus bring a new perspective into the very active topic of ice sheet responses to ocean forcing (e.g., Straneo and Heimbach, 2013; Jenkins et al., 2016).

BIBLIOGRAPHY

Deser, C., Alexander, M. A., and Timlin, M. S. (2003). Understanding the Persistence of Sea Surface Temperature Anomalies in Midlatitudes. *J. Clim.*, 16(1):57–72.

Deser, C., Phillips, A., Bourdette, V., and Teng, H. (2012). Uncertainty in climate change projections: The role of internal variability. *Climate Dynamics*, 38(3-4):527–546.

Harrison, W. D., Elsberg, D. H., Echelmeyer, K. A., and Krimmel, R. M. (2001). On the characterization of glacier response by a single time-scale. *Journal of Glaciology*, 47(159):659–664.

Hasselmann, K. (1976). Stochastic climate models Part I. Theory. *Tellus*, 28(6):473–485.

Hawkins, E. and Sutton, R. (2009). The potential to narrow uncertainty in regional climate predictions. *Bulletin of the American Meteorological Society*, 90(8):1095–1108.

IPCC (2013). Climate Change 2013: The Physical Science Basis. Contribution of Working Group I to the Fifth Assessment Report of the Intergovernmental Panel on Climate Change. Technical report, Cambridge.

Jenkins, A., Dutrieux, P., Jacobs, S., Steig, E. J., Gudmundsson, G. H., Smith, J., and Heywood, K. J. (2016). Decadal ocean forcing and Antarctic Ice Sheet response: lessons from the Amundsen Sea. *Oceanography*, 29(4):106–117.

Jóhannesson, T., Raymond, C., and Waddington, E. (1989). Time–Scale for Adjustment of Glaciers to Changes in Mass Balance. *Journal of Glaciology*, 35(121):355–369.

Leclercq, P. W., Oerlemans, J., Basagic, H. J., Bushueva, I., Cook, A. J., and Le Bris, R. (2014). A data set of worldwide glacier length fluctuations. *Cryosphere*, 8:659–672.

Lorenz, E. N. (1963). Deterministic Nonperiodic Flow. *Journal of the Atmospheric Sciences*, 20(2):130–141.

Lüthi, M. P. (2009). Transient response of idealized glaciers to climate variations. *Journal of Glaciology*, 55(193):918–930.

Marzeion, B., Jarosch, A., and Hofer, M. (2012). Past and future sea-level change from the surface mass balance of glaciers. *The Cryosphere*, 6(6):1295.

Oerlemans, J. (2001). *Glaciers and climate change*. Balkema.

Robel, A. A., Roe, G. H., and Haseloff, M. (2018). Response of Marine-Terminating Glaciers to Forcing: Time Scales, Sensitivities, Instabilities, and Stochastic Dynamics. *Journal of Geophysical Research: Earth Surface*, 123(9):2205–2227.

Roe, G. H. and Baker, M. B. (2014). Glacier response to climate perturbations: An accurate linear geometric model. *Journal of Glaciology*, 60(222):670–684.

Straneo, F. and Heimbach, P. (2013). North Atlantic warming and the retreat of Greenland's outlet glaciers. *Nature*, 504(7478):36–43.

Wallace, J. M., Fu, Q., Smoliak, B. V., Lin, P., and Johanson, C. M. (2012). Simulated versus observed patterns of warming over the extratropical Northern Hemisphere continents during the cold season. *Proceedings of the National Academy of Sciences of the United States of America*, 109(36):14337–14342.

Chapter 2

IDENTIFYING DYNAMICALLY INDUCED VARIABILITY IN GLACIER MASS-BALANCE RECORDS

Chapter 2, in full, is a reprint of a manuscript published in *Journal of Climate*:

Christian, J. E., N. Siler, M. Koutnik, and G. Roe, 2016: Identifying Dynamically Induced Variability in Glacier Mass-Balance Records. *J. Climate*, 29, 8915–8929, https://doi.org/10.1175/JCLI-D-16-0128.1.

2.1 Abstract

Glacier mass balance provides a direct indicator of a glacier's relationship with local climate, but internally-generated variability in atmospheric circulation adds a significant degree of noise to mass-balance timeseries, making it difficult to correctly identify and interpret trends. This study applies "dynamical adjustment" to seasonal mass-balance records to identify and remove the component of variance in these timeseries that is associated with large-scale circulation fluctuations ("dynamical adjustment" here refers to a statistical method and not a glacier's dynamical response to climate). Mass-balance records are investigated for three glaciers: Wolverine and Gulkana in Alaska, and South Cascade in Washington. North Pacific sea-level pressure and sea-surface temperature fields perform comparably as predictors, each explaining 50–60% of variance in winter balance and 25–35% in summer balance for South Cascade and Wolverine Glaciers. Gulkana glacier, located farther inland, is less closely linked to North Pacific climate variability, with the predictors explaining roughly 30% of variance in winter and summer balance. To investigate the degree to which this variability

affects trends, adjusted mass-balance timeseries are compared to those in the raw data, with common results for all three glaciers: winter balance trends are not significant initially, and do not gain robust significance after adjustment despite the large amount of circulation-related variability. However, the raw summer balance data have statistically significant negative trends that remain after dynamical adjustment. This indicates that these trends of increasing ablation in recent decades are not due to circulation anomalies and are consistent with anthropogenic warming.

2.2 Introduction

2.2.1 Glaciers and climate variability

Variations in climate occur in response to both external forcing and internally-generated variability. External forcings are generally defined as mechanisms outside of the climate system that change the underlying radiative balance of the planet; such forcings can be natural (e.g., changes in volcanic or solar activity) or anthropogenic (e.g., greenhouse gas and aerosol emissions, changes in land use), in origin (e.g., IPCC 2013). Internal variability is also fundamental to the climate system and occurs even in the absence of external forcing; these variations arise as chaotic fluctuations in oceanic and atmospheric circulation, and are integrated by components of the climate system operating on a range of timescales (e.g., IPCC 2013). Though such variability is essentially stochastic in nature (e.g., Hasselmann 1976), there are preferred modes of variability that emerge on interannual to decadal timescales. A large body of research exists on these persistent patterns and their origins in the coupled atmosphere-ocean system (e.g., Deser et al. 2010 and references therein) as well as on the effects of time-varying atmospheric dynamics on hemisphere-scale temperature trends (Wallace et al. 1995). Model developments and increases in computational power over the past decade have allowed for improved understanding of how this internal variability differs from external forcing. For example, Deser et al. (2012) integrated an ensemble of identical global climate models with identical external forcing scenarios, but with minor perturbations in the

initial climate state between ensemble members. The resulting divergence among the model integrations can be due only to internal variability. Deser et al. (2012) demonstrated that internal variability can dominate over external forcing in regional climate trends even on multidecadal timescales (see also Wallace et al. 2013). Glaciers interact with their local climate via their mass balance: the accumulation and ablation (i.e., melt) of snow and ice each year. Worldwide glacier retreat is a highly visible and widely cited result of a changing climate. However, glaciers respond not only to external forcings, but also to interannual variability in temperature and precipitation (e.g., Oerlemans 2001; Roe and Baker 2014) associated with internal climate variability. Large year-to-year fluctuations can make it difficult to identify and attribute trends in the global archive of mass-balance records. However, when combined with other climate data, the variability itself can yield information about the large-scale climate processes that drive glacier changes. For example, Bitz and Battisti (1999) examined correlations between the mass-balance records of several Western North American glaciers and indices of prominent modes of climate variability, as well as meteorological data from local to synoptic scales. Their analyses provide insight into the dynamical links between North Pacific climate and the targeted glaciers, and the relevant differences between the glaciers' climatic settings. In this study, we build on these analyses of the signatures of large-scale climate variability in glacier mass-balance records, with the added objective of improving the identification of trends in mass balance.

2.2.2 Dynamical adjustment

For any climate record that spans only a few decades, identifying the effect of anthropogenic forcing can be problematic: trend estimates may lack statistical significance due to the background noise of inter-annual variability. Furthermore, the trends themselves may be biased by limited temporal or spatial sampling of low-frequency, internally-generated fluctuations (e.g., Casola et al. 2009; Wallace et al. 2012). "Dynamical adjustment" is a method that seeks to extract the component of the variance in a climate timeseries that is attributable to large-scale atmospheric circulation anomalies (i.e., dynamically-induced variability) rather

than to external forcing. With this component removed, the adjusted timeseries has less variance and may exhibit a different trend. For example, Wallace et al. (2012) dynamically adjusted observed surface air temperatures poleward of 40°N and concluded that 0.7°C of the ∼1.7°C warming trend in wintertime temperatures from 1965–2000 was dynamically induced. With adjusted trends unbiased by internal effects, such analyses can clarify the anthropogenic signal in a target climate timeseries. A number of studies in recent decades have developed and used this method. Although not all were referred to as "dynamical adjustment", they nonetheless established the objective of evaluating the role of dynamically induced variability. These studies analyzed surface-temperature records using a variety of approaches, including regression of the temperature fields themselves (Wallace et al., 1995), with established climate indices (e.g., Hurrell 1996; Bitz and Battisti 1999; Thompson et al. 2000) and with Sea Level Pressure (SLP) fields (Thompson et al. 2009). More recent studies have adjusted additional climate variables such as snowpack, air temperature, and hurricane activity (Smoliak et al. 2010; Wallace et al. 2012; Smoliak et al. 2015), and are based on the method of Partial Least Squares (PLS) regression (see Abdi 2010). PLS regression decomposes a set of predictor variables into components of variability that are optimized to explain the variability in a variable of interest (the predictand). In the context of dynamical adjustment, the predictors are grid points of a time-varying field (e.g., sea level pressure, sea surface temperature) that is assumed to have a dynamical link to the predictand (e.g., regional temperature, snowpack). We present the PLS regression algorithm in section 3. Note that in our context, the term "dynamical adjustment" should not be confused with the dynamics of a glacier's geometrical adjustment to climate changes. In this study, "dynamical adjustment" will refer only to the methodology described above. We apply a PLS-based dynamical adjustment to glacier mass-balance records using SLP and Sea Surface Temperature (SST), independently, as predictors. SLP has been used previously for dynamical adjustments (Smoliak et al. 2010; Wallace et al. 2012; Smoliak et al. 2015), and its variability is a widely used indicator of circulation changes on a range of timescales. SLP patterns control the direction and magnitude of near-surface winds, and thus are strongly linked to variability

in surface temperature and precipitation (e.g., Wallace and Hobbs 2006). This relationship makes SLP a clear candidate for dynamically adjusting glacier mass-balance records. SST is related to glacier change through a number of pathways. It is established that the onshore flow of warm, moist marine air masses during storms links SSTs to snowpack in coastal mountains (Casola et al. 2009), and by extension in this study, to the accumulation/winter balance of glaciers in Western North America. Furthermore, SST and SLP variability are closely related via dynamical coupling between the ocean and atmosphere. For example, Deser and Phillips (2009) showed that SST variability is related to recent decadal trends in North Pacific atmospheric circulation. At the same time, SST also responds to higher frequency atmospheric pressure variations, as demonstrated by Johnstone and Mantua (2014), who found that the leading mode of monthly variability in North Pacific SST resembles a lagged response to the 11-month running mean of SLP variability. The coupling of atmospheric pressure and ocean temperature on timescales from months to decades motivates our investigation of both SLP and SST datasets as predictors for glacier mass-balance variability.

2.3 Study area and datasets

2.3.1 Target Glaciers

We focus our study on the mass-balance records of three United States Geological Survey (USGS) benchmark glaciers: Wolverine Glacier in Alaska's Kenai Range, Gulkana Glacier in the Alaska Range, and South Cascade Glacier in Washington State's Cascade Range (Fig. 2.1). These glaciers have the longest continuous mass-balance records in North America, with winter balance (B_w), summer balance (B_s), and annual balance (B_a) data available from 1959–2011 for South Cascade Glacier (WGMS 2012; 2013), and from 1966–2015 for Wolverine and Gulkana Glaciers (Fig. 2.1) (O'Neel et al. 2016). Monitoring is ongoing, but more recent measurements for South Cascade were not released at the time of our analysis.

In addition to having long-term, high-quality mass-balance records, the glaciers exist in distinct climate settings. Accordingly, their balance records show some characteristic differ-

ences: Wolverine Glacier receives ample moisture from the Gulf of Alaska (approximately 50km away), and has a large mean-winter balance rate (B_w = 2.2 meters-water-equivalent per year, m w.e. yr^{-1}) and also large variability (standard deviation, σ = 0.9 m w.e. yr^{-1}); Gulkana Glacier is ∼300 km inland and blocked from much of this precipitation by high coastal mountains (e.g., Rasmussen and Conway, 2004), and thus experiences a continental climate with less precipitation and less variability (B_w = 1.3 m w.e. yr^{-1}, σ = 0.3 m w.e. yr^{-1}). Meanwhile at lower latitudes, South Cascade Glacier is 250km inland from the Pacific but is only partially blocked from onshore moisture flow by the Olympic Mountains, and still resides in a maritime climate as evidenced by its high winter accumulation and variability (B_w = 2.8 m w.e. yr^{-1}, σ = 0.6 m w.e. yr^{-1}).

The long-term mean mass-balance values are −0.4, −0.5, and −0.6 m w.e. yr^{-1} for Wolverine, Gulkana, and South Cascade, respectively, indicating that all three glaciers have been out of equilibrium with the average climate over the study period. However, as stated previously, Wolverine and South Cascade show significant variability in annual balance (σ = 1.2 and 1.0 m w.e. yr^{-1}), such that years of positive annual balance are not uncommon. For Gulkana, the mean annual balance is comparable in magnitude to the standard deviation (σ = 0.6 m w.e. yr^{-1}), and indeed there are only seven years of positive balance in the 50-year record, with the most recent in 2003.

2.3.2 Mass-balance data

The glacier-averaged balance values reported by the USGS are calculated from point measurements of accumulation and ablation, which are converted to meters-water-equivalent based on density measurements, and then extrapolated over the whole glacier area using empirical altitude-dependent relations. Wolverine and Gulkana each have three index sites at which point mass balance is measured, though measurements at additional sites have been made intermittently to constrain results. Additionally, Digital Elevation Models (DEMs) from aerial photogrammetry are used to update the area-altitude distribution used for extrapolation from point balance to glacier-wide balance as the glacier's geometry changes, linearly

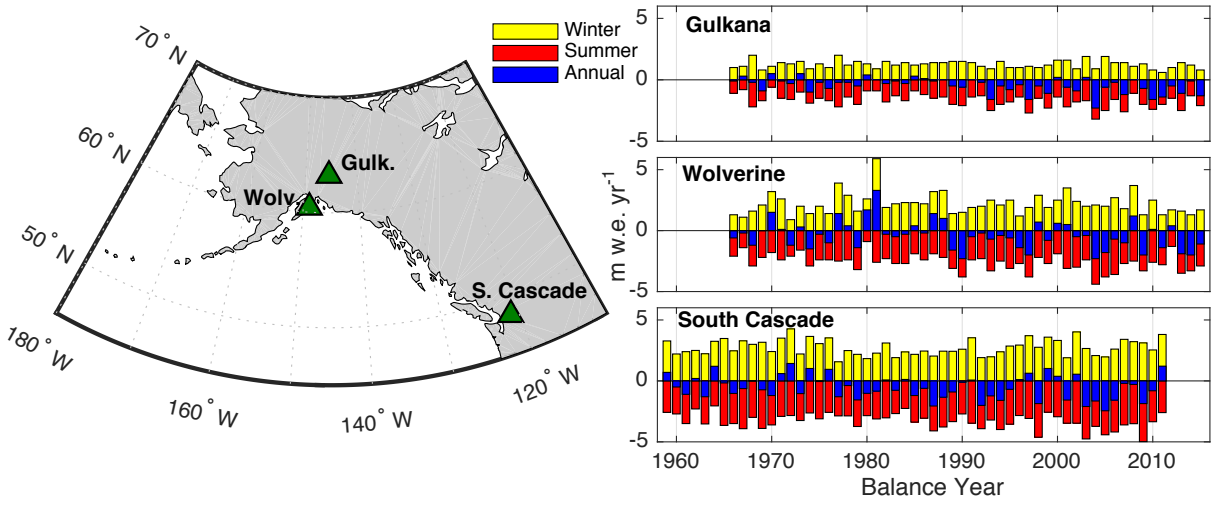

Figure 2.1: Locations of three target glaciers (left). Panels (right) show mass-balance records for each glacier, each with winter (yellow), summer (red), and annual (blue) data.

interpolating between years with available DEMs (Van Beusekom et al. 2010; O'Neel et al. 2014). South Cascade currently uses six fixed index sites (Bidlake et al. 2010). Snow depth, which is often more easily measured than ablation, is frequently measured in additional locations on the glaciers in order to mitigate the effects of local irregularities. Maximum accumulation and ablation values for each index site are often derived quantities, because measurements rarely fall precisely at the transition between accumulation and ablation seasons, and furthermore, these dates may not be synchronous across the glacier. For all three glaciers, temperature and precipitation measurements from nearby meteorological stations are used to estimate the dates of these transitions and to model the accumulation/ablation that occurred between the measurement date and the seasonal transition. Complete descriptions of the models and conventions used to generate the mass-balance datasets are available in USGS technical reports: for example, Bidlake et al. (2010) for South Cascade Glacier, and Van Beusekom et al. (2010) for Wolverine and Gulkana Glaciers. For our purposes, we use B_w, B_s, and B_a in their available forms as estimates of glacier-wide change from season

to season. We discuss the potential effects of observational error in section 5.

2.3.3 Sea level pressure

The SLP predictor is derived from 2.5° × 2.5° monthly mean SLP data from NCEP/NCAR Reanalysis (Kalnay et al. 1996). In order to match the respective seasons of the mass-balance timeseries, averages of winter (October–March) and summer (April–September) SLP are used. The domain is restricted to 20–70°N and 150–250°E. Our results are not qualitatively sensitive to the domain, provided that the most of the North Pacific is included. However, the fraction of mass-balance variability explained by the predictor declines somewhat with significantly larger or smaller domains.

2.3.4 Sea surface temperature

For the SST predictor, 1° × 1° monthly values come from the Met Office Hadley Centre's sea ice and sea surface temperature data set, HadISST1 (Rayner et al. 2003). The global mean is subtracted from the SST field at each time, and we use the resulting anomaly fields as the SST predictor. This removes the global, long-term warming signal associated with external radiative forcing (e.g., IPCC 2013), and in principle retains trends unique to the study domain, though this residual is small compared to the global mean trend. The domain is the same as that for SLP, except it is further restricted by removing all grid points that experience sea ice cover, even if only seasonally. Seasonal averages are taken as with SLP.

2.4 Method of Partial Least Squares (PLS) Regression

Using a time-varying field (i.e., multiple predictor timeseries) to explain variability in the predictand preserves spatial information, but since the individual predictors are spatially indexed observations of the same climate variable, they may be highly correlated. While this could be problematic for some regression techniques, the PLS method eliminates this problem by decomposing the predictor set into orthogonal patterns of variability.

This idea is common to a number of statistical approaches for analyzing variability in climate data. For example, Principal Component Analysis (PCA) decomposes a single dataset into a set of patterns that best capture its own variability, and Maximum Covariance Analysis (MCA, see e.g., Bretherton et al. 1992; von Storch and Zwiers 1999) identifies patterns that maximize covariance between two different variables. Like MCA, PLS regression identifies common patterns between different climate variables, but here the constraint is one-way: the predictor is decomposed into patterns that explain the maximum amount of variance in the predictand. This makes PLS especially suitable for dynamical adjustment, where the primary goal is to identify the large-scale origins of variability in the predictand.

Dynamical adjustment using PLS regression proceeds as follows. Let $\mathbf{X}$ be an $n \times m$ matrix with n observations in time at m spatial points (i.e., m predictors), which has been standardized to zero mean and unit variance in time. In the case of a gridded dataset such as SST or SLP, the grid is reshaped into a $1 \times m$ vector for each observation time (where m is the product of the original grid's length and width), yielding the $n \times m$ matrix for the whole observational period. Let $\mathbf{Y}$ be the predictand timeseries of n observations, also standardized to zero mean and unit variance. In our case, $\mathbf{Y}$ is an $n \times 1$ vector, though PLS regression can be generalized to the case that the predictand is a matrix. First, a correlation map, $\mathbf{W}$, is created using detrended timeseries:

$$\mathbf{W} = \frac{1}{n-1}\mathbf{X}'^{T}\mathbf{Y}', \tag{1}$$

where the prime denotes that the predictand and each predictor grid point have been detrended in time. This is done so that the correlation map is not biased by trends, which could more easily be correlated without a dynamical link. $\mathbf{W}$ is thus an $m \times 1$ vector that can be reshaped back into the predictor's physical (grid) dimensions to provide a map of the detrended correlations between predictor and predictand at each observation point (see Fig. 2.1a). $\mathbf{W}$ is weighted by the cosine of latitude (denoted $\mathbf{W}_c$) to equally distribute influence by area, and finally normalized to unit magnitude. Brackets $\langle \mathbf{A} \rangle$ hereafter denote

the following normalization for a generic variable $\mathbf{A}$:

$$\langle \mathbf{A} \rangle = \mathbf{A} / \sqrt{\mathbf{A}^T \mathbf{A}}. \tag{2}$$

Next, the predictor is projected onto $\langle \mathbf{W}_c \rangle$:

$$\mathbf{t} = \mathbf{X} \langle \mathbf{W}_c \rangle, \tag{3}$$

where $\mathbf{t}$ is an index in time $(n \times 1)$ that expresses the variations of the spatial correlation patterns. Here we note the similarity with PCA, in that $\mathbf{t}$ is analogous to the principal component of an empirical orthogonal function of $\mathbf{X}$, where here we simply enforce that the function is the correlation map $\mathbf{W}_c$. The index $\mathbf{t}$ then determines regression coefficients that are used to remove variance from both the predictor and the predictand. Let $\mathbf{P}$ be the vector of regression coefficients for the set of predictor variables, $\mathbf{X}$:

$$\mathbf{P} = \mathbf{X}^T \langle \mathbf{t} \rangle, \tag{4}$$

and β the regression coefficient for the predictand, $\mathbf{Y}$:

$$\beta = \langle \mathbf{t}^T \rangle \mathbf{Y}. \tag{5}$$

Then, the index is subtracted from the predictor and predictand weighted by $\mathbf{P}$ and β, which yields the *dynamically adjusted* variables:

$$\mathbf{X}_{adj} = \mathbf{X} - \mathbf{t}\mathbf{P}^T \quad and \quad \mathbf{Y}_{adj} = \mathbf{Y} - \beta \mathbf{t}. \tag{6}$$

The fractions of variance in $\mathbf{X}$ and $\mathbf{Y}$ explained by $\mathbf{t}$ are given, respectively, by

$$(\mathbf{P}^T\mathbf{P})/\sum_m\sum_n |X_{mn}|^2 \quad and \quad \beta^2/\sum_n |Y_n|^2. \tag{7}$$

Note that, in general, the respective fractions of variance explained in $\mathbf{X}$ and $\mathbf{Y}$ are not equal, since PLS finds patterns that maximize variance in $\mathbf{Y}$ explained by $\mathbf{X}$.

At this stage, the PLS regression has removed from $\mathbf{X}$ the component of its own variability that explains the most variance in $\mathbf{Y}$. And from $\mathbf{Y}$, it has removed the component of variability that can be attributed to variability in $\mathbf{X}$. In our context of PLS-based dynamical adjustment, the pattern regressed out of $\mathbf{X}$ is interpreted as a mode of large-scale climate variability that drives changes in glacier mass balance. However, there may in fact be multiple independent modes whereby the predictor fields drive the predictand, and thus more associated co-variability may remain between $\mathbf{X}_{adj}$ and $\mathbf{Y}_{adj}$. Much of the utility of PLS regression comes from the capability to reiterate the regression with $\mathbf{X}_{adj}$ and $\mathbf{Y}_{adj}$ as predictor and predictand. Further iterations yield a series of indices, $\mathbf{t}_1, \mathbf{t}_2 \ldots \mathbf{t}_n$. These indices are mutually orthogonal and thus the total variance explained is additive.

Successive iterations typically explain progressively less variance, and will eventually fail to yield significant or physically meaningful adjustments. Previous studies (Smoliak et al. 2010; Smoliak et al. 2015; Wallace et al. 2012) have used cross-validation to determine the number of PLS modes that should be considered in analysis. We follow in this vein, using a procedure outlined in Abdi (2010), which evaluates the predictive skill of the PLS modes when applied to an observation left out of the regression. This method indicated that between one and four modes had predictive power depending on the variables used. However, this metric – especially with relatively short records – is not guaranteed to inform physical significance. Thus, for all dynamical adjustments presented here, we consider the two leading modes for the sake of consistency. This involves some risk of retaining insignificant modes (or omitting significant modes), but since the modes beyond the leading pattern explain a small amount of variance, they are unlikely to project strongly onto mass-balance trends and

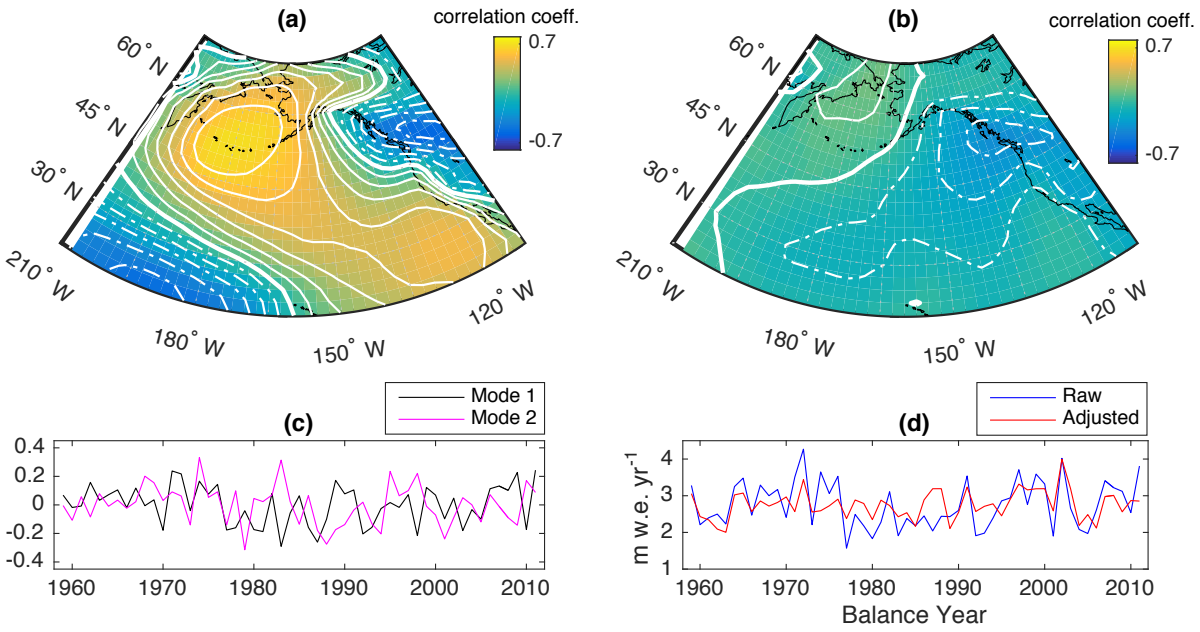

Figure 2.2: Adjustment for South Cascade Glacier winter balance using SLP. (a) The leading correlation map between SLP and winter balance. Contour interval is 0.1, with bold indicating the zero contour and dashed contours indicating negative correlations. (b) The second correlation map. (c) The two leading indices associated with SLP variability, to be regressed out of the winter balance record. (d) The original winter balance record and the adjusted timeseries, which remains after the dynamically-induced variability has been removed.

significantly bias our conclusions.

2.5 Results

2.5.1 Raw data

We begin by characterizing the noise and trends in the raw mass-balance records using standard statistical metrics. We use a straightforward version of the t-statistic to evaluate trend significance (see e.g., Casola et al., 2009; Roe 2011). For a given mass-balance record, the t-value is given by

$$\tilde{t} = \frac{\Delta B}{\sigma}\sqrt{\frac{\nu - 2}{12}}, \tag{8}$$

where ΔB is the magnitude of total change in mass balance as estimated by a least-squares linear fit to the data over the observing period, σ is the standard deviation of the detrended residual, and ν is the number of degrees of freedom. The critical t-value for a given threshold of confidence and number of degrees of freedom can be found in standard statistics tables, and we can then solve for a critical $\Delta B/\sigma$ (the "signal-to-noise ratio") needed to declare a trend significant.

A variable with persistence (i.e., serial correlation) on the order of the sampling interval Δt has fewer independent degrees of freedom than observations. In order to account for the possibility of persistence, we estimate ν from the autocorrelation function of the timeseries. One straightforward metric based on Bartlett (1946) states that the 95% confidence bound for a lag-1 autocorrelation ($r_{\Delta t}$) indistinguishable from zero is $1.96/\sqrt{N}$, where N is the number of observations. After linear detrending, all of the mass-balance records fall below this threshold of ~ 0.27, indicating that the test does not provide evidence of persistence. Another method, based on Leith (1973), assumes a red noise process with a decorrelation (e-folding) time τ estimated from $r_{\Delta t}$. In this case,

$$\nu = \frac{-N\Delta t}{2\tau}, \quad where \quad \tau = \frac{-\Delta t}{\ln\left(r_{\Delta t}\right)}. \tag{9}$$

Following this metric, ν/N approaches 1 as $r_{\Delta t}$ approaches e^{-2} (~ 0.13). Again, $r_{\Delta t}$ for all records fall below this threshold. On this basis we conclude that the observations lack persistence and thus each timeseries is consistent with N independent degrees of freedom. We discuss the sensitivity of our conclusions to the choice of ν in the next section.

The critical t-value, and thus the critical signal-to-noise ratio, also depends on whether a one-tailed or two-tailed test is used; that is, whether trends breaching the chosen confidence

Table 2.1: Trends in mass-balance records, reported as $mw.e.yr^{-1}$ per decade, based on data from 1959–2011 for South Cascade and 1966–2015 for Wolverine and Gulkana. Values in bold are trends that are statistically significant at 95% based on a 2-tailed Student's t-test.

	Winter	*Summer*	*Annual*
South Cascade	0.02	**-0.16**	−0.15
Wolverine	−0.03	**-0.21**	**-0.23**
Gulkana	−0.03	**-0.17**	**-0.20**

level can come from one or both sides of the t-distribution. A one-tailed test can enhance detectability provided the *sign* of the trend can reasonably be assumed *a priori*. However, considering that internal climate variability can have a considerable impact on decadal climate trends (e.g., Deser et al. 2012; Wallace et al. 2012), and lacking an *a priori* assumption about the sign of this trend contribution, we argue that a two-tailed significance test is most rigorous for this study. This allows for either positive or negative trends to be detected, but requires a higher signal-to-noise ratio for significance at a given confidence level.

For the three target glaciers, we see a common pattern. All three have negative trends in summer balance, significant at the 5% level (Table 1). However, none of the glaciers have statistically significant trends in winter balance. Although several studies have documented declining snowpack in Washington's Cascade Mountains (e.g., Mote et al. 2005; Casola et al. 2009; Stoelinga et al. 2010), winter balance depends on a different hypsometric signature on the landscape as well as other local effects specific to the glacier's setting within the mountain range (e.g., avalanching, wind deposition, microclimates) and thus may not exhibit the same trends as regional snowpack.

Finally, driven by the summertime contribution, the annual mass balance has a negative trend for all three glaciers, but is significant only for Gulkana.

2.5.2 Adjustment of winter balance

We now apply dynamical adjustment to investigate what fraction of each mass-balance record can be attributed to variability in large-scale atmospheric circulation. We first present results for winter mass balance, as they demonstrate the clearest dynamical link between predictors and predictand. For South Cascade Glacier, the leading SLP predictor pattern explains 53% of variance in winter balance. The spatial pattern of the leading SLP mode (Fig. 2.1a) shows that variability in winter accumulation is strongly correlated with the strength of the Aleutian Low, a persistent wintertime pattern of low surface-pressure and cyclonic circulation in the North Pacific. Variability in this feature reflects shifts in the latitude and intensity of the winter stormtrack, and thus variability of precipitation over South Cascade Glacier (e.g., Bitz and Battisti 1999).

A second iteration of PLS-regression yields a second pattern explaining an additional 10% of the variance in the original record (Fig. 2.1b). In general, spatial patterns for successive modes are more difficult to interpret physically, since the remaining correlations after the preceding mode(s) have been removed are weaker and less spatially coherent. Additionally, the constraint that modes are mutually orthogonal can obscure physical interpretations, given that dynamical processes are not necessarily linearly independent (e.g., Hannachi et al. 2007). The two orthogonal indices $(\mathbf{t}_1, \mathbf{t}_2)$ generated from these patterns are shown in Fig. 2.1c, and their combined effect is seen in Fig. 2.1d: the adjusted timeseries has 63% less variance than the raw winter balance record.

Using SST as a predictor returned similar results for South Cascade winter balance: the leading patterns explained 47% and 12% of variance, respectively. The spatial correlation patterns are distinct for SST, with the leading pattern resembling the spatial signature of the Pacific Decadal Oscillation (e.g., Mantua et al. 1997) (see Fig. 2.3a). However, the indices (Fig. 2.3c) produced from SST are strongly correlated with those of SLP ($r = 0.84$ for leading mode), indicating that the dynamical adjustment extracts a common element of variance in South Cascade Glacier's mass-balance driven by the coupled ocean-atmosphere

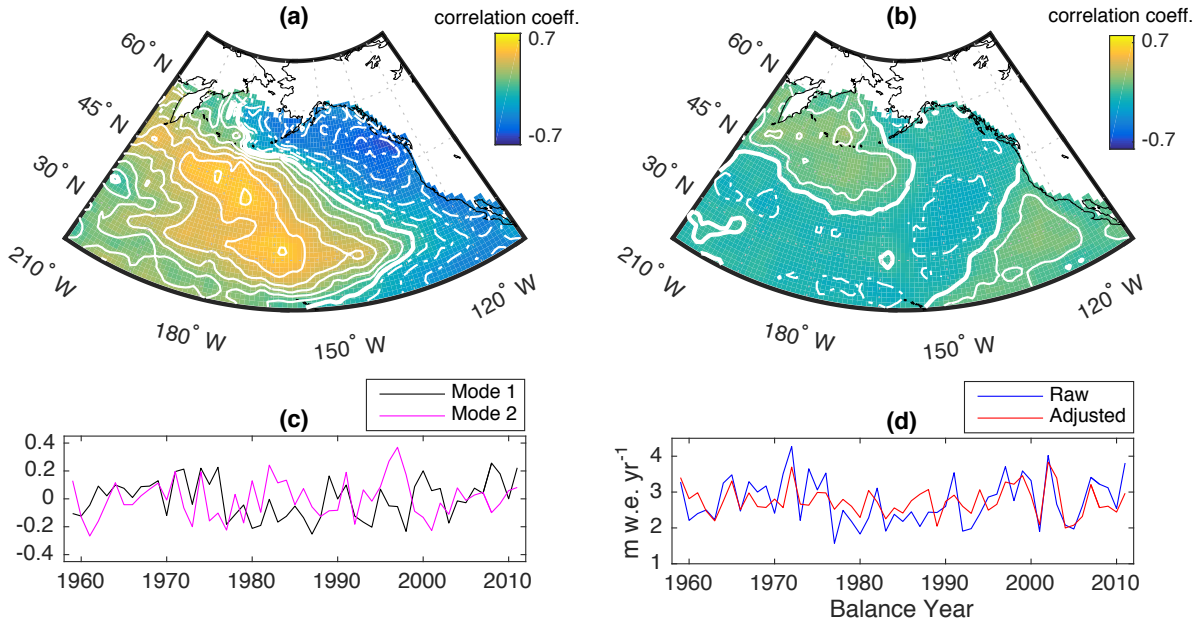

Figure 2.3: As for Fig. 2.1, but using SST as predictor for South Cascade winter balance. (a) The leading correlation map for SST. Contour interval is 0.1, with bold indicating the zero contour and dashed contours indicating negative correlations. (b) The second correlation map. (c) The two leading indices associated with SST variability. (d) The original and adjusted timeseries.

system. Similar to results using SLP, the adjustment with SST removes 59% of the original variance in B_w (Fig. 2.3c).

The dynamical adjustments for Wolverine glacier accounted for similar, albeit slightly weaker, components of variance in winter balance. The first two SLP patterns explained 46% and 9% of variance, and the SST patterns explained 34% and 9%, respectively. Notably, the leading correlation patterns associated with SLP and SST have similar structure but opposite polarity to their respective counterparts for South Cascade Glacier (Fig. 2.4). As a result, the leading indices for Wolverine and South Cascade Glaciers are strongly negatively correlated ($r \sim -0.9$ for SLP, -0.8 for SST). For the years that the mass-balance observations overlap for all three glaciers (1966–2011), the records themselves are moderately anti-correlated

($r = -0.42$), a relationship that has been attributed to circulation anomalies that shift winter storms toward southeast Alaska and away from Washington state, or vice versa (e.g., Walters and Meier 1989; Bitz and Battisti 1999; Rasmussen and Conway 2004). Additionally, Bitz and Battisti (1999) showed that winter balance has different temperature sensitivities between these settings, with warmer winters more favorable for accumulation in Alaska and the opposite for Washington. This may then be a coupled temperature and precipitation signal; it is difficult to say which dominates from the patterns alone, although the end effect is reflected in winter accumulation. The adjusted records for Wolverine and South Cascade glaciers are effectively uncorrelated ($r = -0.05$ using SLP), reinforcing that the adjustment is indeed identifying and removing the dynamical contribution to mass-balance variability.

Winter mass balance for Gulkana Glacier showed a much weaker connection to the predictors: SLP and SST patterns explained $23\% + 7\%$ and $22\% + 6\%$, respectively. Recalling that Gulkana's winter-balance record has comparatively little variability to begin with (Fig. 2.1), the year-to-year changes in accumulation that are driven by internal North Pacific climate variability are quite small, consistent with its more continental setting.

In summary, by applying dynamical adjustment we can account for almost two-thirds of the total variance in the maritime glaciers' winter accumulation, indicating a close connection between internal variability in North Pacific circulation and winter mass-balance; however, the case of Gulkana Glacier, with less than one third of variance explained, suggests that this relation is muted for continental glaciers, which are buffered by coastal mountains and long overland fetches.

2.5.3 Adjustment of summer balance

For the maritime glaciers (South Cascade and Wolverine), warm-season (April–Sept) SLP and SST explain substantially less variance in the summer balance records. South Cascade Glacier is more closely linked with SLP than SST, with two predictor patterns explaining $28\%+7\%$ of variance for SLP, compared with only $15\%+6\%$ for SST. (The second modes may not in fact be significant, but are reported here for the sake of consistency.) For Wolverine

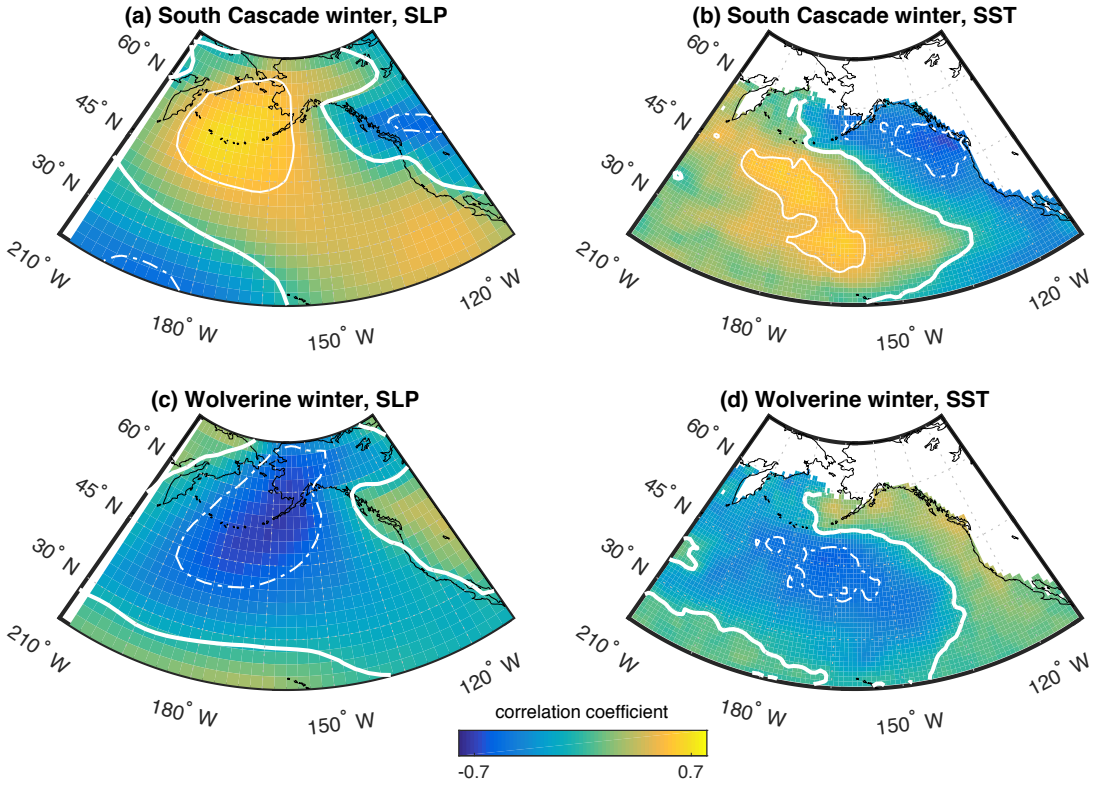

Figure 2.4: Comparison of leading winter correlation patterns for South Cascade (a, b) and Wolverine (c, d) Glaciers using SLP (a, c) and SST (b, d) as predictors. Contour interval is 0.5, with bold indicating the zero contour and dashed contours indicating negative correlations. Note the similar structure but opposite polarity between patterns corresponding to the two glaciers.

Glacier, both predictors explain roughly the same total variance, with $21\% + 8\%$ for SLP, and $24\% + 4\%$ for SST. The variance explained by summer SLP for Gulkana Glacier ($22\% + 9\%$) is similar to that of the maritime glaciers, but it is notable in that it makes Gulkana the only glacier with comparable amounts of dynamically induced variability in summer and winter mass balance. This is broadly consistent with the rule of thumb that continental glaciers, being further removed from the ocean's moisture-laden storms and moderating effect on temperature, are comparatively more sensitive to melt-season climate (e.g., Medwedeff and

Roe 2016). It is perhaps not surprising that summer SSTs are a weak predictor for Gulkana Glacier's summer balance, explaining only 15% of total variance.

By far the strongest summer SST relationship is the leading mode for Wolverine Glacier, explaining 24% of variance. The correlation map (Fig. 2.5a) shows what may be an intuitive result for this glacier situated closest to the Pacific: near-shore SST and summer balance are anti-correlated, i.e., years of anomalously warm ocean surface are associated with more summer melt. Correlation maps for the leading summer SLP patterns (associated with $\sim$ 20% of variance for each glacier) all show moderately positive correlation with SLP to the south of each glacier (Fig. 2.5b–d). However, the links between summer climate anomalies and summer balance are weaker than for winter, consistent with generally less vigorous circulation in summer.

2.5.4 Adjusted trends

Our analyses show that a substantial amount ($\sim$30–60%) of variance in mass balance is explained by variability in SLP and SST. We can now return to one of our main motivating questions: what is the role of natural variability in the observed trends in mass-balance records? It is important to note that, although the correlation map $\mathbf{W}$ (Eq. 1) is generated from detrended data, the component of variance removed from the predictand may itself contain a linear trend. This is because the index $\mathbf{t}$ and the regression coefficients β and $\mathbf{P}$ contain data that have been standardized but not detrended (see Eq. 3–5). Thus low-frequency variance that might be projecting onto the linear trend can in principle be removed from the mass-balance records – indeed this is one motivation for pursuing dynamical adjustment. Though all of the dynamically adjusted mass-balance records necessarily have reduced overall variance, removing this low-frequency variance may yield residual time series ($\mathbf{Y}_{adj}$ in Eq. 6) that have enhanced or reduced trends, affecting the interpretations of observed trends and their causes.

Since both the noise and the trend are affected by the dynamical adjustment, we revisit the t-statistic (Eq. 8) as a way to compare the raw and adjusted mass-balance records. Recall

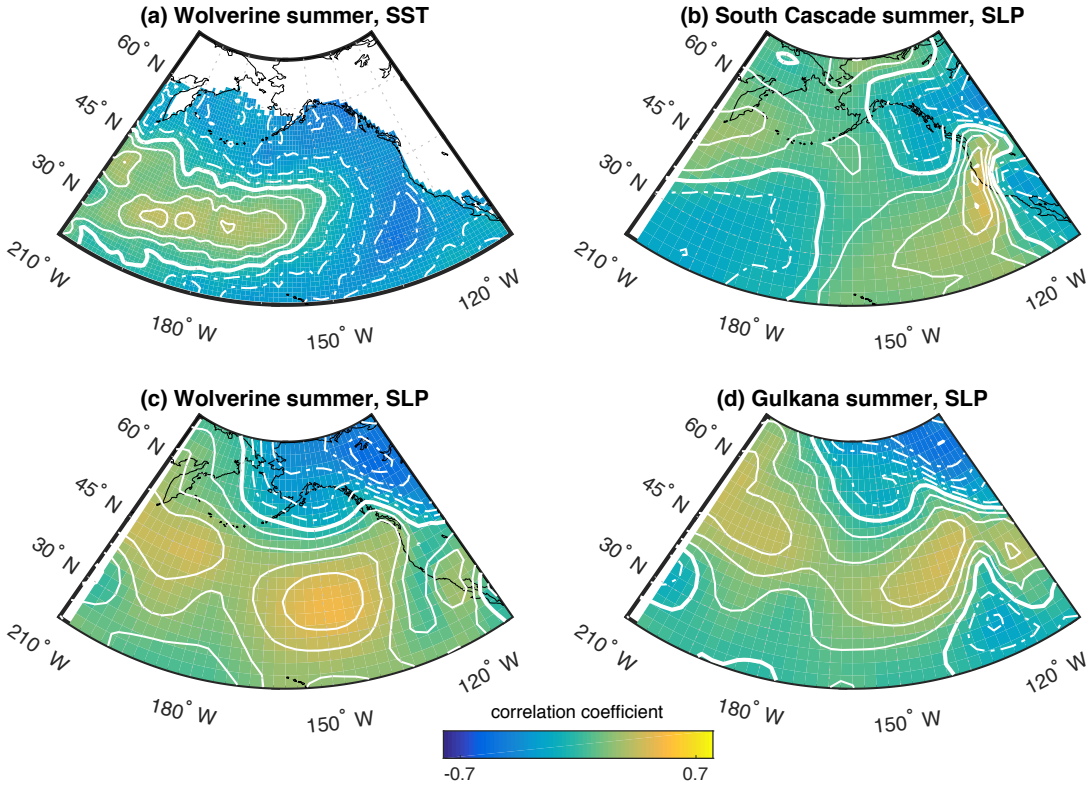

Figure 2.5: Selected correlation patterns for summer mass balance. Contour interval is 0.1, with bold indicating the zero contour and dashed contours indicating negative correlations. (a) Wolverine Glacier's summer balance is negatively correlated with SST near the western coast of North America. (b–d) For all three glaciers, summer balance is positively correlated with SLP in regions to the south.

that the significance of a trend in a given number of independent observations depends on the signal-to-noise ratio, $\Delta B/\sigma$. This ratio is a useful metric for comparing the relative significance of trends, and for significance at the 5% level, our records requires $\Delta B/\sigma > 0.98$ for $N = 53$ years (South Cascade) and $\Delta B/\sigma > 1.00$ for $N = 50$ years (Wolverine and Gulkana). Table 2 shows $\Delta B/\sigma$ for all raw records and adjustments, and we note that trends in the South Cascade and Wolverine winter records are not significant in raw or adjusted form. Gulkana's adjusted winter balance trend barely breaches the threshold for significance

‘

Table 2.2: Signal to noise ratios ($\Delta B/\sigma$) for raw mass-balance records and adjustments using SLP and SST as predictors. Bold values indicate statistical significance at 95% based on a 2-tailed Student's t-test.

	South Cascade			*Wolverine*			*Gulkana*		
	Raw	SLP	SST	Raw	SLP	SST	Raw	SLP	SST
Winter	0.13	0.68	0.17	0.15	0.70	0.29	0.47	**1.04**	0.88
Summer	**1.48**	**1.58**	**2.44**	**1.66**	**2.15**	**1.92**	**1.67**	**2.45**	**2.35**

at 95% when using SLP as a predictor, but just short of it using SST. However, all three of the summer records have significant trends in raw form and improved signal-to-noise ratios after adjustment. In other words, the trends in summer mass balance are not associated with low-frequency circulation variability, and are more consistent with an external forcing.

2.6 Sensitivity

2.6.1 Methods for testing trend significance

Several factors should be borne in mind when interpreting these results. First of all, recall that the threshold for trend significance is dependent on the number of degrees of freedom (ν) estimated from the timeseries' autocorrelation (Eq. 9). Given that the autocorrelation functions are rather noisy for these short timeseries, it is worth considering significance estimates for the case $\nu < N$, to account for the possibility that sampling effects have obscured weak persistence. While this does increase the critical signal-to-noise ratio for significance, we find that our conclusions are robust to different choices of ν. Consider a decorrelation time twice the maximum allowed for our initial assumption that $\nu = N$, which then cuts ν in half. If $\nu = 25(26)$, the critical $\Delta B/\sigma$ for 95% confidence required by the t-test is 1.49(1.45) for a timeseries of 50(53) years. Even in this case, the interpretation would remain that all summer trends are significant at 95%, both before and after dynamical

adjustment (see Table 2).

As an alternative to the t-test, we also applied the method of phase randomization to test for trend significance (see e.g., Theiler et al. 1992; Vafeiadis et al. 2008). In this framework, a random phase rotation is applied to each Fourier frequency component of the detrended timeseries. After transformation back into the time domain, this yields a surrogate timeseries where the spectrum and autocorrelation structure have been preserved. A large ensemble (10^4–10^5) of these surrogate datasets can then provide a distribution of trends that arise merely from under-sampling the spectrum of the original timeseries. The observed trends for raw and adjusted summer balance fell well beyond the central 95% of the distribution. However, the method of phase randomization has some caveats for short timeseries, namely that the probability distributions of surrogate data are not well-preserved. Thus, while consistent with the other trend tests, this method may not stand on its own in this application.

2.6.2 Choice of predictor variable

Additionally, we find that the trend changes after adjustments vary with the choice of predictor (however, the significance at 95% changes only for Gulkana Glacier's winter balance, where both trends are near the threshold). While SLP and SST are dynamically linked and yield highly correlated indices (see section 4.2), their trend adjustments are not consistent. For South Cascade and Wolverine Glaciers, SLP and SST adjust the mass-balance trends in opposite directions, in both the summer and winter cases (Fig. 2.6). This is consistent with the overall result that circulation variability has not contributed substantially to the trends over the period of observation.

In addition to the choice between SLP and SST, we also assessed the sensitivity to the choice of data source for the same climate variable. The Met Office HadSLP2 dataset is an alternative SLP dataset, providing monthly means on a $5^\circ \times 5^\circ$ grid (Allan 2006). Results using this predictor are qualitatively equivalent to those using NCEP/NCAR reanalysis: the correlation patterns and respective amounts of variance explained are very similar, and the

trend adjustments are also minimal.

2.6.3 Observational error

Both predictor and predictand datasets contain some degree of observational and sampling error. The datasets for the Alaskan glaciers have been reanalyzed, as described by Van Beusekom et al. (2010) and in the supplementary material of O'Neel et al. (2014). Work by the USGS addresses both systemic and isolated errors in reported balance data, and ongoing efforts include calibrating field measurements with geodetic methods using available DEMs.

What are the effects of remaining measurement error on dynamical adjustment? Since PLS regression operates only on anomalies, it is insensitive to systemic biases in mass-balance data (unlike, for example, estimates of cumulative balance). Random errors, however, may confound correlation maps and trend estimates. But while a large error in one year's reported mass balance certainly could bias an initial linear trend estimate, it is unlikely to be erroneously *removed* by dynamical adjustment, and thus the *changes* to trends (or lack thereof) should be relatively insensitive to this form of uncertainty. Furthermore, the cases in which the statistics are shored up by a physical interpretation, as in the relationship between South Cascade, Wolverine, and the Aleutian Low (section 4.2), suggest that observational or sampling errors in the mass balance or predictor datasets are not necessarily a barrier for identifying relevant dynamical patterns.

2.6.4 Conventional mass balance vs. reference surface mass balance

While we have focused on partitioning the effects of internal climate variability and external forcing on mass balance changes, it is also important to consider the effect that a changing glacier geometry can have on mass balance measurements. Terminus changes constitute a negative feedback by changing the ablation area, while thickness changes can counteract this by lowering or raising surface elevation across the glacier. These processes have motivated analyses of reference-surface mass balances, which are calibrated to a constant glacier hypsometry (e.g., Elsberg et al. 2001; Huss et al. 2012). Reference-surface values were

available for Wolverine and Gulkana glaciers through 2009 (Van Beusekom et al. 2010), and we found that dynamically adjusting these data produced qualitatively similar results to those using conventional balance. Trend estimates are slightly different for reference surface balances, but summer trends retained significance, suggesting that they are not principally a geometrical effect.

2.6.5 Length of timeseries

Finally, the length of the predictand timeseries has some interesting implications. We focus on the USGS benchmark glaciers in part because they offer long uninterrupted records, and thus offer more information to be compared with the other climate datasets. However, the trend biases caused by the low-frequency components of natural variability can be more dramatic in shorter records. This is a familiar challenge associated with limited sampling, but it means that the skill of dynamical adjustment in terms of removing dynamically-induced trends is sensitive to record length. As an illustrative example, we consider separate adjustments for two halves of the South Cascade winter record (Fig. 2.7). In the raw data, the periods from 1959–1984 and 1985–2011 have markedly different trends, a feature that is lost when a linear trend is estimated for the whole record. The separate adjustments yield more dramatic trend changes than with the entire record. For example, winter balance from 1985–2011 has a strong positive trend ($\Delta B/\sigma = 1.35$; significant at 90% but not at 95%), but this is nearly completely removed by dynamical adjustment, indicating that it is associated with circulation variability. Of course, the half-and-half split is arbitrary, and we do not attempt here to define an optimal timeseries length for adjustment. However, given the preponderance of one- to two-decade mass-balance records for glaciers around the world (Medwedeff and Roe 2016), these may be important considerations for future applications of dynamical adjustment.

2.7 Summary and conclusions

We have applied PLS-based dynamical adjustment to seasonal glacier mass balance and have found this to be a useful method for analyzing dynamically-induced variability, explaining from about one-third of summer variance to well over half of winter variance in these records. Building on its previous applications to regional averages or fields (e.g., snowpack, SAT, Hurricane activity), we find that the method of dynamical adjustment is also capable of identifying relationships between large-scale circulation and more localized processes (i.e., accumulation and ablation on individual glaciers).

For winter balance, dynamical adjustment shows that a large portion of accumulation variability is explained by North Pacific variability, and is captured in comparable proportions by both SLP and SST reanalysis fields. The effect is strongest for the maritime glaciers (South Cascade and Wolverine), explaining over half of the variance. The adjustments also demonstrated that the primary source of dynamically-induced variability for these glaciers is variability in the Aleutian Low. For summer balance, dynamical adjustment using SLP as a predictor explained approximately one third of variance for all glaciers, but substantially less when using SST. The variability left unexplained by dynamical adjustment is likely the aggregate of many factors, including the nuances of regional climate, mountain meteorology, and the noise and sampling effects inherent in the climate and mass-balance datasets. Further analysis using meteorological data and/or regional climate models could provide insight into such processes, as well as the limits of the relationships that can be resolved with dynamical adjustment.

Dynamical adjustment also reveals whether trends in time series are related to circulation variability. We found that, despite the large degree of circulation-related variability in seasonal mass balance, the dynamical adjustment did not change the trends substantially. However, by accounting for the possibility of a dynamically-induced bias, we have a refined view of mass-balance change for these glaciers. The negative trends in summer balance, which are significant in the raw data, persist with a greater signal-to-noise ratio

when dynamically-induced variability is removed. This supports an interpretation that the trends are externally forced and associated with anthropogenic greenhouse warming. However, no statistically significant trends exist in adjusted winter balance (with the exception of Gulkana's winter balance, but its significance is not robust to the choice of predictor). This strengthens the interpretation that anthropogenic trends in accumulation over the glaciers have yet to emerge.

The absence of winter trends is common to many winter mass-balance records (Medwedeff and Roe 2016), and may simply reflect the different temperature sensitivities of accumulation and ablation. In theory, warming winters would eventually cause a decline in accumulation as the average freezing level climbs, though in dry, cold settings the initial effect may instead be increased precipitation due to a greater atmospheric moisture capacity. Indeed, winter warming and elevated freezing levels have been observed in Northwestern North America, but the actual effect on winter balance varies depending on the hypsometric profile of the glacier and the baseline climatology (Arendt et al. 2009). It follows that the time of emergence – and even the sign – of winter balance trends under warming may vary considerably by region and by glacier. Since such changes would inevitably exist amid natural variability, dynamical adjustment could be a useful method for diagnosing any new trends that emerge.

The general question of the relative importance of external forcing and internal variability in observed trends is an important one. Several studies have addressed it for glacier mass balance in different ways (e.g., Huss et al. 2010; Marzeion et al. 2014). Huss et al. (2010) concluded from running-mean correlations that up to half of the 21st century declines in mass balance in the Swiss Alps could be accounted for by the Atlantic Multidecadal Oscillation. Dynamical adjustment would provide an alternative analysis method that could address the same question, and would supply the associated correlation patterns that could be evaluated for dynamical mechanisms. Marzeion et al. (2014) used ensembles of global climate models to estimate the magnitude of natural mass-balance variability relative to simulated trends, aggregated into different regions. Dynamical adjustment would provide a complementary analysis here, too.

Finally, it is also important to understand how much of a model's projection of a future climate trajectory may be attributable to internal variability (e.g., Deser et al. 2012). By identifying the variability associated with circulation patterns in the modern climate, dynamical adjustment could again be used to constrain the externally forced portion of the climate projection. Dynamical adjustment is thus a versatile tool, whose wider application to a variety of glacier mass-balance settings and problems may prove useful.

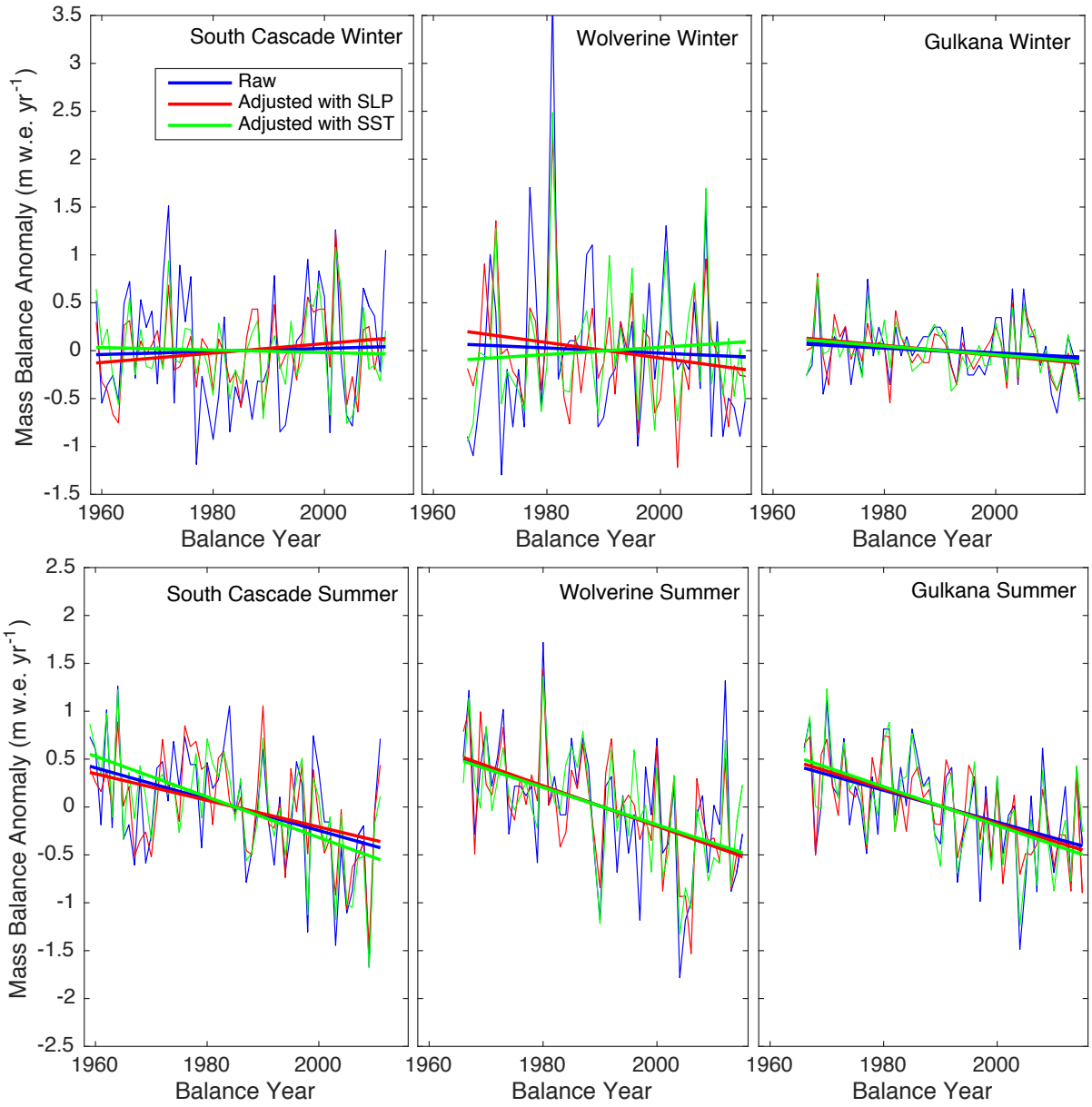

Figure 2.6: Raw and adjusted data for all glaciers, with linear trends plotted in bold. South Cascade and Wolverine Glaciers demonstrate that the change in trends is sensitive to the choice of predictor. Also note that for both predictors, the adjustment shifts the trends in South Cascade and Wolverine winter balance in opposite directions. This is a direct result of their opposing correlation structures (section 4.2). Any trends in the predictors in the highly (anti-)correlated areas yield opposing trends in the associated indices.

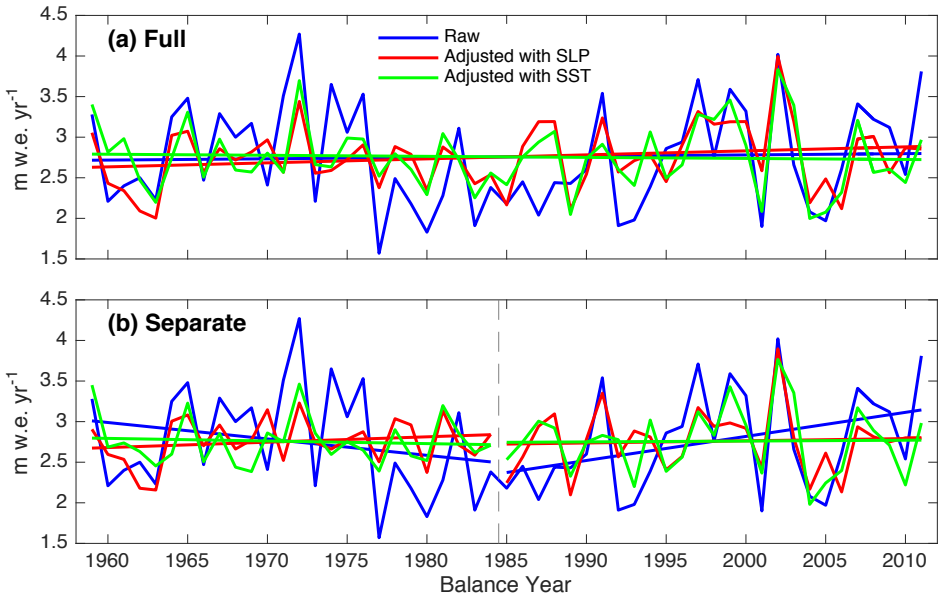

Figure 2.7: Dynamical adjustment and trend estimates are sensitive to the length of the record being analyzed. Timeseries and linear trend estimates are shown for each period for raw and adjusted data. (a) Adjustments to South Cascade winter balance for the whole record. (b) Adjustments performed separately for the periods 1959–1984 and 1985–2011 (separated by dashed line). The opposing trends are almost completely removed by dynamical adjustment, indicating that they are associated with circulation variability.

ACKNOWLEDGMENTS

We gratefully acknowledge the USGS Climate and Land Use Change program for maintaining the benchmark glacier-monitoring program. We also thank Shad O'Neel for helpful discussion regarding mass-balance measurements and uncertainty. Finally, we thank editor Peter Huybers and three anonymous reviewers for comments that greatly improved the manuscript. J.E.C was supported by the National Science Foundation Graduate Research Fellowship Program.

BIBLIOGRAPHY

Abdi, H. (2010). Partial least squares regression and projection on latent structure regression (PLS Regression). *Wiley Interdisciplinary Reviews: Computational Statistics*, 2(1):97–106.

Allan, R. and Ansell, T. (2006). A new globally complete monthly historical gridded mean sea level pressure dataset (HadSLP2): 1850-2004. *Journal of Climate*, 19(22):5816–5842.

Arendt, A., Walsh, J., and Harrison, W. (2009). Changes of glaciers and climate in northwestern North America during the late twentieth century. *Journal of Climate*, 22(15):4117–4134.

Bartlett, M. S. (1946). On the theoretical specification and sampling properties of autocorrelated time-series. *Supplement to the Journal of the Royal Statistical Society*, 8(1):27–41.

Bidlake, W. R., Josberger, E. G., and Savoca, M. E. (2010). Modeled and measured glacier change and related glaciological, hydrological, and meteorological conditions at South Cascade Glacier, Washington, balance and water years 2006 and 2007. Technical report, U. S. Geological Survey.

Bitz, C. and Battisti, D. (1999). Interannual to Decadal Variability in Climate and the Glacier Mass Balance in Washington, Western Canada, and Alaska. *Journal of Climate*, 12(11):3181–3196.

Bretherton, C. S., Smith, C., and Wallace, J. M. (1992). An intercomparison of methods for finding coupled patterns in climate data. *Journal of climate*, 5(6):541–560.

Casola, J. H., Cuo, L., Livneh, B., Lettenmaier, D. P., Stoelinga, M. T., Mote, P. W., and Wallace, J. M. (2009). Assessing the Impacts of Global Warming on Snowpack in the Washington Cascades. *Journal of Climate*, 22(10):2758–2772.

Deser, C., Alexander, M. A., Xie, S.-P., and Phillips, A. S. (2010). Sea surface temperature variability: Patterns and mechanisms. *Annual Review of Marine Science*, 2:115–143.

Deser, C., Phillips, A., Bourdette, V., and Teng, H. (2012). Uncertainty in climate change projections: the role of internal variability. *Climate Dynamics*, 38(3-4):527–546.

Deser, C. and Phillips, A. S. (2009). Atmospheric circulation trends, 1950-2000: The relative roles of sea surface temperature forcing and direct atmospheric radiative forcing. *Journal of Climate*, 22(2):396–413.

Elsberg, D., Harrison, W. D., Echelmeyer, K. A., and Krimmel, R. M. (2001). Quantifying the effects of climate and surface change on glacier mass balance. *Journal of Glaciology*, 47(159):649–658.

Hannachi, A., Jolliffe, I., and Stephenson, D. (2007). Empirical orthogonal functions and related techniques in atmospheric science: A review. *International Journal of Climatology*, 27(9):1119–1152.

Hasselmann, K. (1976). Stochastic climate models part 1. Theory. *Tellus*, 28(6):473–485.

Hurrell, J. W. (1996). Influence of variations in extratropical wintertime teleconnections on Northern Hemisphere temperature. *Geophysical Research Letters*, 23(6):665–668.

Huss, M., Hock, R., Bauder, A., and Funk, M. (2010). 100-year mass changes in the Swiss Alps linked to the Atlantic Multidecadal Oscillation. *Geophysical Research Letters*, 37(10).

Huss, M., Hock, R., Bauder, A., and Funk, M. (2012). Conventional versus reference-surface mass balance. *Journal of Glaciology*, 58(208):278–286.

IPCC (2013). *Climate change 2013: The Physical Science Basis. Working Group I contribution to the Fifth assessment report of the Intergovernmental Panel on Climate Change*. Stocker, T.F., D. Qin, G.-K. Plattner, M. Tignor, S.K. Allen, J. Boschung, A. Nauels,

Y. Xia, V. Bex and P.M. Midgley, Eds. Cambridge University Press, Cambridge, United Kingdom and New York, NY, USA, 1535 pp.

Johnstone, J. A. and Mantua, N. J. (2014). Atmospheric controls on northeast Pacific temperature variability and change, 1900–2012. *Proceedings of the National Academy of Sciences*, 111(40):14360–14365.

Kalnay, E., Kanamitsu, M., Kistler, R., Collins, W., Deaven, D., Gandin, L., Iredell, M., Saha, S., White, G., Woollen, J., et al. (1996). The NCEP/NCAR 40-year reanalysis project. *Bulletin of the American meteorological Society*, 77(3):437–471.

Leith, C. (1973). The standard error of time-average estimates of climatic means. *Journal of Applied Meteorology*, 12(6):1066–1069.

Mantua, N. J., Hare, S. R., Zhang, Y., Wallace, J. M., and Francis, R. C. (1997). A Pacific interdecadal climate oscillation with impacts on salmon production. *Bulletin of the american Meteorological Society*, 78(6):1069–1079.

Marzeion, B., Cogley, J. G., Richter, K., and Parkes, D. (2014). Attribution of global glacier mass loss to anthropogenic and natural causes. *Science*, 345(6199):919–921.

Medwedeff, W. and Roe, G. H. (2016). A statistical analysis of global glacier mass balance observations. *In press*.

Mote, P. W., Hamlet, A. F., Clark, M. P., and Lettenmaier, D. P. (2005). Declining mountain snowpack in western North America. *Bulletin of the American meteorological Society*, 86(1):39–49.

Oerlemans, J. (2001). *Glaciers and climate change*. CRC Press.

O'Neel, S., Hood, E., Arendt, A., and Sass, L. (2014). Assessing streamflow sensitivity to variations in glacier mass balance. *Climatic change*, 123(2):329–341.

O'Neel, S., Sass, L., McNeil, C. J., and McGrath, D. (2016). USGS Benchmark Glacier Mass Dataset. Technical report, USGS Alaska Science Center, Anchorage, AK.

Rasmussen, L. and Conway, H. (2004). Climate and glacier variability in western North America. *Journal of Climate*, 17(9):1804–1815.

Rayner, N., Parker, D., Folland, C., Horton, E., Alexander, L., and Rowell, D. (2003). The global sea-ice and sea surface temperature (HadISST) data sets. *J. Geophys. Res.*

Roe, G. H. (2011). What do glaciers tell us about climate variability and climate change? *Journal of Glaciology*, 57(203):567–578.

Roe, G. H. and Baker, M. B. (2014). Glacier response to climate perturbations: an accurate linear geometric model. *Journal of Glaciology*, 60(222):670–684.

Smoliak, B. V., Wallace, J. M., Lin, P., and Fu, Q. (2015). Dynamical Adjustment of the Northern Hemisphere Surface Air Temperature Field: Methodology and Application to Observations. *Journal of Climate*, 28(4):1613–1629.

Smoliak, B. V., Wallace, J. M., Stoelinga, M. T., and Mitchell, T. P. (2010). Application of partial least squares regression to the diagnosis of year-to-year variations in Pacific Northwest snowpack and Atlantic hurricanes. *Geophysical Research Letters*, 37(3).

Stoelinga, M. T., Albright, M. D., and Mass, C. F. (2010). A new look at snowpack trends in the Cascade Mountains. *Journal of Climate*, 23(10):2473–2491.

Theiler, J., Eubank, S., Longtin, A., Galdrikian, B., and Farmer, J. D. (1992). Testing for nonlinearity in time series: the method of surrogate data. *Physica D: Nonlinear Phenomena*, 58(1-4):77–94.

Thompson, D. W., Wallace, J. M., and Hegerl, G. C. (2000). Annular modes in the extratropical circulation. Part II: Trends. *Journal of Climate*, 13(5):1018–1036.

Thompson, D. W., Wallace, J. M., Jones, P. D., and Kennedy, J. J. (2009). Identifying signatures of natural climate variability in time series of global-mean surface temperature: Methodology and insights. *Journal of Climate*, 22(22):6120–6141.

Vafeiadis, T., Bora-Senta, E., and Kugiumtzis, D. (2008). Evaluation of linear trend tests using resampling techniques. *Communications in Statistics?Simulation and Computation®*, 37(5):907–923.

Van Beusekom, A. E., O'Neel, S. R., March, R. S., Sass, L. C., and Cox, L. H. (2010). Re-analysis of Alaskan benchmark glacier mass-balance data using the index method. *US Geological Survey Scientific Investigations Report*, 5247:16.

Von Storch, H. and Zwiers, F. (1999). Statistical analysis in climate research.

Wallace, J. M., Deser, C., Smoliak, B. V., and Phillips, A. S. (2015). *Attribution of climate change in the presence of internal variability*, volume 6. World Scientific Series on Asia–Pacific Weather and Climate.

Wallace, J. M., Fu, Q., Smoliak, B. V., Lin, P., and Johanson, C. M. (2012). Simulated versus observed patterns of warming over the extratropical Northern Hemisphere continents during the cold season. *Proceedings of the National Academy of Sciences*, 109(36):14337–14342.

Wallace, J. M. and Hobbs, P. V. (2006). *Atmospheric science: an introductory survey*, volume 92. Academic press.

Wallace, J. M., Zhang, Y., and Renwick, J. A. (1995). Dynamic contribution to hemispheric mean temperature trends. *Science*, 270(5237):780.

Walters, R. A. and Meier, M. F. (1989). Variability of glacier mass balances in western North America. *Aspects of climate variability in the Pacific and the Western Americas*, pages 365–374.

WGMS (2012). *Fluctuations of Glaciers 2005-2010 (Vol. X).* Zemp, M., Frey, H., Gner-Roer, I., Nussbaumer, S.U., Hoelzle, M., Paul, F. and W. Haeberli, Eds. ICSU(WDS)/IUGG(IACS)/UNEP/UNESCO/WMO, World Glacier Monitoring Service, Zurich, Switzerland.

WGMS (2013). *Glacier Mass Balance Bulletin No. 12 (2010–2011).* Zemp, M., Nussbaumer, S. U., Naegeli, K., Gner-Roer, I., Paul, F., Hoelzle, M., and W. Haeberli, Eds. ICSU(WDS)/IUGG(IACS)/UNEP/UNESCO/WMO, World Glacier Monitoring Service, Zurich, Switzerland, 106 pp.

Chapter 3

COMMITTED RETREAT: CONTROLS ON GLACIER DISEQUILIBRIUM IN A WARMING CLIMATE

Chapter 3, in full, is a reprint of "Committed retreat: controls on glacier disequilibrium in a warming climate" authored by J Christian, M Koutnik, and G Roe, as it appears in *Journal of Glaciology*, 2018. The dissertation author was the primary investigator and author of this paper.

3.1 Abstract

The widespread retreat of mountain glaciers is a striking emblem of recent climate change. Yet mass-balance observations indicate that many glaciers are out of equilibrium with current climate, meaning that observed retreats do not show the full response to warming. This is a fundamental consequence of glacier dynamics: mountain glaciers typically have multidecadal response timescales, and so their response lags centennial-scale climate trends. A substantial difference between transient and equilibrium glacier length persists throughout the warming period; we refer to this length difference as "disequilibrium". Forcing idealized glacier geometries with gradual warming shows that the glacier response timescale fundamentally governs the evolution of disequilibrium. Comparing a hierarchy of different glacier models suggests that accurate estimates of ice thickness and climatology, which control the timescale, are more important than higher-order ice dynamics for capturing disequilibrium. Current glacier disequilibrium has previously been estimated for a selection of individual glaciers; our idealized modeling shows that sustained disequilibrium is a fundamental response of glacier dynamics, and is robust across a range of glacier geometries. This implies that many mountain glaciers are committed to additional, kilometer-scale retreats, even without further

warming. Disequilibrium must also be addressed when calibrating glacier models used for climate reconstructions and projections of retreat in response to future warming.

3.2 Introduction

Many natural phenomena, including thermodynamic, geophysical, and biological systems, can be described as reservoirs with inputs (e.g., mass, energy, information) that produce a related output. The behavior of these systems depends fundamentally on the extent to which they integrate their inputs. This is often characterized by a response time, or "memory", that is related to the capacity of the reservoir and the characteristic input and output rates. This timescale determines how quickly the system can respond to a perturbation.

When a gradual forcing is applied, an "equilibrium response" can be defined as the state at which the system would be in equilibrium with the forcing at any given instant. This state evolves with the forcing. However, because the system has a memory of its previous states, the actual system state lags the equilibrium response by an amount that depends on its response time. This basic concept has major implications in the context of a changing climate system, which has subcomponents that respond on a wide range of timescales. One of the most striking examples is the rate of surface warming in response to anthropogenic CO_2 emissions. Transient warming lags the equilibrium response due to the vast thermal inertia of the ocean (e.g., Wigley and Schlesinger, 1985). In turn, warming surface temperatures constitute a gradual forcing for other systems with long response times: lagged responses have also been investigated for sea-level rise (e.g., Meehl et al., 2005) and forest die back (Jones et al., 2009), among many other environmental responses to warming.

In this paper, we investigate these concepts for the case of the retreat of mountain glaciers in a warming climate. Previous studies have noted that many glaciers are out of equilibrium with the modern climate and thus committed to additional change (e.g., Bahr et al., 2009; Mernild et al., 2013; Marzeion et al., 2017, 2018). Indeed, standard mass-balance measurements report surface mass balance over the evolving glacier area (e.g., WGMS, 2017), and so the widely noted negative mass balance of most of the world's glaciers (e.g., IPCC, 2013;

Medwedeff and Roe, 2017) necessarily implies they are out of equilibrium. A number of studies have gone a step further, calculating glacier extents that would be in equilibrium with recent climate observations. Such studies have targeted South Cascade Glacier, Washington (Rasmussen and Conway, 2001), Haig Glacier, Canada (e.g., Adhikari and Marshall, 2013), Morteratsch Glacier, Switzerland (Zekollari et al., 2014; Zekollari and Huybrechts, 2015), Great Aletsch Glacier, Switzerland (Jouvet et al., 2011), as well as collections of glaciers in the Alps (Lüthi et al., 2010; Carturan et al., 2013) and Bhutan (Rupper et al., 2012). These studies have highlighted a striking discrepancy between current and equilibrium glacier geometries in specific settings; here, we explore the fundamental controls on this response. We first illustrate the basic behavior of glacier retreat with a simple model, and introduce metrics for characterizing the discrepancy between the evolving transient and equilibrium length responses. We then present experiments in which we use several additional models of varying complexity to evaluate how ice dynamics, glacier geometry, and climate variability control the transient glacier response to gradual warming.

3.2.1 Illustrating disequilibrium with a simple glacier model

A mountain glacier can be conceptualized as an open system with memory: it integrates mass accumulated across its surface into a reservoir of ice, and this reservoir adjusts its extent to maintain a balance between input in the accumulation zone and output in the ablation zone. The simplest representation of this behavior is a first-order differential equation for fluctuations of length, L', around a steady state, $\bar{L}$, caused by mass-balance perturbations, b':

$$\frac{dL'}{dt} + \frac{L'}{\tau} = \beta b', \tag{3.1}$$

where $\beta = \bar{L}/H$. H is a characteristic ice thickness and τ is the glacier response timescale, given by

$$\tau = \frac{H}{b_t}, \tag{3.2}$$

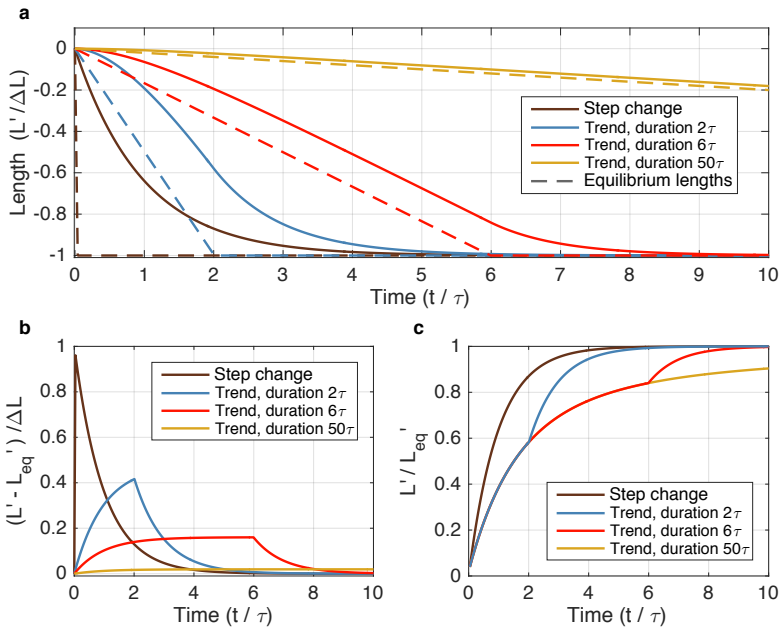

Figure 3.1: The response of a simple glacier model to a step function and sustained trends in climate forcing. (a) Normalized length response to a climate forcing. Solid lines show the transient response, dashed lines show the instantaneous equilibrium length. The climate forcing is applied as a step function (black), and as a trend over periods of 2τ (blue), 6τ (red), and 50τ (gold), where τ is the glacier response timescale. (b) Degree of disequilibrium in normalized length. (c) Fractional equilibration, which proceeds identically for all climate trends until the forcing stops.

where b_t is the (negative) annual mass balance rate at the terminus. β is a geometric parameter that scales the length responses to mass balance perturbations; as we will see, it is related to the glacier's length sensitivity. In this model, the glacier's length is the only degree of freedom, so Eqn (3.1) is a mass-conservation statement equating ice-volume change to imbalance between input and output rates (e.g., Jóhannesson et al., 1989). The basic model represented by Eqns (3.1) and (3.2) has been widely used to explore glacier responses to climate perturbations (e.g., Jóhannesson et al., 1989; Harrison et al., 2001; Oerlemans, 2001, 2007; Roe and O'neal, 2009). While various formulations for the response timescale and glacier-sensitivity parameters have been proposed, members of this family of models all resolve the same basic behavior. For an instantaneous mass-balance change Δb at $t = 0$, the glacier asymptotically approaches a new geometry described by $\bar{L} + \Delta L$, where accumulation and ablation are again balanced. The solution of Eqn (3.1) for this case is

$$L'(t) = \Delta L(1 - e^{-t/\tau}), \tag{3.3}$$

where $\Delta L = \tau\beta\Delta b$.

Another important analytical solution to Eqn (3.1) is the case of a linear trend in mass balance ($\dot{b} = db/dt$), starting at $t = 0$:

$$L'(t) = \tau\beta\dot{b}[t - \tau(1 - e^{-t/\tau})], \tag{3.4}$$

For $t \gg \tau$, Eqn (3.4) approaches $L'(t) = \tau\beta\dot{b}(t - \tau)$. Thus, at long timescales, there is a lag of τ behind the length at which the glacier would remain in equilibrium with the climate as it changes. We refer to this evolving length as the glacier's equilibrium response, defined by

$$L'(t) = \tau\beta\dot{b}t. \tag{3.5}$$

Figure 3.1a shows the responses of a glacier with an arbitrary timescale τ to mass-balance changes imposed instantaneously or as linear trends. Results are plotted as normalized by τ in time and $|L|$ in length. Solid lines show the transient length changes and dashed lines show the equilibrium responses (Eqn 3.5). Four rates of forcing are shown: the same total

mass balance change Δb is applied instantaneously (black), or gradually applied over periods of 2τ (blue), 6τ (red), and 50τ (gold).

We will refer to the difference between transient and equilibrium responses (L' and L'_{eq}; solid and dashed lines) at any given time as the "disequilibrium". Figure 3.1b shows this metric for each forcing, again normalized by $|\Delta L|$. For mass-balance trends, the degree of disequilibrium approaches a constant (see the case of the 6τ trend in Fig. 3.1b), which depends on the rate of forcing. The response to a slow trend (50τ, gold curves in Fig. 3.1) approaches a limiting case in which the glacier responds quasi-statically, and its degree of disequilibrium is negligible.

During a warming period, the degree of disequilibrium is a measure of a glacier's overextension, and thus the amount of additional retreat that is already guaranteed even with no further climate change. Climate researchers have introduced the concept of "committed warming" as a quantity describing the warming that will still occur even if anthropogenic forcing stabilized (e.g., Hansen et al., 1985; Wigley and Schlesinger, 1985; Wigley, 2005); similar metrics exist for committed sea-level rise and ice-sheet loss (e.g., Meehl et al., 2005; Price et al., 2011; Goldberg et al., 2015). The reference state used to define the committed change varies in the literature. In this paper, we use the term "committed retreat" to refer to the additional retreat that must occur for the glacier to reach equilibrium should warming stop abruptly at a given time. In this sense, its magnitude is equivalent to the degree of disequilibrium, though committed retreat also has a time-dependence: once the forcing stops, the realization of committed retreat is still governed by τ.

The ratio L'/L'_{eq} is another way to express a glacier's lagged response to a climate trend. At any instant in time, this is the fraction of the total (equilibrium) adjustment that the glacier has attained for the amount of climate change that has already occurred. We will refer to this as"fractional equilibration". It is a useful measure of the committed retreat in the context of the changes that have already been observed. For example, a fractional equilibration of 33% would mean that twice as much retreat as has already occurred is committed to happen in the future, if the climate stopped changing at that moment. Figure 3.1c shows

the evolution of L'/L'_{eq}. Note that the fractional equilibration progresses identically for all three rates of gradual forcing (blue, red, and gold curves) until the forcing stops.

Figure 3.1 highlights some very general behavior discussed in the previous section: systems with memory produce a lagged response when a gradual forcing is applied, and their degree of disequilibrium can be significant when the duration of the forcing is similar to the response timescale. Most mountain glaciers have response times between $\sim$ 10 and 100 years (e.g., Jóhannesson et al., 1989; Oerlemans, 2001)—similar in order to the duration of anthropogenic climate forcing to date ($\sim$ 100 years; IPCC, 2013). The results from this simple model show that neither the instantaneous nor the quasi-static limits realistically describe recent glacier changes, nor those that can be expected in the near future. However, applying these concepts to observations or projections requires using models that capture the relevant dynamics and can incorporate glacier and climate observations. To evaluate the important factors for understanding glacier disequilibrium in today's climate, we present several experiments using idealized glacier geometries forced with gradual warming trends. In the next section, we describe the four models used, and the idealized glacier settings. We then compare the hierarchy of models to evaluate the importance of ice dynamics. Next, we investigate the role of glacier geometry by assessing response times across a range of geometries, and by considering uncertainty in ice thickness. Finally, we consider several issues that climate variability can bring to estimating or modeling glacier disequilibrium.

3.3 Methods

3.3.1 Linear models

The simplest model we consider in our experiments is given by Eqns (3.1) and (3.2). However, this model assumes that the glacier has a single dynamical stage: mass-balance fluctuations cause an immediate tendency on the glacier length, L', damped exponentially on the timescale τ. Roe and Baker (2014) evaluated the ability of Eqn (3.1) to emulate the behavior of a shallow-ice flowline model as a function of frequency, f. Equation (3.1) performs well at

low frequencies ($f \ll 1/\tau$), but the single dynamical stage exaggerates the high-frequency response. Roe and Baker (2014) developed a new linear model that incorporates three stages of glacier response: changes in ice thickness drive changes in ice flux that, in turn, drive changes in glacier length. Their model takes the form of a third-order ordinary differential equation:

$$\left(\frac{d}{dt} + \frac{1}{\epsilon\tau}\right)^3 L' = \frac{1}{\epsilon^3\tau^2}\beta b', \tag{3.6}$$

where τ and β are defined as above, and $\epsilon = 1/\sqrt{3}$. Following the terminology in Roe and Baker (2014), we will refer to Eqns (3.1) and (3.6) as 1-stage and 3-stage models, respectively. The 3-stage model is governed by the same response-time parameter as the 1-stage, but in a different functional form (that is, it arises from the same geometric considerations, but is not an e-folding timescale). As noted above, the two models differ primarily at high-frequencies; however, these differences remain relevant at long timescales when the forcing is a continuous trend. This is evident in the long-term limits of the 1-stage and 3-stage responses to a linear mass-balance trend, $\dot{b}$, starting at $t = 0$. The 1-stage solution is given by Eqn (3.4), and the 3-stage solution is

$$L'(t) = \tau\left[1 - \frac{3\epsilon\tau}{t}(1 - e^{t/\epsilon\tau}) + e^{-t/\epsilon\tau}\left(\frac{t}{2\epsilon\tau} + 2\right)\right]\beta\dot{b}t. \tag{3.7}$$

For $t \gg \tau$, Eqn (3.7) approaches $L'(t) = \tau\beta\dot{b}(t - 3\epsilon\tau)$, indicating a greater lag behind the equilibrium response than the 1-stage model. The fractional equilibration also highlights this difference. For each model, it is obtained by dividing $L'(t)$ (Eqn 3.4 for 1-stage, Eqn 3.7 for 3-stage) by the equilibrium length response ($L'_{eq}(t)$; Eqn 3.5). The factor ($\tau\beta\dot{b}t$) drops out, leaving

$$\left.\frac{L'}{L'_{eq}}\right|_{1-stage} = 1 - \frac{\tau}{t}(1 - e^{-t/\tau}), \tag{3.8}$$

and

$$\left.\frac{L'}{L'_{eq}}\right|_{3-stage} = 1 - \frac{3\epsilon\tau}{t}(1 - e^{-t/\epsilon\tau}) + e^{-t/\epsilon\tau}(\frac{t}{2\epsilon\tau} + 2). \tag{3.9}$$

Both expressions depend only on the glacier's response time and the duration of the trend. The exponentials in Eqns (3.8) and (3.9) decay fastest, leaving terms proportional to $1/t$ in the long-time limit. However, the 1-stage fractional equilibration asymptotes to $1 - \tau/t$, whereas the 3-stage model asymptotes to a slower $1 - 3\epsilon\tau/t$ approach to unity, on account of its greater lag behind the equilibrium response.

Several other analytical glacier models exist in the literature. For example, Harrison et al. (2003) and Lüthi (2009) both developed dynamical models for area and volume fluctuations, which effectively have two stages of adjustment. Here we limit our selection of analytical models to the 1-stage and 3-stage frameworks. These provide a range in complexity, and allow for straightforward comparison as they are based on a common set of parameters, but, as discussed above, represent different assumptions about glacier dynamics.

3.3.2 Nonlinear flowline models

In order to more comprehensively capture glacier dynamics, we use numerical models that explicitly represent ice deformation in response to driving stresses. These models ultimately stem from the Stokes equations,

$$\nabla \cdot \sigma_{ij} = -\rho g_i \tag{3.10}$$

and

$$\nabla \cdot u_i = 0, \tag{3.11}$$

where σ_{ij} is the Cauchy stress tensor, ρ is the density of ice, g_i is acceleration due to gravity, and u_i are velocity components. Equation (3.10) expresses local balance between surface forces (stress gradients) and body forces (gravity) per unit volume of ice, while Eqn (3.11) expresses conservation of mass. These equations are linked by a constitutive relation (Glen, 1955) that relates driving stresses to strain rates $\dot{\epsilon}_{ij}$ (and therefore to velocities):

$$\dot{\epsilon}_{ij} = A\, S_e^{n-1} S_{ij}. \tag{3.12}$$

A is the creep parameter that follows an Arrhenius relationship, which we hold constant (see Table 3.1), and we use a flow exponent of $n = 3$. S_{ij} is the deviatoric stress tensor, defined

as the Cauchy stress tensor minus its isotropic pressure component, and $S_e^2 = \frac{1}{2} S_{ij} S_{ij}$ is a scalar effective stress. Finally, a continuity equation gives the evolution of local ice thickness, h:

$$\frac{dh}{dt} = b - \nabla \cdot \mathbf{F} \tag{3.13}$$

where b is the local surface mass balance rate, and $\mathbf{F}$ is the vertically-integrated ice flux. Here basal mass balance terms are neglected, and it is assumed that bed geometry is constant in time, making Eqn (3.13) equivalent to the evolution of the ice surface.

The nonlinear relationship between stress and strain (Eqn 3.12) can require significant numerical computation to solve in its full form, and for this reason it is often advantageous to seek approximations to the Stokes equations. A common one in glaciology is the shallow-ice approximation (SIA), in which it is assumed that gravitational driving stress is balanced only by basal shear stress (e.g., Hutter and Hughes, 1984). If x is the horizontal coordinate along a glacier flowline, z is the vertical coordinate, and s is the free ice surface, the driving stress is given by

$$\sigma_{xz} = \sigma_{zx} = -\rho g_z h \frac{ds}{dx}, \tag{3.14}$$

and all other terms in the stress tensor are neglected. In contrast, "full-Stokes" solutions make no such truncations and solve for the full stress state. The SIA is valid in the limit of shallow aspect ratios ($H/L \ll 1$) and has been shown to be a reasonable approximation for mountain glacier geometries, although its performance declines for smaller glaciers and steeper bed slopes (e.g., Le Meur et al., 2004; Leysinger Vieli and Gudmundsson, 2004; Adhikari and Marshall, 2011). Intermediate "higher order" modeling frameworks exist that resolve some, but not all, additional stress components (e.g., Pattyn, 2002; Hindmarsh, 2004); in this study, however, we limit our comparison to SIA and full-Stokes models.

We run both a SIA and a full-Stokes model for a two-dimensional flowline, that is, assuming a constant glacier width and neglecting the influence of lateral boundaries. The SIA equations are integrated using finite differences and explicit time stepping (e.g., Oerlemans, 2001; Roe, 2011) on a 25 m grid. For our full-Stokes simulations, we use the finite-element

model Elmer/Ice (Gagliardini et al., 2013) with a horizontal element size of 25 m and 10 vertical layers. For both models, we incorporate a simple Weertman-style sliding law (e.g., Weertman, 1964; Cuffey and Paterson, 2010):

$$S_b = C u_b^m. \tag{3.15}$$

S_b is the basal shear stress, u_b is the sliding velocity, and m is the Weertman exponent, or the inverse of the flow exponent n (i.e, $m = 1/3$). C is a constant sliding coefficient; however, note that the sliding velocity depends nonlinearly on the basal shear stress. We assume an altitude-dependent mass-balance function $b(z)$ for the flowline models:

$$b(z) = \bar{P} - \mu(\bar{T}_{z=0} - \Gamma z), \tag{3.16}$$

where P is the mean annual accumulation, uniform across the glacier surface, and $\bar{T}_{z=0}$ is the mean melt-season temperature at sea level. μ is a melt factor, relating mass balance to melt-season temperature, and Γ is the atmospheric temperature lapse rate.

3.3.3 Steady-state glacier geometries

Our model domains are idealized mountain glaciers with uniform bed slopes. We first consider two geometries: glacier 1 has a bed slope of $\tan(\phi) = 0.2$ (11.3), and glacier 2 has a slope of $\tan(\phi) = 0.2$ (5.7). Both have a maximum elevation of 2500 m above sea level (Fig. 3.2a). Table 3.1 displays the mass-balance and dynamical parameters used in the models. We use values for sliding and deformation parameters (C and A) that are considered typical for mountain glaciers (see e.g., Budd et al., 1979; Oerlemans, 2001; Roe, 2011). Our sliding relation (Eqn 3.15) is a simplified version of that presented in Oerlemans (2001), and subsequently in Roe (2011) and Roe and Baker (2014). These studies used $C = (H_s/f_s)^m$, where H_s is ice thickness and f_s is a sliding parameter, which they set at 5.7e-20 $\mathrm{Pa}^{-3}\ \mathrm{s}^{-1}\ \mathrm{m}^2$ following Budd et al. (1979). For simplicity, we treat H_s as constant, set at 50 m for glacier 1 and 100 m for glacier 2. These values fall between initial mean thickness, and thickness after a 2 °C warming (described in the next section). Using the above value for f_s, this gives

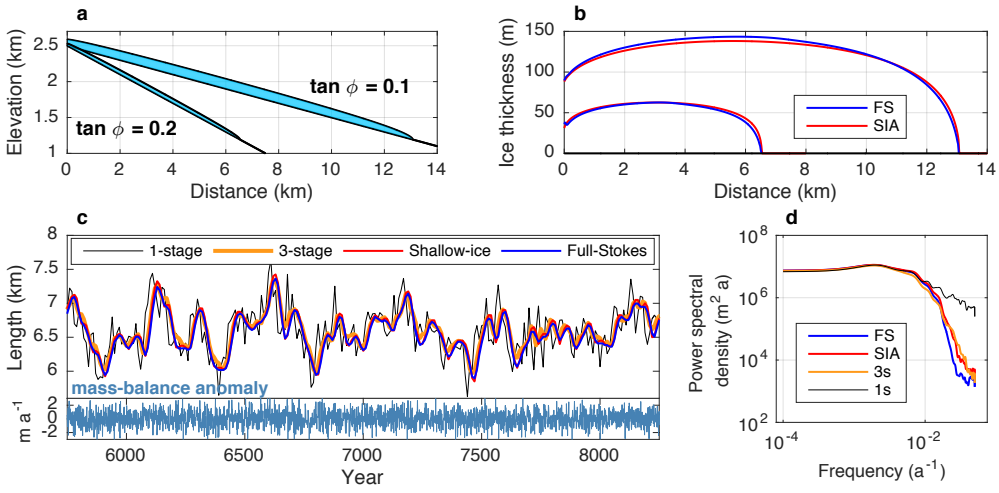

Figure 3.2: Idealized glacier geometries and response to climate variability. (a) Equilibrium configuration for the two geometries used throughout this study. (b) Equilibrium ice thickness profiles generated with the full-Stokes (blue) and shallow-ice (red) models. The mean ice thickness for these profiles is used to determine τ in the 1- and 3-stage models. (c) Length response of all four models to white-noise interannual variability ($\sigma_T = 0.7$ °C and $\sigma_P = 0.7$ a^{-1}), for glacier 1. 2.5 ka of a 10 ka model run is shown. The mass-balance anomaly is shown in the lower panel. (d) Power spectral density for the length responses to variability (glacier 1). Both (c) and (d) show that the 1-stage response has more variance at high frequencies, but the other three models agree closely.

Table 3.1: Glacier and climate parameters for glaciers 1 and 2. The first group of parameters are those imposed in the flowline models, while the second group are calculated from the full-Stokes model and used to calibrate the linear models.

Parameter	**Symbol**	**Value**	**Units**
		Glac. 1 (Glac. 2) if different	
Max. elevation	Z_{max}	2500	m
Bed slope	$\tan\phi$	0.2 (0.1)	
Melt season temp. at sea level	$\bar{T}_{z=0}$	20	°C
Accumulation	$\bar{P}$	4	m a^{-1} (ice equiv.)
Melt factor	μ	0.5	m a^{-1} °C^{-1}
Lapse rate	Γ	6.5	°C km^{-1}
Deformation parameter	A	1.9e-24	Pa^{-3} s^{-1}
Sliding coefficient	C	3.03e-4 (3.82e-4)	Pa $s^{1/3}$ $m^{-1/3}$
Steady-state length	$\bar{L}$	6.55 (13.1)	km
Characteristic thickness	$\bar{H}$	54 (123)	m
Terminus mass balance rate	b_t	-2.12	m a^{-1} (ice equiv.)
$\bar{L}/H$	β	121 (107)	
Response time ($\tau = H/b_t$)	τ	25 (57)	a

the constant sliding coefficients in Table 3.1. Our climate parameters are consistent with a temperate, maritime setting. With the values in Table 3.1, Eqn (3.16) gives equilibrium lengths of 6.55 km (glacier 1) and 13.1 km (glacier 2). Since an ice elevation-mass balance feedback is not included, the equilibrium lengths are analytical functions of the mass-balance profile and the bed geometries.

The full-Stokes and SIA models agree closely on their equilibrium thickness profiles, shown in Fig. 3.2b. For the smaller, steeper glacier (1), mean ice thicknesses are 53 m (full-Stokes) and 54 m (SIA); and for the larger glacier (2), 123 m (full-Stokes) and 120 m (SIA). The similar thicknesses, in turn, imply good agreement on estimated response times (Eqn

3.2; $\tau = -H/b_t$). Using mean thicknesses for H, and with b_t set by Eqn (3.16), Eqn (3.2) gives $\tau = 25$ years for glacier 1, and $\tau = 57$ years for glacier 2 (using full-Stokes thickness; 56 years for the SIA thickness). It should be noted that terminus ablation rate for both glaciers is lower than those observed on many glaciers; this is a consequence of their constant width.

We use the full-Stokes steady-state geometries to calibrate the 1-stage and 3-stage linear models (see the second group of parameters in Table 3.1). The elevation, temperature, and lapse rate parameters we have chosen (Table 3.1) dictate that some summer melt occurs at all elevations (i.e., $\bar{T}_{Zmax} > 0$), making Eqn (3.16) a continuous, linear function over our domain. This means that both temperature anomalies (T') and precipitation anomalies (P') correspond to uniform mass-balance anomalies. These mass-balance anomalies constitute the forcing for the linear models, and are given by

$$b' = P' - \mu T'. \tag{3.17}$$

The linear model parameters presented here are a simple case of those derived for the 1-stage model in Roe and O'neal (2009) and for the 3-stage model in Roe and Baker (2014), which were generalized to allow for a region where no melt occurs.

These synthetic geometries are meant to represent two generic mountain glaciers with distinct response times, rather than specific settings. However, to put their response times in context with glaciers around the world, we turn to (Roe et al., 2017, supplemental material), who estimated τ, according to Eqn (3.2), for 37 glaciers based on data from existing glacier inventories. For example, their timescale estimates for Blue Glacier in the Olympic Mountains ($\tau \sim 28$ years) and Hintereisferner in the Austrian Alps ($\tau \sim 30$ years) are comparable to our glacier 1 ($\tau = 25$ years). Our glacier 2 ($\tau = 57$ years) is similar in timescale to Saskatchewan Glacier in the Canadian Rockies, Gries Glacier in the Swiss Alps, or Storglacin in northern Sweden ($\tau \sim 50, 59$ and 60 years, respectively), among others. The largest glaciers in the Alps likely have even longer response times, with estimates for individual glaciers approaching or exceeding a century

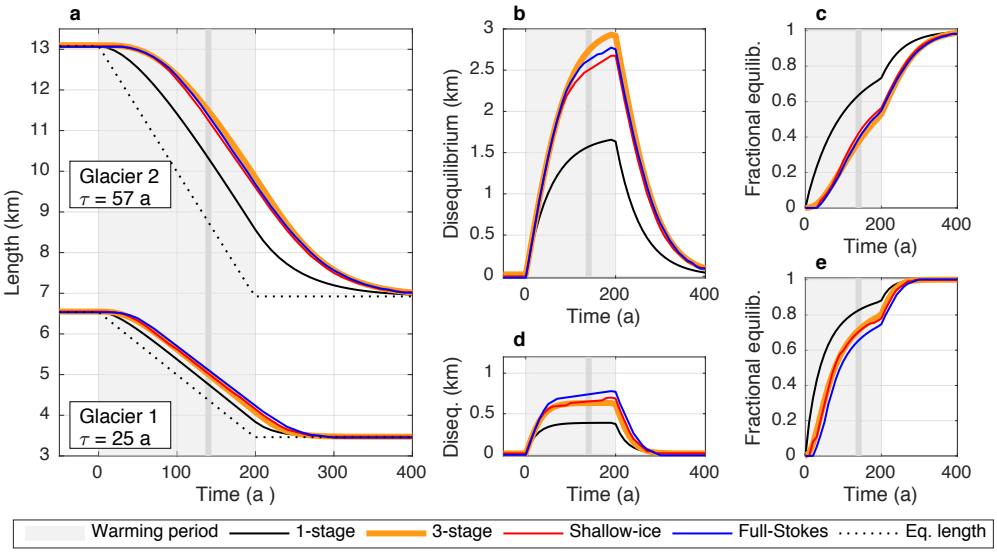

Figure 3.3: The role of model complexity in response to a trend. (a) Length responses to a 2 °C warming over 200 years, for all four models. The dashed lines show length at which the glaciers would be in equilibrium if the climate were to stabilize at that time. (b) Disequilibrium, defined as the difference between transient and equilibrium length, for glacier 2. (c) Fractional equilibration for glacier 2. (d) and (e): as for (b) and (c), but for glacier 1. The gray vertical line in each panel marks 140 years into the warming period as a reference point for current disequilibrium assuming anthropogenic forcing began ca. 1880.

3.4 Results

3.4.1 Model Complexity

The 1-stage model illustrated the basic response to a climate trend (Fig. 3.1); a next step is to investigate the responses of the more realistic models introduced in the previous section. Using a hierarchy of models, we can ask what is the simplest model that can accurately characterize a glacier's disequilibrium in a warming climate?

While our ultimate interest is retreat due to a warming trend, forcing the different models with stochastic climate variability is a good way to evaluate their relative performance as a function of frequency. We imposed 10,000 years of white noise (i.e., equal power at all frequencies) in both temperature and precipitation, with $\sigma_T = 0.7$ °C and $\sigma_P = 0.7$ m a^{-1}.

The resulting standard deviation in mass balance is 0.78 m a^{-1}, consistent with variability observed in maritime climates (e.g., Medwedeff and Roe, 2017). A 2500-year segment of our model output for the smaller glacier geometry is shown in Fig. 3.2c; it is immediately clear that the 1-stage model is an outlier, with much more high-frequency variability than the other three models. This is evident also in the power spectrum (Fig. 3.2d): the 1-stage model has considerably less damping at high frequencies, consistent with the results of Roe and Baker (2014). The standard deviations of the length fluctuations, σ_L, are 335 m, 267 m, 295 m, and 284 m for the 1-stage, 3-stage, SIA, and full-Stokes models, respectively. These represent departures of 18% (1-stage), 6% (3-stage) and 4% (SIA) with respect to the full-Stokes model. Thus, it appears that for small fluctuations around a mean state, the simplified dynamics of the 3-stage and SIA models hold up as reasonable approximations, while the 1-stage model should be treated with caution, especially on short timescales.

We now investigate our central question of the transient response to a climate trend. In the following analyses, we stipulate a linear trend in melt-season temperature of 2 °C over 200 years, and no changes in precipitation, typical of the observed midlatitude trends over the last century (e.g. IPCC, 2013). Figure 3.3a shows the length responses of all four models and both geometries. All models exhibit a significant lag behind the equilibrium response (dashed line). However, the 1-stage model's tendency to respond too quickly means that it underestimates the glacier's lag behind the changing climate. The good agreement among 3-stage, SIA, and full-Stokes models suggests that the basic transient response to warming is not significantly affected by higher-order ice dynamics, consistent with the conclusions of previous studies (e.g. Leysinger Vieli and Gudmundsson, 2004). Figures 3.3b and 3.3c show the disequilibrium and fractional equilibration (as defined in section 3.1.1), respectively, for glacier 2 (τ = 57 years), and 3.3d and 3.3e show results for glacier 1 (τ = 25 years). The degree of disequilibrium is much more pronounced for the longer timescale glacier, consistent with its longer memory of previous, cooler climate states. It is important to note that the absolute length changes are greater for glacier 2 on account of its shallower bed slope. However, in terms of the fractional equilibration, we see that, by the end of the 200-year

Table 3.2: Parameters and initial geometries for three glaciers with similar timescales. Results from the SIA model (bottom group) are inputs in the 3-stage model.

Parameter	**Symbol**	**Glacier 2**	**Glacier 3**	**Glacier 4**	**Units**
Bed slope	$\tan\phi$	0.1	0.125	0.2	
Deformation parameter	A	1.9e-24	2.4e-24	2.4e-24	$\mathrm{Pa}^{-3}\ \mathrm{s}^{-1}$
Sliding coefficient	C	3.82e-4	n/a	n/a	$\mathrm{Pa\ s}^{1/3}\ \mathrm{m}^{-1/3}$
Max. elevation	Z_{max}	2500	3000	2500	m
Melt season temp. (sea level)	$\bar{T}_{z=0}$	20	21	21	°C
Mean ice thickness	H	120	176	91	m
Terminus balance rate	b_t	−2.12	−3.25	−1.63	$\mathrm{m\ a}^{-1}$ (ice equiv.)
Response timescale	τ	57	54	56	a

warming period, the 3-stage, SIA, and full-Stokes models all show that the "slower" glacier 2 has only worked through about half of its total adjustment to a 2 °C warming; glacier 1 is about three quarters of its way to equilibrium. The vertical lines in each panel mark 140 years into the warming as a rough comparison for the current state of glaciers, assuming anthropogenic forcing started around 1880 (e.g. IPCC, 2013). The basic physics of a lagged response to a trend implies that glaciers with long response times can be assumed to be significantly out of equilibrium with our current climate, both in an absolute and fractional sense.

3.4.2 Three different glaciers with the same response time

The marked difference in the responses of glaciers 1 and 2 to gradual warming shows the important role of the response time in setting the disequilibrium. Despite the simple form of the response time (Eqn 3.2), a number of geometric, climatic, and rheological parameters are implicitly represented in the characteristic values H and b_t. Given the range that these parameters may take for different glaciers around the world, it is important to consider the

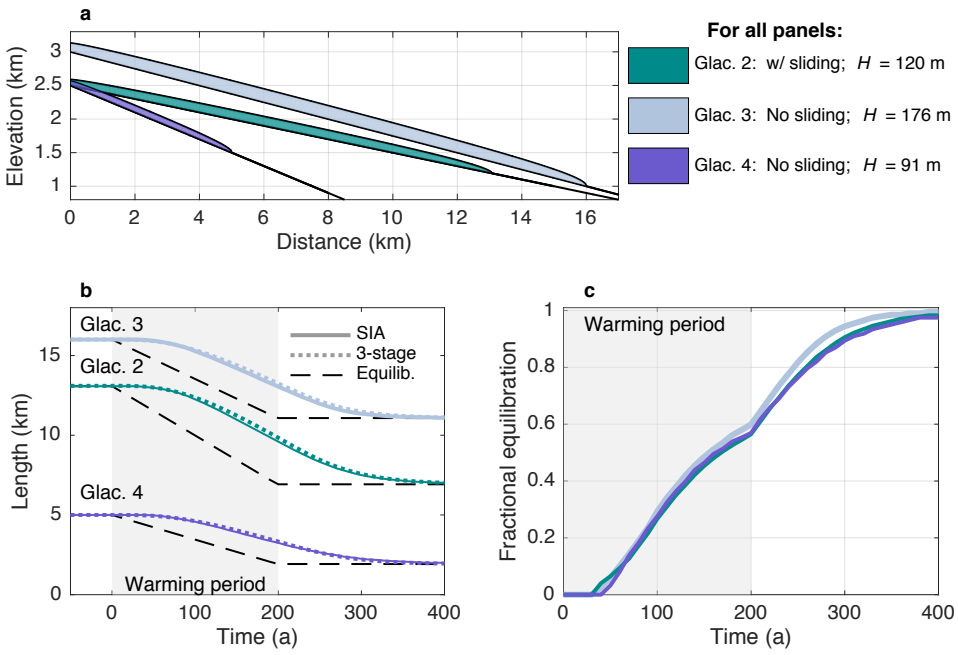

Figure 3.4: Three glaciers with 55-year response timescales. (a) Initial equilibrium profiles for the three glaciers. Glacier 2 is the same as the larger glacier in the main text. Glaciers 3 and 4 do not have basal sliding. (b) Length responses of each glacier in response to a 2 °C warming over 200 years. Solid lines are the SIA model response, dotted lines the 3-stage model response, and black dashed lines show the instantaneous equilibrium lengths. (c) Fractional equilibration for each glacier (for clarity, only SIA responses are shown). Despite their different geometries and dynamics, the glaciers' transient responses are nearly identical in a fractional sense.

applicability of Eqn (3.2) across a range of parameter space. As an illustrative example, we present two additional idealized glaciers with different parameters for rheology, mass-balance, and bed-geometry. However, these parameters have been tuned in such a way to give response times (54 and 56 years) comparable to that of glacier 2 (57 years).

For simplicity, we only compare the SIA and 3-stage models in this section. Table 3.2 displays the parameters and resulting geometries for glaciers 2–4 , and SIA thickness profiles are shown in Fig. 3.4a. Glacier 3 is slightly steeper than glacier 2, but does not slide over its bed, resulting in a greater steady-state mean ice thickness (176 m). Glacier 4 is steeper yet, and even with no sliding, has a mean thickness of only 91 m. Despite its smaller dimensions, it has a long response time because its terminus does not extend very far into lower, warmer elevations. All glaciers have the same accumulation rate of 4 m a^{-1} ice equivalent, but the maximum elevations and melt season temperatures have been manipulated to give terminus positions, and thus mass-balance rates (b_t), that yield the desired response times.

The 3-stage model parameters are again based on the SIA equilibrium geometries. Figure 3.4b shows 3-stage and SIA length responses to the same gradual warming (2 °C over 200 years), which again agree closely. Owing to their different geometries, the length sensitivities (and thus equilibrium responses) are slightly different for the three glaciers. However, as Fig. 3.4c shows, their responses are nearly identical in terms of fractional equilibration. Thus, we conclude that a glacier's fractional equilibration depends on its timescale (e.g, Fig. 3.3c vs. 3.3e), but not on the glacier's length sensitivity (Fig. 3.4). This point is demonstrated analytically by the 3-stage solution for fractional equilibration (Eqn 3.9). Furthermore, that the 3-stage model, which is blind to the details of sliding vs. deformation, can emulate the SIA responses for each case suggests that glacier geometry encapsulates ice dynamics well enough to dictate the basic response to forcing. This makes τ, which is based on geometry and mass balance, a versatile metric for understanding glacier responses across a wide range of settings.

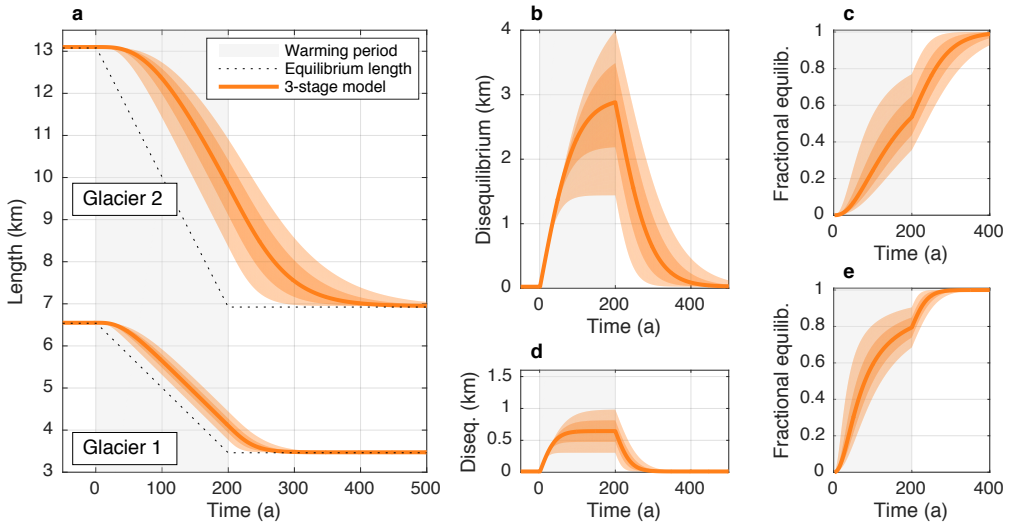

Figure 3.5: The spread of responses due to uncertainty in ice thickness. (a) Orange shaded regions show $\pm 1\sigma_L$ and $2\sigma_L$ bounds for uncertainty in timescale ($\sigma_\tau = \tau/4$), generated with the 3-stage model. The dashed line shows equilibrium length. (b, c) Associated spread in disequilibrium and fractional equilibration for glacier 2. (d, e) As for (b) and (c), but for glacier 1.

3.4.3 Uncertainty in response time

The essential lagged nature of the glacier response to a trend is robust across a range of geometries (Figs. 3.3 and 3.4), but it depends on τ, and, via Eqn (3.2), ice thickness. In reality, ice thickness is often uncertain, and different estimation methods can yield different τ for the same glacier (e.g. Oerlemans, 2001; Harrison et al., 2001). So, we now evaluate how uncertainty in τ affects disequilibrium. The good agreement with the SIA and full-Stokes flowline models makes the 3-stage model an efficient analytical tool. In the previous sections, we had the benefit of thickness profiles generated by the numerical models, and our results show that the mean ice thickness was an appropriate characteristic value to use in calculating τ. However, direct ice-thickness measurements on mountain glaciers are uncommon, and for more complex geometries, the mean may not be the best characteristic thickness for τ. Thus, we will use thickness in the following experiments to directly manipulate the response

timescale.

We consider a broad uncertainty in thickness: a Gaussian probability distribution with a standard deviation of $\sigma_H = \bar{H}/4$, where $\bar{H}$ is the mean thickness of the original flowline profiles that calibrated the 3-stage model. This gives $\sigma_H = 13$ m for glacier 1, and $\sigma_H = 31$ m for glacier 2. With this value, the $\pm 2\sigma_H$ range is equal to $\bar{H}$ itself. Since τ is directly proportional to H, this yields a probability distribution for τ that also has the $\pm 2\sigma_\tau$ range equal to $\bar{\tau}$. Figure 3.5a shows the resulting length responses to our 2 °C warming trend, with shaded regions showing the $\pm 1\sigma$ and $\pm 2\sigma$ bounds. The effect of timescale uncertainty is a sustained spread in length responses and, accordingly, in disequilibrium (Figs. 3.5b and 3.5d) and fractional equilibration (Figs. 3.5c and 3.5e). Errors in the response timescale introduce very long-term effects: the spread grows throughout the warming period, and persists well after the climate has re-stabilized. For instance, for glacier 2, the $\pm 1\sigma$ range in timescale (a spread of 28 years) yields a spread of ~ 1.3 km in length after 200 years of warming, or, to use the fractional metric, a range of ~ 60 years to reach 80% equilibration.

While ice thickness is a directly tunable parameter for the 3-stage model, the effects of timescale uncertainty are also relevant to flowline modeling approaches where ice thickness depends in part on the rheological parameters and basal conditions. We used this dependence to tune flowline ice thicknesses in section 3.3.2; similarly, Roe and Baker (2014) also showed that the response time (Eqn 3.2) captures glacier response over a range of flowline model parameters. This suggests that errors in flowline model ice thickness, whatever their source, would cause errors in the length response similar to those in Fig. 3.5.

3.4.4 Uncertainties due to climate variability

So far, we have considered the length response to a gradual warming in the framework of an idealized climate with no variations other than the imposed trend. In reality, however, any external climate forcing will occur in the midst of natural climate variability, which will continue to force low frequency glacier length fluctuations (see Fig. 3.2c) on top of the retreat due to long-term warming. Figure 3.6a shows this behavior with an ensemble

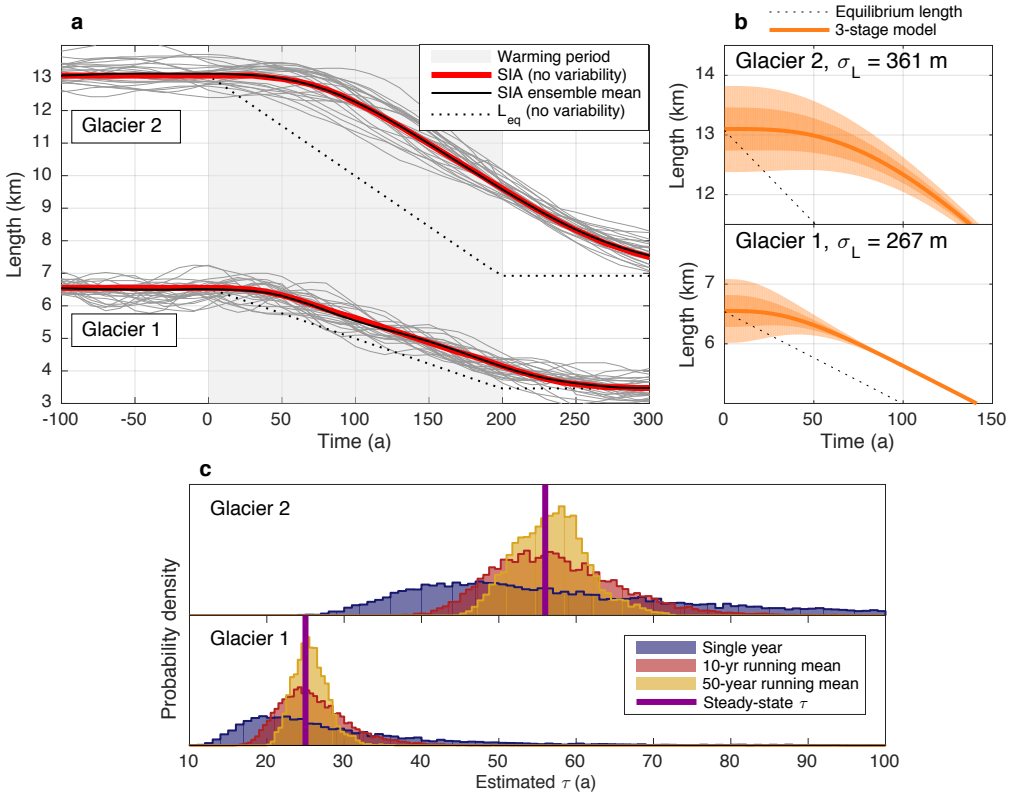

Figure 3.6: Uncertainties due to climate variability. (a) An ensemble of length responses from the SIA model for a 2 °C warming over 200 years, plus 100 realizations of white-noise variability (only 25 are shown). The ensemble mean (black) closely follows the length response to warming with no variability (red). The instantaneous equilibrium length for warming with no variability is plotted for reference (dashed line). (b) Uncertainty in initial state due to unknown climate history prior to the onset of warming (t=0). Shaded regions show the $\pm 1\sigma_L$ and $2\sigma_L$ bounds for the same level of variability as in (a). Initial disequilibrium decays toward the long-term retreat trajectory. (c) Distributions of estimated timescale generated by tracking $\bar{H}$ and b_t through 10 000 years of noise-driven fluctuations. Blue is the distribution when sampling $\bar{H}$ and b_t from a single year; red is the distribution for 10-year means; gold is the distribution for 50-year means; and the purple line shows the steady-state value.

of length responses for different realizations of white-noise temperature and precipitation variability, $\sigma_T = 0.7\,^{\circ}\mathrm{C}$ and $\sigma_P = 0.7\ \mathrm{m\ a^{-1}}$, superimposed upon the standard warming trend. The responses shown are 25 of 100 realizations generated using the SIA model, which was initialized from a steady-state configuration 200 years before the onset of warming in order to allow the fluctuations of each member to de-correlate. The 3-stage model gives similar results, but is omitted for clarity. The fact that the ensemble mean is almost exactly equal to the trajectory for warming without variability reinforces that sustained disequilibrium is still the fundamental response in a noisy, warming climate. While variability may temporarily kick the glacier closer to its equilibrium length, it still has a restoring tendency back to the lagged state. We use a relatively high level of variability in these experiments to illustrate the potential uncertainties; it can be expected that a setting with less interannual variability would yield results more closely resembling the basic, lagged response.

These noise-driven fluctuations have several implications that must be considered for modeling the response of any glacier to climate warming. The possibility that the glacier was mid-fluctuation at the onset of the trend amounts to an uncertainty in initial conditions if the preceding climate is unknown. We illustrate this for the fluctuations driven by our standard interannual variability ($\sigma_T = 0.7\ ^{\circ}\mathrm{C}$ and $\sigma_P = 0.7\ \mathrm{m\ a^{-1}}$). Figure 3.6b shows the $\pm 1\sigma$ and $\pm 2\sigma$ bounds, where initial length anomalies are described by the Gaussian probability distributions with widths of σ_L for each glacier. The impact of this uncertainty declines with time, on a timescale governed by τ. Initial-condition uncertainty does not therefore play a large role 140 years after the onset of the trend. While for the case considered here, the initial uncertainty arises from interannual climate variability, the same concept would apply to other poorly-constrained climate histories. For example, accounting for little-ice-age excursions might entail a much larger uncertainty in initial conditions (e.g., Matthews and Briffa, 2005).

Additional impacts of climate variability on glacier disequilibrium are the basic statistical challenges in defining the mean climate, trends, variability, and any parameters that rely on these estimates. The pre-trend climatology, equilibrium length, and the onset and magnitude

of the climate trend are all uncertain quantities in a noisy climate; the accuracy of their estimates will vary depending on the level of climate variability and the length and quality of observational records. Estimates of the response timescale ($\tau = -H/b_t$) will also be affected by climate variability and the resulting glacier fluctuations. Even with observations, defining the characteristic values for ice thickness (here, the mean, $\bar{H}$) and terminus ablation rates (b_t) over decadal timescales may be uncertain due to sampling errors. Both $\bar{H}$ and the terminus elevation (and therefore b_t) will vary with the glacier's low-frequency response to noise, but the dominant effect is simply the year-to-year variability in mass balance at the terminus. To investigate the effects on response-time estimates, we used the SIA model to track $\bar{H}$ and b_t yearly through 10 000 years of climate noise for both glaciers (again, with $\sigma_T = 0.7$ °C and $\sigma_P = 0.7$ m a^{-1}). From the $\bar{H}$ and b_t timeseries, we calculated τ for each individual year. We then took running means of the $\bar{H}$ and b_t timeseries to create distributions representing estimates of τ based on 10 and 50 years of observations. The probability densities for these distributions are shown in Fig. 3.6c. Not surprisingly, a single year gives a poor estimate of τ, as shown by the broad, blue curves. The 10-year (red) and 50-year (gold) estimates converge on the steady-state values of $\tau = 25$ and 57 years (vertical purple lines), but still have a substantial spread. While only the linear models require τ as an input parameter, this uncertainty is relevant for numerical flowline models as well. These sampling errors will still come to bear on the calibration of the glacier geometry, mass balance, and flow parameters, choices that must be made for any model, and which we have shown here fundamentally affect glacier response.

3.5 Discussion

3.5.1 The committed retreat of mountain glaciers

The result that transient glacier retreat lags the equilibrium response to a climate trend stems fundamentally from the multi-decadal response times common to most mountain glaciers. Our focus on idealized glaciers, rather than specific settings, helps to demonstrate this basic

behavior and the factors that affect it. Our comparison of several idealized geometries shows that a glacier's fractional equilibration during a climate trend depends strongly on its response time (glacier 1 vs. glacier 2 in Fig. 3.3), but not on its length sensitivity (glaciers 2–4 in Fig. 3.4). Figure 3.4 also shows that the fractional equilibration is the same for different parameter combinations that yield approximately the same value for $\tau = -H/b_t$. This makes τ a fundamental and useful parameter for categorizing glacier responses across a wide range of settings and geometries. Some general conclusions can thus be drawn about committed glacier retreat around the world based on estimated response times and observed climate trends (see, e.g., Roe and others, 2017). Consider that our synthetic 54–57-year glaciers are less than 50% into their adjustments to the total warming that has occurred in 140 years (see Fig. 3.4c). Given the observed global surface warming of roughly 1°C in the last century (e.g. IPCC, 2013), our results imply that longer-timescale glaciers ($\tau > 50$ years) are substantially out of equilibrium today. In other words, their observed retreats are startling underestimates of the total retreat already built in by the industrial-era warming that has occurred to date. For large glaciers with shallow slopes and large length sensitivities, absolute disequilibrium may be on the order of kilometers (see Fig. 3.3b). This is consistent with several detailed modeling studies that have assessed committed retreat for large valley glaciers in the Alps. For example, Zekollari et al. (2014) estimated the committed retreat of Morteratsch Glacier, based on 2001–10 climate, at nearly 2 km, while Jouvet et al. (2011) calculated a striking 6 km commitment for Great Aletsch Glacier based on 1989–2008 climate.

Additionally, while we have focused here on length changes, committed retreat also implies committed volume loss, which has direct implications for committed sea-level change (e.g. Mernild et al., 2013; Marzeion et al., 2017, 2018). While volume tends to react more quickly than length (e.g. Oerlemans, 2001), the committed loss should still depend on τ, making the distribution of individual response times an important consideration for regional or global estimates of committed volume change, and the associated impacts on sea-level and hydrology. Given some level of current disequilibrium, how certain is a glacier's committed retreat? For any component of the climate system, committed change is a useful metric be-

cause it is based on forcing that has occurred thus far, and is thus partitioned from changes associated with the much less certain future of anthropogenic forcing. However, a choice of definition must be made as to the way in which forcing is hypothetically stabilized. We've based committed retreat on an abrupt stabilization of temperature, as warming is a direct forcing on glacier extent (and is more robust than precipitation trends for most glaciers around the world; see, e.g., Roe et al., 2017). However, the relevant forcing is different for other aspects of the climate system. Early studies on committed climate warming were based on a fixed atmospheric composition (e.g. Hansen et al., 1985; Wigley and Schlesinger, 1985; Wigley, 2005), but this approach did not account for the finite lifetime of atmospheric greenhouse gases. As greenhouse gas emissions are the primary source of anthropogenic forcing (e.g. IPCC, 2013), more recent approaches calculate the climate commitment based on zero additional emissions. Although there is a broad spread of uncertainty, the central estimates are that if all anthropogenic emissions ceased today, the natural decline of greenhouse gases and the delayed ocean response would offset each other, leaving global temperatures approximately flat for the next few centuries (Solomon et al., 2009; Armour and Roe, 2011; Mauritsen and Pincus, 2017). These studies suggest that the observed warming to date constitutes a hard lower bound from which to calculate committed glacier retreat. And while calculating retreat based on current temperatures is an idealized approach, it is consistent with recent literature on committed change in the climate system.

3.5.2 Implications for climate reconstructions

The fact that glaciers lag their equilibrium response to a climate trend has important consequences for inferring past climates using numerical glacier models. A failure to account for current disequilibrium in the glacier state can render estimates of past climate significantly in error. Let dL/dT_{eq} be defined as the equilibrium sensitivity of a glacier to a change in mean temperature. For a glacier model, this is a fixed function of the parameters chosen by the modeler. In principle, one can use the model to infer the climate change required for a length change ΔL_{eq}, between two equilibrium climate states. Assuming only changes in

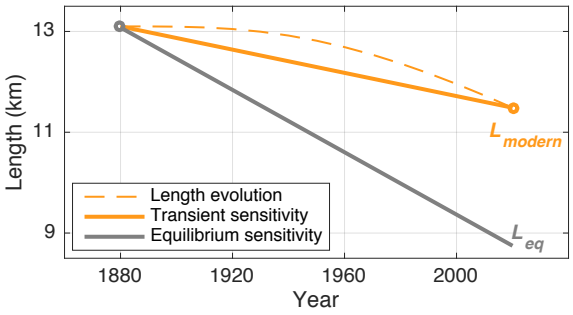

Figure 3.7: Transient vs. equilibrium sensitivity. The dashed orange line shows the 3-stage length response of glacier 2 to the 1 °C century^{-1} warming, beginning in 1880. Transient length sensitivity inferred from terminus retreat (solid orange line) underestimates the glacier's equilibrium sensitivity (gray line). The transient sensitivity is -1.1 km °C-1, while the true equilibrium sensitivity is -2.9 km °C^{-1}.

temperature, this can be written as:

$$\Delta T_{eq} = \frac{\Delta L_{eq}}{dL/dT_{eq}}. \tag{3.18}$$

However, because of the modern disequilibrium, an error is incurred if the modern length is used in calculating ΔL_{eq}. For example, consider a moraine recording the glacier's equilibrium preindustrial extent, from which ΔL_{eq} in Eqn (3.18) is set to $L_{moraine} - L_{modern}$. However, using glacier 2 as an example ($\tau = 57$ years), the modern glacier has retreated less than halfway to its equilibrium length, so this assumed ΔL_{eq} would underestimate the true equilibrium length change:

$$\Delta L = (L_{moraine} - L_{modern}) \leqslant \frac{1}{2} \cdot \Delta L_{eq}|^{true}. \tag{3.19}$$

There are multiple possible consequences of the error. First, if the model sensitivity is correct, the resulting estimate of ΔT_{eq} is less than half as large as the true climate change. The other possibility is that the glacier model parameters are tuned in a way that renders the model less than half as sensitive as it should be. This latter pitfall will occur when ΔT_{eq} is constrained by instrumental or proxy records. Figure 3.6 illustrates this for glacier 2's response to a

1°C per century warming (dashed line), beginning in 1880. The average rate of retreat over the last 140 years (solid orange line) gives a transient sensitivity of -1.1 km $^{\circ}C^{-1}$, whereas the equilibrium sensitivity (gray line) is actually -2.9 km $^{\circ}C^{-1}$. A model tuned to the transient sensitivity would miscalculate any climate changes further in the past, and would also underestimate the natural glacier variability, σ_L. Finally, some combination of errors in ΔT_{eq} and the sensitivity is also possible. Whatever the case, it is clear that initializing a model in steady-state with contemporary climate and length observations, when the target glacier is in fact far out of equilibrium, means building significant error into any analyses that rely on the model.

A number of approaches for reconstructing climate from glacier records exist (see, e.g., a review by Mackintosh et al., 2017, and references therein). However, the effects of disequilibrium have not been emphasized in the reconstruction literature. The consequences of ignoring current disequilibrium would vary by methodology and by glacier, but our results suggest that disequilibrium should be factored into any length sensitivity estimates or model calibrations based on current geometry. Errors would be particularly problematic for estimates of late-Holocene climate changes relative to the modern climate, and for glaciers with long response times. They become less of an issue for larger glacier changes, such as retreat from the last glacial maximum, where the modern disequilibrium is a smaller fraction of the overall change; or, for glaciers with fast response times, whose current state is closer to equilibrium.

3.5.3 Implications for glacier projections

Modeling glacier retreat is also a vital part of predicting and adapting to impacts of glacier change in a warming climate, such as sea-level and hydrological changes (e.g. IPCC, 2013). Uncertain emissions scenarios and regional climate variability introduce a large amount of uncertainty into localized projections (e.g. Deser et al., 2014), but because the metric of committed retreat is independent of future forcing by construction, it can provide a useful bound for assessing future impacts. Current disequilibrium is also important to assess because the

model sensitivity issues discussed above also apply to projections of future retreat: whatever the future forcing scenario, initializing glacier models in steady state with the current climate will introduce errors into the predicted retreat and the glacier's contributions to catchment hydrology.

Another point related to future glacier change is that over the initial period of gradual warming (that is, up to a few multiples of τ), terminus retreat accelerates even as the rate of warming remains steady. This acceleration can be conceptualized in the three-stage framework of Roe and Baker (2014): melt-driven thinning reduces flux into the terminus region, eventually making ablation more efficient at driving terminus retreat. This sequence is more drawn out for longer response timescales, and our results suggest that glaciers with 50+ year response times have not emerged from this early stage of adjustment to anthropogenic warming. In other words, their recent responses may be characterized more by thinning than by terminus retreat. Indeed, dramatic thinning has been observed for many mountain glaciers (see e.g. Paul et al., 2004), and may be a precursor to increased retreat for long-timescale glaciers. These stages of response should thus be considered when interpreting recent or future changes in retreat rates.

3.5.4 The role of higher-order ice dynamics

In addition to considering model tuning and initialization, the representation of ice dynamics is also an important decision that the modeler faces, and the degree of complexity required ultimately depends on the question being asked: shallow-ice solutions can give errors in the spatial pattern of ice thickness or velocities (e.g. Le Meur et al., 2004; Greve and Blatter, 2009; Adhikari and Marshall, 2011, 2013); however, Adhikari and Marshall (2013) also showed that the discrepancies between higher- and lower-order solutions were greater for advance scenarios than for retreat. Leysinger Vieli and Gudmundsson (2004) compared full-Stokes and SIA model responses to step changes in climate, making the important point that accurate mass-balance information may be more critical than higher-order dynamics for modeling glacier responses to climate changes. The close agreement between our SIA and

full-Stokes simulations indicate that higher-order stresses do not play a large role in the basic, lagged response to gradual warming, consistent with the insights of Leysinger Vieli and Gudmundsson (2004) and Adhikari and Marshall (2013). We find that accurate ice thickness and mass balance, which robustly characterize the response time, are more important than model complexity for representing disequilibrium, provided that 3-stage (as opposed to 1-stage) dynamics are used if a linear model is chosen (see also discussion in Roe and Baker, 2014). However, a uniform bed geometry and absence of lateral effects make it more likely that SIA (and 3-stage) assumptions hold. Several studies have shown that the choice of model dynamics may affect the steady-state thickness distribution (e.g. Le Meur et al., 2004; Adhikari and Marshall, 2013). Thus, for modeling experiments that target specific glacier geometries, the inclusion of higher-order stresses may become important for representing the degree of disequilibrium through the response time, even if higher-order mechanics do not play a major role in retreat.

3.5.5 Outlook

Estimates of past climate change, and predictions of future glacier retreat must take the current disequilibrium of glaciers into account. However, without perfect knowledge of the system, there is an unavoidable quandary here: current climate is typically well observed, but current disequilibrium may be uncertain because the response time can only be estimated approximately (e.g., Fig. 3.5). On the other hand, while the disequilibrium was less (though not necessarily absent) at the start of the industrial era, the climate then may be less certain. Nevertheless, records of glacier front position at the beginning of the industrial era are abundant (e.g. Leclercq et al., 2014), and several global datasets of temperature extend back to 1880 (e.g. **?**). Our opinion is that in many parts of the world, sufficient climate and glacier data exist to incorporate disequilibrium into interpretations of glacier change and model initialization. One approach is a dynamic calibration, using a model of at least 3-stage complexity, to account for transient effects and identify glacier and climate parameters (e.g., Table 3.1) together with their uncertainties that best reproduce the observed retreat.

Such a calibrated model could then be used to estimate older climate changes or future glacier responses. Dynamic calibration has been applied to a number of well-observed glaciers (e.g. Oerlemans, 1997; Lüthi et al., 2010; Jouvet et al., 2011; Zekollari et al., 2014). Additionally, Roe et al. (2017) applied this approach, using the 3-stage model, to compare natural glacier variability with observed retreats around the world. In any event, it is vital to produce reconstructions and projections that reflect uncertainties in model parameters. Because each glacier setting is unique, modeling efforts are often targeted to a single glacier, and it is easy for calibration choices to be made that affect the model sensitivity. As the results of this paper demonstrate, the errors can be severe when modern glaciers are assumed to be near equilibrium.

3.6 Summary and Conclusions

Because many mountain glaciers have response timescales that are similar in order to the period of time over which humans have been changing the climate, we should not assume that they are close to equilibrium in response to this forcing (see Fig. 3.1). We explored the factors that influence this disequilibrium and that modelers must take into account to properly capture the transient response. Specifically, we considered (1) the representation of ice dynamics; (2) the glacier's geometry, and therefore its response timescale; and (3) the effects of climate variability on model initialization and glacier response. Our main findings in these areas are summarized as follows:

1. A comparison of four models of ice dynamics forced by the same ramp warming showed that, at a minimum, 3-stage linear dynamics were necessary to accurately capture a glacier's degree of disequilibrium. The 1-stage linear model captures the basic phenomenon of disequilibrium, but underestimates its magnitude by roughly a factor of two in our results; this is because it too-rapidly translates mass-balance perturbations into length changes. A number of other low-order glacier models exist in the literature; our comparisons indicate that accurately capturing the lag between forcing and

terminus response (or equivalently, the phase lag in the cross spectrum Roe and Baker, 2014), as the 3-stage does, is a prerequisite for any analytical model used to estimate disequilibrium. The 3-stage model emulates the response of the flowline models very well, despite its dependence on fixed parameters linearized about a mean state. Roe and Baker (2014) showed that the 3-stage parameters could be calibrated for more complex valley geometries, and could still reasonably emulate flowline model output for terminus fluctuations. However, they noted greater disagreement for large excursions that spanned slope breaks in the glacier bed. It can be expected that linear-response models will become less accurate when modeling a retreat that traverses significant changes in the valley geometry. Thus, while the 3-stage model succeeded here in modeling time-varying glacier retreat, more complex geometries may call for at least SIA or higher-order flowline models.

2. In contrast to the close agreement of 3-stage and flowline model outputs, the distribution of responses associated with uncertainty in ice thickness, and thus timescale, is quite broad (Fig. 3.5). This is ultimately a simple result—adjusting the timescale, by construction, adjusts how quickly the glacier can respond to a climate change, and thus how much it lags a trend. However, because this lag is unyielding, errors related to the response timescale are persistent, and necessarily bear upon estimates of current disequilibrium and projections of future retreat.

3. Random, interannual climate variability introduces several complications when modeling transient glacier retreat. Terminus fluctuations due to a noisy mass balance history imply an uncertainty in initial conditions, but the effects of an initial length perturbation decay and are of negligible significance after a few multiples of τ. However, a noisy climate can also have persistent impacts on modeled glacier responses, because mass balance variability and glacier fluctuations mean that estimates of glacier parameters are subject to sampling errors. Even with multi-decade running means, substantial year-to-year variability can mean non-trivial uncertainty in the mean value of τ (Fig.

3.6c), and thus the degree of disequilibrium. Finally, length responses to an ensemble of noisy, warming climates demonstrate that, while climate variability can cause glacier retreat to slow or even reverse for a short period, the terminus does indeed fluctuate around its lagged, not equilibrium, trajectory (Fig. 3.6a). So, while climate variability inevitably clouds our metrics for quantifying it, glacier disequilibrium should be considered a robust phenomenon in the global aggregate, and as the warming trend continues.

While individual glacier dynamics can be quite complicated, a simple lesson from our work is clear: mountain glaciers with multi-decadal response times are among the many components of the climate system whose modern state is one of both realized and committed change. We have already witnessed significant glacier retreat over the past century but the disequilibrium of these systems with the modern climate means that responses to continued climate warming are inextricably compounded by ongoing adjustment to the warming of the past decades. However, if estimates of the glacier timescale, length sensitivity, and the warming trend are available, current disequilibrium can be accounted for when calibrating models and interpreting observations. The basic behavior and dependencies discussed here can provide a framework for refining reconstructions of past climate, estimates of current glacier state, and projections of future glacier retreat.

3.7 Acknowledgements

We thank three anonymous reviewers for thorough and thoughtful comments that helped us clarify the manuscript. We are also grateful to Benjamin Smith (Applied Physics Laboratory, U. Washington) for assistance with and access to modeling resources; and to the scientific editor, Ralf Greve, for helpful comments and effective handling of the manuscript. JEC was supported by the National Science Foundation Graduate Research Fellowship Program (DGE-1256082).

BIBLIOGRAPHY

Adhikari, S. and Marshall, S. J. (2011). Improvements to shear-deformational models of glacier dynamics through a longitudinal stress factor. *Journal of Glaciology*, 56(206):1003–1016.

Adhikari, S. and Marshall, S. J. (2013). Influence of high-order mechanics on simulation of glacier response to climate change: Insights from Haig Glacier, Canadian Rocky Mountains. *Cryosphere*, 7(5):1527–1541.

Armour, K. C. and Roe, G. H. (2011). Climate commitment in an uncertain world. *Geophysical Research Letters*, 38(1).

Bahr, D. B., Dyurgerov, M., and Meier, M. F. (2009). Sea-level rise from glaciers and ice caps: A lower bound. *Geophysical Research Letters*, 36(3).

Budd, W. F., Keage, P. L., and Blundy, N. A. (1979). Empirical studies of ice sliding. *Journal of Glaciology*, 23(89):157–170.

Carturan, L., Filippi, R., Seppi, R., Gabrielli, P., Notarnicola, C., Bertoldi, L., Paul, F., Rastner, P., Cazorzi, F., Dinale, R., and Dalla Fontana, G. (2013). Area and volume loss of the glaciers in the Ortles-Cevedale group (Eastern Italian Alps): Controls and imbalance of the remaining glaciers. *Cryosphere*, 7(5):1339–1359.

Cuffey, K. and Paterson, W. (2010). *The physics of glaciers, 4th Edition*. Academic Press.

Deser, C., Phillips, A. S., Alexander, M. A., and Smoliak, B. V. (2014). Projecting North American climate over the next 50 years: Uncertainty due to internal variability. *Journal of Climate*, 27(6):2271– 2296.

Gagliardini, O., Zwinger, T., Gillet-Chaulet, F., Durand, G., Favier, L., De Fleurian, B., Greve, R., Malinen, M., Martín, C., Räback, P., Ruokolainen, J., Sacchettini, M., Schäfer, M., Seddik, H., and Thies, J. (2013). Capabilities and performance of Elmer/Ice, a new-generation ice sheet model. *Geoscientific Model Development*, 6(4):1299–1318.

Glen, J. W. (1955). The creep of polycrystalline ice. *Proceedings of the Royal Society of London. Series A. Mathematical and Physical Sciences*, 228(1175):519–538.

Goldberg, D. N., Heimbach, P., Joughin, I., and Smith, B. (2015). Committed retreat of Smith, Pope, and Kohler Glaciers over the next 30 years inferred by transient model calibration. *Cryosphere*, 9(6):2429–2446.

Greve, R. and Blatter, H. (2009). *Dynamics of ice sheets and glaciers*. Springer Science & Business Media.

Hansen, J., Russell, G., Lacis, A., Fung, I., Rind, D., and Stone, P. (1985). Climate response times: Dependence on climate sensitivity and ocean mixing. *Science*, 47(159):659–664.

Harrison, W. D., Elsberg, D. H., Echelmeyer, K. A., and Krimmel, R. M. (2001). On the characterization of glacier response by a single time-scale. *Journal of Glaciology*, 47(159):659–664.

Harrison, W. D., Raymond, C. F., Echelmeyer, K. A., and Krimmel, R. M. (2003). A macroscopic approach to glacier dynamics. *Journal of Glaciology*, 49(164):13–21.

Hindmarsh, R. C. A. (2004). A numerical comparison of approximations to the Stokes equations used in ice sheet and glacier modeling. *Journal of Geophysical Research: Earth Surface*, 109(F01012).

Hutter, K. and Hughes, T. J. (1984). Theoretical Glaciology. *Journal of Applied Mechanics*.

IPCC (2013). Climate Change 2013: The Physical Science Basis. Contribution of Working Group I to the Fifth Assessment Report of the Intergovernmental Panel on Climate Change. Technical report, Cambridge.

Jóhannesson, T., Raymond, C., and Waddington, E. (1989). Time–Scale for Adjustment of Glaciers to Changes in Mass Balance. *Journal of Glaciology*, 35(121):355–369.

Jones, C., Lowe, J., Liddicoat, S., and Betts, R. (2009). Committed terrestrial ecosystem changes due to climate change. *Nature Geoscience*, 2(7):484–487.

Jouvet, G., Huss, M., Funk, M., and Blatter, H. (2011). Modelling the retreat of Grosser Aletschgletscher, Switzerland, in a changing climate. *Journal of Glaciology*, 57(206):1033–1045.

Le Meur, E., Gagliardini, O., Zwinger, T., and Ruokolainen, J. (2004). Glacier flow modelling: A comparison of the Shallow Ice Approximation and the full-Stokes solution. *Comptes Rendus Physique*, 5(7):709–722.

Leclercq, P. W., Oerlemans, J., Basagic, H. J., Bushueva, I., Cook, A. J., and Le Bris, R. (2014). A data set of worldwide glacier length fluctuations. *Cryosphere*, 8(2):659–672.

Leysinger Vieli, G. J.-M. C. and Gudmundsson, G. H. (2004). On estimating length fluctuations of glaciers caused by changes in climatic forcing. *Journal of Geophysical Research: Earth Surface*, 109(F1).

Lüthi, M. P. (2009). Transient response of idealized glaciers to climate variations. *Journal of Glaciology*, 55(193):918–930.

Lüthi, M. P., Bauder, A., and Funk, M. (2010). Volume change reconstruction of Swiss glaciers from length change data. *Journal of Geophysical Research: Earth Surface*, 115(4).

Mackintosh, A. N., Anderson, B. M., and Pierrehumbert, R. T. (2017). Reconstructing Climate from Glaciers. *Annual Review of Earth and Planetary Sciences*, 45:649–80.

Marzeion, B., Champollion, N., Haeberli, W., Langley, K., Leclercq, P., and Paul, F. (2017). Observation-Based Estimates of Global Glacier Mass Change and Its Contribution to Sea-Level Change. *Surveys in Geophysics*, 38(1):105–130.

Marzeion, B., Kaser, G., Maussion, F., and Champollion, N. (2018). Limited influence of climate change mitigation on short-term glacier mass loss. *Nature Climate Change*, 8(4):305–308.

Matthews, J. A. and Briffa, K. R. (2005). The 'Little Ice Age': Re-evaluation of an evolving concept. *Geografiska Annaler, Series A: Physical Geography*, 87(1):17–36.

Mauritsen, T. and Pincus, R. (2017). Committed warming inferred from observations. *Nature Climate Change*, 7(9):652–655.

Medwedeff, W. G. and Roe, G. H. (2017). Trends and variability in the global dataset of glacier mass balance. *Climate Dynamics*, 48(9-10):3085–3097.

Meehl, G. A., Washington, W. M., Collins, W. D., Arblaster, J. M., Hu, A., Buja, L. E., Strand, W. G., and Teng, H. (2005). How much more global warming and sea level rise? *Science*, 307(5716):1769–1772.

Mernild, S. H., Lipscomb, W. H., Bahr, D. B., Radić, V., and Zemp, M. (2013). Global glacier changes: A revised assessment of committed mass losses and sampling uncertainties. *Cryosphere*, 7(5):1565–1577.

Oerlemans, J. (1997). A flowline model for Nigardsbreen, Norway: projection of future glacier length based on dynamic calibration with the historic record. *Annals of Glaciology*, 24:382–389.

Oerlemans, J. (2007). Estimating response times of Vadret da Morteratsch, Vadret da Palü , Briksdalsbreen and Nigardsbreen from their length records. *Journal of Glaciology*, 53(182):357–362.

Oerlemans, J. J. (2001). *Glaciers and climate change*. A.A. Balkema Publishers.

Pattyn, F. (2002). Transient glacier response with a higher-order numerical ice-flow model. *Journal of Glaciology*, 48(162):467–477.

Paul, F., Kääb, A., Maisch, M., Kellenberger, T., and Haeberli, W. (2004). Rapid disintegration of Alpine glaciers observed with satellite data. *Geophysical Research Letters*, 31(21).

Price, S. F., Payne, A. J., Howat, I. M., and Smith, B. E. (2011). Committed sea-level rise for the next century from Greenland ice sheet dynamics during the past decade. *Proceedings of the National Academy of Sciences of the United States of America*, 108(22):8978–8983.

Rasmussen, L. A. and Conway, H. (2001). Estimating South Cascade Glacier (Washington, U.S.A.) mass balance from a distant radiosonde and comparison with Blue Glacier. *Journal of Glaciology*, 47(159):579–588.

Roe, G. H. (2011). What do glaciers tell us about climate variability and climate change? *Journal of Glaciology*, 57(203):567–578.

Roe, G. H. and Baker, M. B. (2014). Glacier response to climate perturbations: An accurate linear geometric model. *Journal of Glaciology*, 60(222):670–684.

Roe, G. H., Baker, M. B., and Herla, F. (2017). Centennial glacier retreat as categorical evidence of regional climate change. *Nature Geoscience*, 10(2):95–99.

Roe, G. H. and O'neal, M. A. (2009). The response of glaciers to intrinsic climate variability: observations and models of late-Holocene variations in the Pacific Northwest. *Journal of Glaciology*, 55(193):839–854.

Rupper, S., Schaefer, J. M., Burgener, L. K., Koenig, L. S., Tsering, K., and Cook, E. R. (2012). Sensitivity and response of Bhutanese glaciers to atmospheric warming. *Geophysical Research Letters*, 39(19).

Solomon, S., Plattner, G.-K., Knutti, R., and Friedlingstein, P. (2009). Irreversible climate change due to carbon dioxide emissions. *Proceedings of the National Academy of Sciences*, 106(6):1704–1709.

Weertman, J. (1964). The Theory of Glacier Sliding. *Journal of Glaciology*, 5(39):287–303.

WGMS (2017). Fluctuations of Glaciers Database. Technical report, World Glacier Monitoring Service, Zurich, Switzerland.

Wigley, T. M. (2005). The climate change commitment. *Science*, 307(5717):1766–1769.

Wigley, T. M. and Schlesinger, M. E. (1985). Analytical solution for the effect of increasing CO2 on global mean temperature. *Nature*, 315(6021):649–652.

Zekollari, H., Fürst, J. J., and Huybrechts, P. (2014). Modelling the evolution of Vadret da Morteratsch, Switzerland, since the Little Ice Age and into the future. *Journal of Glaciology*, 60(224):1155–1168.

Zekollari, H. and Huybrechts, P. (2015). On the climate-geometry imbalance, response time and volume-area scaling of an alpine glacier: Insights from a 3-D flow model applied to Vadret da Morteratsch, Switzerland. *Annals of Glaciology*, 56(70):51–62.

Chapter 4

DIFFERENCES IN THE TRANSIENT RESPONSE OF INDIVIDUAL GLACIERS: A CASE STUDY IN THE WASHINGTON CASCADES

Chapter 4, in full, is a manuscript in preparation for submission, authored by J Christian, E Carnahan, M Koutnik, G Roe, and E Whorton. The dissertation author was the primary investigator and author of this paper.

4.1 Abstract

Most mountain glaciers have response times from 10^1–10^2 years. Observed glacier changes necessarily depend on the response time, as do assessments about future change. We investigate variations in individual response times and transient responses for 383 glaciers in the Cascade mountains of Washington State, USA. We estimate a distribution of sub-decadal to multi-decadal response times times based on simple geometric arguments. Many of the largest glaciers in the Cascades have short response times due to steep slopes and low termini. This range of response times, while fairly typical, implies consequential differences in the transient response of individual glaciers. Applying recent analytical methods suggests that the glaciers in the Cascades with multi-decadal response times have only realized about half of their full response to anthropogenic warming, while those with short response times have remained close to equilibrium. Differences in the response time also have hydrological implications. A simple transient model for glacier runoff suggest that it has already peaked in the Cascades in response to anthropogenic warming, but the possibility of additional peaks depends on the response time. These variable transient responses arise simply from a range of different glacier geometries, and can thus be expected in other regions as well. These

effects should be considered when estimating parameters for poorly-observed glaciers, and simple geometric arguments can provide a first line of analysis.

4.2 Introduction

Glacier retreat over approximately the last century is one of the most prominent icons of anthropogenic climate change. At the global scale, glacier loss contributes substantially to sea level rise, but terminus retreat also has important impacts at local scales (Moore et al., 2009). Changes to seasonal streamflow, stream temperature, and geohazards can depend directly on the response of a few key glaciers. And despite the ubiquity of glacier retreat around the world (Leclercq et al., 2014) and confident attribution to climate change (Roe et al., 2017), differences exist in the scale and pace of observed retreat, even amongst glaciers in the same mountain range. Understanding the basis for these differences is thus important for understanding local observations and impacts, and is a prerequisite for making reliable projections.

In this study, we focus on differences associated with fundamental transient glacier dynamics. We estimate individual glacier response times based on geometric attributes provided in the Randolph Glacier Inventory version 6 (RGI Consortium, 2017, hereafter RGI6) We focus on the glaciers of the Cascade mountains of Washington State, USA, which have a long history of glaciological research, and which constitute important local resources. The goal of this study is not to produce a detailed simulation of these glaciers, but rather to assess, based on robust principles, how transient responses vary within the population of glaciers. To that end, we analyze elements of glacier change where the response times found in the Cascades imply a consequential range of behaviors for individual glaciers. These include the degree of disequilibrium with current climate, the response to climate variability, and changes in glacier runoff.

4.2.1 Theoretical background

The response time of the terminus position to climate variations is of fundamental importance in glacier dynamics. Numerous approaches to estimating the response time or "memory" exist. Analytical expressions can be derived from geometry and mass balance (e.g., Jóhannesson et al., 1989; Harrison et al., 2001) or geometry and velocity (e.g., Oerlemans, 2001). Alternatively, characteristic times can be estimated from terminus and climate observations (Harper, 1993; Oerlemans, 2007) or numerical model output (e.g., Leysinger Vieli and Gudmundsson, 2004; Zekollari et al., 2014, 2020). Essentially all of these approaches give response times on the order of 10^1–10^2 years for most mountain glaciers.

We use a response time τ proposed by Jóhannesson et al. (1989):

$$\tau = -H/b_t, \tag{4.1}$$

where H is a characteristic thickness and b_t is the (negative) annual mass balance rate near the glacier terminus. Eq. 4.1 is a straightforward reservoir timescale: τ depends on the volume associated with a given length change (H), and the input/output rates in the region where the change occurs (b_t). Furthermore, H and b_t implicitly capture the essential dynamics of a glacier in steady state: it has evolved towards the thickness and terminus position necessary for ice flow to balance the pattern of accumulation and melt imposed by the landscape and climate.

Simplified models have been developed on the assumption that these same dynamics—implicitly represented in the glacier geometry—govern climate-driven departures from steady state. We use a linear model for glacier length that assumes a response time given by Eq. 4.1 (Roe and Baker, 2014, hereinafter RB14). The model accurately captures transient terminus behavior for simple glacier geometries (RB14; see also Christian et al., 2018), and provides useful analytical solutions. Length anomalies ($L'(t)$) are described by a 3rd-order ordinary differential equation:

$$\left(\frac{d}{dt} + \frac{1}{\epsilon\tau}\right)^3 L' = \frac{\beta}{\epsilon^3\tau^2} b'(t). \tag{4.2}$$

Here, τ is defined as above; $b'(t)$ are surface-mass-balance anomalies; $\beta = A_{tot}/(wH)$ where A_{tot} is glacier area and w is width near the terminus; and $\epsilon = 1/\sqrt{3}$. It should be noted that τ is not an e-folding timescale in this model. Earlier models assumed length perturbations decay exponentially, but this implies an immediate reaction of the terminus and exaggerates the high-frequency components of glacier response; indeed the RB14 model was developed to overcome this limitation. The length sensitivity to mass balance perturbations is

$$\frac{L'}{b'} = \beta\tau = \frac{A_{tot}}{w\ b_t}, \tag{4.3}$$

which is a simple statement of mass conservation expressing the change in ablation area ($w\ L'$) that must accommodate a perturbation b' applied over the entire glacier (Jóhannesson et al., 1989).

An important consequence of ∼decadal response times in an era of anthropogenic warming is that glacier extents are far out of equilbrium with the current climate (e.g. Lüthi et al., 2010; Zekollari et al., 2014; Christian et al., 2018; Marzeion et al., 2018; Zekollari et al., 2020). Christian et al. (2018) applied the RB14 model to show that the degree of disequilibrium depends fundamentally on τ, and can be described by some simple metrics, illustrated in Fig. 1. If a linear mass-balance trend $b'(t) = \dot{b}t$ begins at $t = 0$, the transient terminus response (L') lags the *equilibrium response* (L'_{eq}, dashed line in Fig. 1a). Hereinafter, *disequilibrium* will refer to the length difference, $L' - L'_{eq}$ (Fig. 1b.). The RB14 model predicts that disequilibrium asymptotes to a constant:

$$L' - L'_{eq}|_{t\gg\tau} = 3\epsilon\tau^2\beta\dot{b}. \tag{4.4}$$

While this expression is a linear approximation, it shows three leading controls on disequilibrium: a factor of the response time ($3\epsilon\tau$), the sensitivity ($\tau\beta$), and the rate of forcing ($\dot{b}$). Disequilibrium, as defined here, is equivalent to the additional committed retreat if the climate were to stabilize at a given time.

Let *fractional equilibration* refer to the evolving ratio of L' to L'_{eq} (Fig. 1c). Length

sensitivity cancels, and so this depends only on τ and the time since the onset of forcing:

$$\frac{L'}{L'_{eq}} = 1 - \frac{3\epsilon\tau}{t}(1 - e^{-t/\epsilon\tau}) + e^{-t/\epsilon\tau}(\frac{t}{2\epsilon\tau} + 2). \tag{4.5}$$

This metric can be used to compare the state of glaciers independent of their sensitivities, or to scale observed retreats (L') to the equilibrium response (L'_{eq}), provided that τ and t can be estimated.

Equations 4.4 and 4.5 are approximations for the component of glacier change that is due to a long-term trend, but climate variability also affects glacier response. Direct observations of terminus position, surface mass balance, or geodetic changes will reflect a combination of these effects. One approach for disentangling them is to analyze sources of the variability, so that the background trends can be better understood (e.g., Harper, 1993; Christian et al., 2016; Bonan et al., 2019; Menounos et al., 2019). This study represents an alternative but complementary approach, which is to assume a simple forcing, and analyze the implications of basic glacier dynamics. We discuss the role of climate variability in a later section, but our central focus is on the century-scale response to climate forcing.

4.3 Response time estimates for the Washington Cascades

The Cascade mountains of Washington State, USA, have a temperate, maritime climate and the largest glacierized area in the contiguous USA (e.g., Fountain et al., 2017). Most of the range's largest glaciers are found on stratovolcanos: Mt. Baker, Glacier Peak, Mt. Rainier, and Mt. Adams (the smaller Mt. Saint Helens, which erupted in 1980, hosts much smaller glaciers). The four major volcanoes are the highest peaks in the Cascades, and their glaciers are characterized by large elevation spans and steep slopes. The non-volcanic peaks of the Cascades host smaller valley and cirque glaciers.

RGI6 reports 1709 glacier outlines for the Cascade range in Washington State. We consider only glaciers with a reported area greater than 0.1 km^2 *and* elevation span greater than 250 m, reducing the sample to 383 glaciers. RGI6 reports basic geometric parameters, but in general, observations of H and b_t exist for only a small fraction of glaciers and are

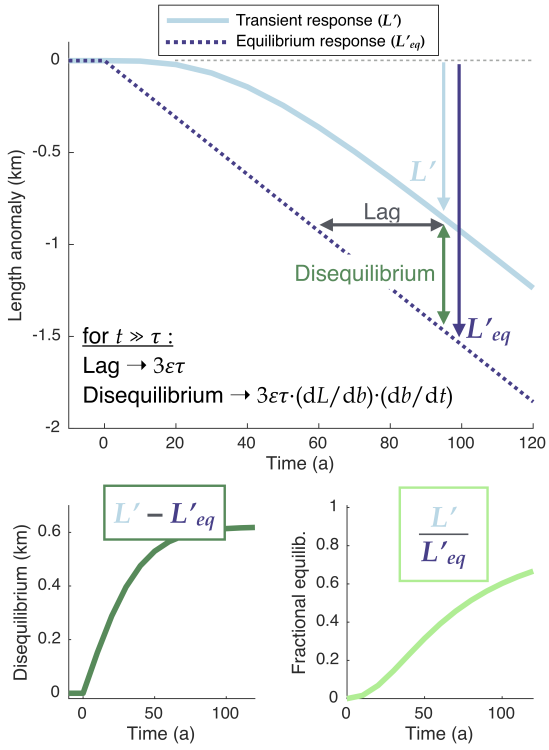

Figure 4.1: Schematic of idealized glacier retreat for a glacier with $\tau = 25$ yrs. Adapted from Christian et al. (2018), fig. 3. (a) Transient (solid) and equilibrium (dashed) length responses to a linear mass balance trend starting at $t = 0$. (b) Disequilibrium is defined as the difference between transient and equilibrium legnth responses, and corresponds to the additional committed retreat at any given time. (c) Fractional equilibration is defined as the ratio of transient to equilibrium responses.

not compiled in the inventory. Haeberli and Hoelzle (1995) and Hoelzle et al. (2007) used a simple algorithm to estimate H and b_t from inventory data, which we adapt here to the Cascades.

4.3.1 Response times

Because ice behaves as a nearly-plastic fluid, most glaciers have maximum basal shear stresses on the order of 10^5 Pa (e.g., Nye, 1952; Cuffey and Paterson, 2010). Thus, assuming a characteristic basal shear stress (S_b) for all glaciers, thickness is estimated on the basis of a glacier's average slope (α):

$$H = \frac{S_b}{f \rho_i g \sin \alpha} \tag{4.6}$$

where $f = 0.8$ is a shape factor, $\rho_i = 900$ kg m^{-3} is the density of glacier ice, and $g = 9.81$ m s^{-1} is gravitational acceleration. α is estimated by $\alpha = \arctan{(Z_{max} - Z_{min})/L_{max}}$ where altitudes (Z_{max}, Z_{min}) and length (L_{max}) are taken from RGI6.

We set $S_b = 1.5 \times 10^5$ Pa, which yields reasonable agreement with observational estimates of mean thickness (Table 1). Note that all but one of these constraints are for volcano glaciers with steep slopes ($\alpha \sim 17$–25°). The exception, South Cascade glacier, is quite flat for the region ($\alpha \sim 10^\circ$), and its thickness observations (maximum of ~ 200 m Hodge, 1979; Fountain, 1994) support that slope is indeed a key predictor for H. As τ is proportional to H in this framework (Eq. 4.1), this is also consistent with empirical studies demonstrating the impact of slope on response time (Leysinger Vieli and Gudmundsson, 2004; Zekollari et al., 2020).

We also considered the global-scale estimates of Huss and Farinotti (2012) (published in Farinotti et al., 2019), who used an inverse method to estimate distributed thickness from surface hypsometry. Their thickness maps agree well with observations on Mt. Baker and Mt. Rainier, but substantially underestimate thickness for South Cascade glacier, raising concerns about representation of other flat valley glaciers in the area. While distributed thicknesses offer major advantages for some applications, the global estimates are not optimized for the

Cascades, and more detailed glacier modeling would need to evaluate assumptions within the numerical estimates against local observations. We proceed with Eq. 4.1, as it focuses on a key geometric constraint (slope) and is commensurate with the simplicity of our analysis.

Figure 4.2a shows the estimated distribution of characteristic thicknesses for the 383 glaciers in our sample. The distribution peaks around 40 m, which is unsurprising for a collection of relatively small glaciers, and consistent with previous applications in other regions Hoelzle et al. (2007). The maximum estimate for H occurs on South Cascade Glacier (123 m), and only two others have estimates greater than 100 m. Again, recall that the method appears to capture a characteristic value closer to the mean than maximum thickness (Table 1).

To estimate b_t, we consider that a glacier is, most simply, a reservoir flowing through a mass balance gradient. To first order, b_t depends on the glacier's span across this gradient. Haeberli and Hoelzle (1995) and Hoelzle et al. (2007) estimated b_t by extrapolating a vertical mass balance gradient (db/dz) from the glacier's mean elevation ($\bar{Z}$) to its terminus (Z_t). We found slightly better agreement with observations when assuming that b_t is proportional to length:

$$b_t = -\frac{db}{dx}\frac{L}{2} \tag{4.7}$$

where db/dx is the mass-balance gradient along the glacier flowline, and L is the length reported by RGI6. In principle, this leaves room for non-elevation factors (e.g., topographic shading, avalanching, wind effects) to contribute to the mass balance profile.

Direct observations of mass balance exist for a handful of glaciers in the Washington Cascades (Table 2), but estimates of db/dz vary widely in the published literature and data. Several glaciers fall in a "typical" range ($\sim$ 5–10 m w.e. yr^{-1} km^{-1}), while gradients more than twice as steep are observed on South Cascade glacier (Meier and Tangborn, 1965; Meier et al., 1971; Baker et al., 2019), and estimates for Nisqually vary between early reports Meier et al. (1971) and recent monitoring Riedel and Larrabee (2015). Furthermore, vertical gradients are hard to constrain from very small glaciers (e.g., Sandalee and Noisy Creek glaciers).

We are left with a picture of uncertain and variable mass-balance gradients throughout the Cascades.

b_t is reported for an additional subset of glaciers (Table 2), and we find that using Eq. 4.7 with $db/dx = 3$ m w.e. yr^{-1} km^{-1} captures the heterogeneity in observed b_t slightly better than applying a vertically-defined gradient. Importantly, it captures the strongly-negative b_t ($\sim$ 5–10 m w.e. yr^{-1}) observed on relatively large glaciers with a range of geometries (e.g., compare South Cascade and Nisqually glaciers). However, a vertical gradient yields a similar overall distribution for the whole sample. We emphasize that in either case, errors may be substantial for individual glaciers.

Figure 4.2b shows the resulting distribution of b_t for the sample. The small scale of most glaciers gives modest values for b_t, while the volcanoes are responsible for the few glaciers with b_t near or exceeding 10 m w.e. yr^{-1}. An important caveat for some of these cases is that several glaciers on Mt. Rainier have extensive debris cover, which can lower melt rates (e.g., Moore et al., 2019). While observations do support strongly-negative b_t, our estimates are likely exaggerated for these glaciers.

Combining estimates of H and b_t yields estimates for τ, whose distribution is shown in Fig 1c. τ falls between 10 and 60 years for $> 90\%$ of glaciers. However the distribution weighted by glacier area (Fig. 1d) skews strongly towards shorter response times. Figure 1e shows the locations of individual glaciers, where the marker size indicates area and color indicates τ. The skewness of the area-weighted distribution is due in large part to the volcanoes, which constitute clusters of large, fast-responding glaciers. Their steep slopes and large spans contribute to small H and large (negative) b_t, and thus short response times. These tendencies on H and b_t are supported by observations, and short response times on the volcanoes have also been proposed based on terminus advances following a period of cool and wet weather in the mid-20th century (e.g., Harper, 1993; Pelto and Hedlund, 2001).

An important point for contextualizing these estimates is that the period of measurements on which they are based (including RGI6 geometries) are somewhat anachronistic. Dates for the RGI6 geometries range from 1959–1985 in this region, and most mass balance

observations correspond to only the last few decades. It is problematic that τ corresponds to an equilibrium geometry in theory, yet glacier observations are concentrated well after the onset of anthropogenic warming ($\sim$ 1880; e.g., IPCC, 2013). For how long is an estimate of τ valid? The answer almost certainly varies by glacier. Christian et al. (2018) showed that Eqs. 4.1 and 4.2 compared well with nonlinear numerical models over the course of a 200-year, 2° C warming for simple geometries. On the other hand, RB14 showed that the linear assumptions break down when the terminus traverses significant geometric variations (e.g. slope breaks). It must be borne in mind that τ will always be an inexact metric in the context of real glaciers undergoing large changes. Nevertheless, if focus is directed toward the basic physical tendencies captured by Eq. 4.1, it can be a useful metric for comparing the responses of glaciers with different attributes. Our estimates of τ, while uncertain for individual glaciers, set us up to investigate what the range of response times implies for the state of glaciers throughout the Washington Cascades.

4.4 Current disequilibrium

We now turn to the "fractional equilibration" metric (Eq. 4.5) to assess the adjustment of these glaciers to the anthropogenic climate trend that commenced in the late 19th century (e.g., IPCC, 2013). The climate anomaly acting on these glaciers over this time period can be decomposed into a linear trend component plus residual variability. We assume that the trend component captures the majority of anthropogenic forcing, and use the analytical solution from the RB14 model (Eq. 4.5) to analyze glacier responses as a function of τ. The following, then, is not a comprehensive reconstruction of glacier retreat, but analysis of how individual response times dictate a major component of glacier evolution in the Cascades. We discuss the role of climate variability and the assumption of linear forcing in the next section.

We would need additional constraints on length history or sensitivity to assess absolute length disequilibrium (Eq. 4.4) for all glaciers. However, fractional equilibration depends only on τ and the duration of the trend, so it allows us to compare glaciers with different

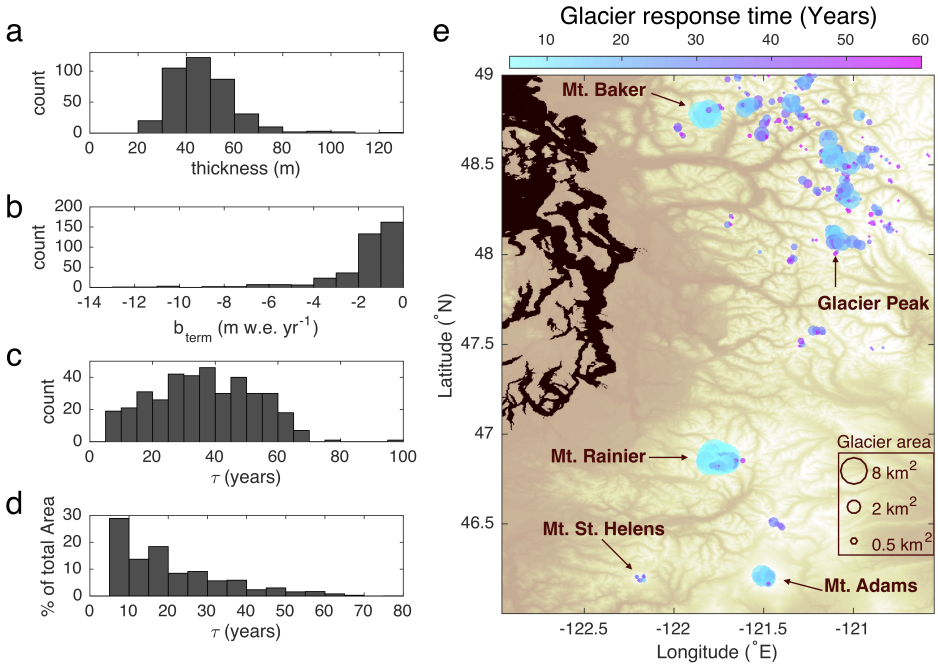

Figure 4.2: Estimated glacier parameters and response times. (a) Distribution of characteristic thickness using shear-stress scaling. (b) Estimated b_t, using $db/dx = 3$ m w.e. yr^{-1} km^{-1}. (c) Estimated response times according to Eq. 4.1. (d) As for (c), but weighted by glacier area reported by RGI. (e) Map of each glacier in our sample. Dot size corresponds to area and color indicates τ. Basemap is topography from the SRTM DEM.

Table 4.1: Comparison of published thickness constraints, numerical results from Huss and Farinotti (2012), and simple shear-stress scaling (Eq. 4.6). Glacier slopes are also shown for reference. Thickness observations come from [1]Driedger and Kennard (1986b), [2]Driedger and Kennard (1986a),[3]Harper (1992),[4]Hodge (1979),[5]Fountain (1994). Ranges for observed h_{max} correspond to histogram bin edges reported in ref. Driedger and Kennard (1986b). The first group are glaciers on Mt. Rainier, and the next are on Mt. Baker.

Glacier$^{(references)}$	Slope (°)	obs. (m)		Huss and Farinotti (2012)(m)		S_b scaling (m)
		$\bar{h}$	h_{max}	$\bar{h}$	h_{max}	H
Emmons$^{(1,2)}$	19	60	183–213	63	150	64
Winthrop$^{(1,2)}$	19	57	91–122	64	176	65
Tahoma$^{(1,2)}$	20	52	122–152	62	196	62
Carbon$^{(1,2)}$	17	90	213–244	79	242	74
Nisqually$^{(1,2)}$	25	48	91–122	56	131	50
Coleman$^{(3)}$	24	39	-	45	114	53
Easton$^{(3)}$	18	51	-	53	108	69
Rainbow$^{(3)}$	19	47	-	53	176	66
South Cascade$^{(2,4,5)}$	10	99	203	53	142	123

geometries and sensitivities. Figure 4.3a shows the evolution of fractional equilibration for all 383 glaciers, assuming a linear forcing beginning in 1880. Figure 4.3b shows the current (2020) distribution of fractional equilibration. The most important and general result is that a fairly typical range of response times implies a wide range in the equilibration of individual glaciers. For example, $\tau = 10$ yrs yields a fractional equilibration of 88% after 140 yrs, while $\tau = 40$ gives only 51%. In other words, the post-industrial retreats observed on fast-responding glaciers, such as those on the volcanoes, account for most of their full, equilibrium response to warming thus far. But observed retreats for those with *multi*decadal response

Table 4.2: Published mass-balance constraints for several glaciers with observations. Sources are [1]Meier and Tangborn (1965) [2]Meier et al. (1971) [3]Baker et al. (2019) [4]Riedel and Larrabee (2015) [5] Riedel and Larrabee (2018) [6]Tangborn et al. (1990) [7]Pelto and Hedlund (2001). Ranges are given where sources suggest different values. Italics indicate glaciers on volcanoes. Note that the observational intervals associated with published constraints vary.

Glacier$^{(references)}$	**observations**		**estimates**	
	db/dz	$-b_t$	$-b_t$ (db/dz = 6 m w.e. yr^{-1} km^{-1})	$-b_t$ (db/dx = 3 m w.e. yr^{-1}
South Cascade$^{(1,2,3)}$	17–22	5–6	1.9	5
Emmons$^{(4)}$	3.2	-	6.6	11.5
Nisqually$^{(2,4)}$	1.8–20	9	8.7	9.3
Noisy Creek$^{(5)}$	8.5	-	1.7	2.3
North Klawatti$^{(5,6)}$	5–8.3	4	3	4.1
Sandalee$^{(5)}$	2.4	-	1.6	1.2
Silver$^{(5)}$	6.3	-	1.2	2.5
Colonial$^{(7)}$	-	4.5	1.2	2
Columbia$^{(7)}$	-	4.5	1.3	2.4
Daniels$^{(7)}$	-	4	1.7	1.3
Easton$^{(7)}$	-	6.5	3.8	6.5
Foss$^{(7)}$	-	4.5	1.6	1.8
Honeycomb$^{(7)}$	-	6	3.3	6
Ice Worm$^{(7)}$	-	4	0.6	1
Kennedy$^{(7)}$	-	6	4.5	4.4
Lewis$^{(7)}$	-	2	0.8	0.8
Lower Curtis$^{(7)}$	-	5.5	1.3	1.7
Lyman$^{(7)}$	-	5	3.7	4.1
Lynch$^{(7)}$	-	4	1.3	1.9
Neve$^{(7)}$	-	4.5	2.8	4.8
Rainbow$^{(7)}$	-	5	3.5	5.8
Yawning$^{(7)}$	-	4	0.4	0.2

times might account for only half of the full response, implying additional committed retreat.

Well-observed glaciers can provide a case study for this disparity. Nisqually and South Cascade glaciers both have more than a century of length observations, and thickness and mass balance measurements provide more-direct constraints on their response times. We consider a plausible range for τ corresponding to the observational estimates of mean and maximum thickness (Table 1), and published values for b_t (Table 2). This gives a range of 5–14 yr for Nisqually, and 20–41 yr for South Cascade. The scaling method estimates 5 and 25 yr, respectively. Figure 4.3c shows the fractional equilibration for each, which are distinct despite uncertainty in τ. We can use current fractional equilibration to estimate their total committed retreat, based on their retreat histories. Leclercq et al. (2014) report a 2.2 km retreat over 1885–2001 for Nisqually and 1.8 km over 1900–2007 for South Cascade glacier. Taking these as L', we can use Eq. 4.5 to solve for L'_{eq} based on τ and t. For the range of τ described above, this implies 180–230 m of additional committed for Nisqually in 2001, and 730–2300 m for South Cascade in 2007 (Fig. 4.3d). For South Cascade glacier, the upper bound would mean much of the remaining glacier is lost. This is consistent with Rasmussen and Conway (2001), who estimated an "equilibrium topography" based on the pattern of mass balance, which was a small fraction of current area. We would expect Eq. 4.5 to break down for such large changes, but the point of this example is to demonstrate the severe disequilibrium implied by a multi-decadal response time, and the contrast with short (decadal) response times.

4.5 The role of climate variability

So far, we have only considered the glacier response to a simple trend in the mean climate since 1880. However, glaciers also integrate year-to-year variability, producing lower-frequency fluctuations (e.g. Oerlemans, 2001; Roe and Baker, 2014). Although the response to external climate forcing now exceeds these fluctuations virtually everywhere (Roe et al., 2017), fluctuations are still superimposed on the overall retreat. The disequilibrium associated with the long-term, forced trend (hereafter, the *forced* disequilibrium) must be

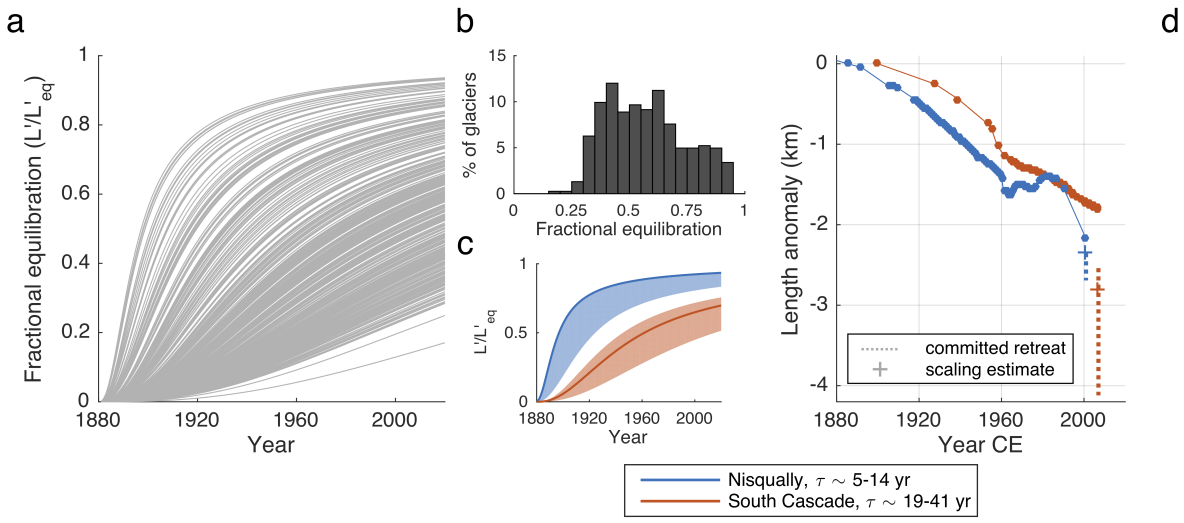

Figure 4.3: The ratio of transient to equilibrium length response evolves according to τ. (a) Fractional equilibration of each glacier (Eq. 4.5) assuming a climate trend began in 1880. (b) The distribution of L'/L'_{eq} today, 140 years into the forcing. A typical range of response times means a large range in current disequilibrium. (c) Fractional equilibration for Nisqually (blue) and South Cascade glaciers (red). The range shown corresponds to τ of 5–14 yr for Nisqually, and 20–41 yr for South Cascade, while the central line corresponds to the scaling estimate. (d) Fractional equilibration can be used to estimate the current equilibrium length based on observed retreat. Despite similar amounts of retreat over the last century, Nisqually and South Cascade glaciers have very different amounts of additional committed retreat. Dashed lines show the range corresponding to uncertainty in τ.

considered in context of these other fluctuations.

For mass balance anomalies b' consistent with white noise (i.e., equal power at all frequencies and no persistence), the RB14 model gives the standard deviation of length anomalies σ_L as

$$\sigma_L = \beta\tau \cdot \psi(\tau) \cdot \sigma_b \tag{4.8}$$

where σ_b is the standard deviation of b'; $\psi(\tau) = \sqrt{[(1-\kappa)(1+4\kappa^2+\kappa^4)]/(1+\kappa)^5}$; and $\kappa = 1 - \Delta t/\epsilon\tau$. Here, $\Delta t = 1$ yr and β, τ, and ϵ are defined as above. σ_L is a function of glacier sensitivity ($\beta\tau$), the damping caused by glacier memory ($\psi(\tau)$ is a decreasing function of τ), and the imposed climate variability (σ_b).

We illustrate these fluctuations with a synthetic example representative of conditions in the Cascades. A synthetic timeseries of b' is shown in Fig. 4.4a. A forced trend (dashed black) of $\dot{b} = 1$ m yr^{-1} century^{-1} begins in 1880. We add white-noise anomalies with $\sigma_b = 1$ m yr^{-1}, consistent with the 59-year record on South Cascade glacier (Baker et al., 2019). The trend thus has a signal-to-noise ratio (SNR) $\Delta b/\sigma_b = 1$ after one century of forcing. Note that b' corresponds to a fixed point or reference surface as opposed to glacier-averaged balance (often denoted B), and therefore includes no effects of changing glacier geometry.

Figure 4.4b shows the response of two idealized glaciers to this forcing, simulated with the RB14 model. We chose parameters giving $\tau = 12$ yr (orange) and 48 yr (blue) to compare relatively short and long response times. Bold lines show the response to the anomalies in Fig. 4.4a, while shading shows the $\pm 1\sigma_L$ bounds given by Eq. 4.8. Climate variability makes the "instantaneous" equilibrium L_{eq} harder to define, but we illustrate it here based on the forced trend (dashed lines). For real glaciers, it can be conceptualized as the long-term mean terminus position, were the external forcing trend to stop.

Recall that the forced disequilibrium approaches $3\epsilon\tau^2\beta\dot{b}$ for $t \gg \tau$ (Eq. 4.4), which is a decent approximation after ~ 140 years of anthropogenic forcing. Dividing Eq. 4.4 by Eq. 4.8 gives a ratio of the long-term forced disequilibrium to the standard deviation of natural

terminus variability. The sensitivity $\beta\tau$ cancels, leaving

$$\frac{3\epsilon\tau}{\psi(\tau)}\frac{\dot{b}}{\sigma_b}. \tag{4.9}$$

The first ratio is an increasing function of τ, and $\dot{b}/\sigma_b$ is the ratio of the forced change in b to the natural variability (i.e., the SNR per unit time, 1 century^{-1} above). Figure 4.4c shows Eq. 4.9 for fixed $\dot{b}/\sigma_b$. A typical range of response times encompasses disequilibrium that can be easily obscured by natural fluctuations, or stand well beyond them. For the synthetic glaciers, the forced disequilibrium is roughly $1\sigma_L$ and $9\sigma_L$ by 2020 (orange and blue stars). $\dot{b}/\sigma_b$ may vary somewhat by glacier, but mass balance anomalies are generally quite regionally coherent (Pelto, 2006; Huybers and Roe, 2009). Roe et al. (2017) found a range from roughly 0.5 to 2 century^{-1} around the world, which we show for reference (dotted lines).

The point remains that the *forced* disequilibrium stands clear of natural fluctuations for glaciers with multi-decade response times, but can obscured for those with short response times. This also helps put the differences in fractional equilibration (Fig. 4.3) in a more practical light. One may ask: if climate change paused today, would we notice the additional committed retreat in the coming decades? The answer is a clear *yes* for multi-decadal response times, but a careful accounting of climate variability would be needed for short response times.

4.5.1 A hiatus in forcing?

The above analyses assume that the external forcing is described by a linear trend, but global-mean temperature records show a hiatus in warming roughly from the 1940s to 1970s (e.g., IPCC, 2013). Records in the Pacific Northwest are noisier, but show a similar pattern which may be enhanced by modes of natural variability, such as the Pacific Decadal Oscillation (Mantua et al., 1997). Figure 4.4c shows April–September mean temperature from the Berkeley Earth dataset (Rohde et al., 2013) at a grid point in the North Cascades (121.5° W, 48.5° N). October–March precipitation from Matsuura and Willmott (2018) is also shown,

indicating slightly wetter conditions as well. The combined effect was favorable for glacier mass balance (Rasmussen, 2009) and is the likely cause of a number of transient glacier advances in the Cascades (e.g., Hubley, 1956; Harper, 1993; Pelto and Hedlund, 2001).

Variations in 20th-century warming likely reflect a combination of internal climate variability and changes in external forcing, and attribution remains an active area of research (e.g., Hegerl et al., 2018). Some hiatus is nonetheless part of the climate history responsible for the recorded and current state of glaciers. The case of a noisy trend (Fig. 4.4a) is still instructive here: variations in decadal trends occur even in uncorrelated white noise (highlighted by the running mean) which can cause glaciers with short memories to advance (Fig. 4.4b). However, distinct phases of forcing are often invoked heuristically in the literature, and it is important to consider what this assumption implies for different glaciers. To illustrate the effects on disequilibrium, we consider a scenario where forcing since 1880 is broken into two linear trends separated by a constant climate from 1940–1970 (Fig. 4.4d). A 30-year hiatus is enough time for the glacier with $\tau = 12$ yrs to very nearly equilibrate, while the glacier with $\tau = 48$ yrs remains far out of equilibrium, and its retreat rate is essentially unchanged. While we are not proposing that a step-wise trend is the optimal model, Fig. 4.4d simply illustrates that τ limits how much a glacier can adjust to multi-decadal changes in the rate of forcing, whatever their source. Previous studies have proposed long response times as the reason that some glaciers failed to advance during the 1940s–1970s (Pelto and Hedlund, 2001; Rasmussen and Conway, 2001), and our estimates for τ are certainly consistent with this idea.

4.5.2 Uncertainties in current equilibration

In Fig. 4.5, we consider how the variations discussed above affect estimates of the current state. We compare three potential sources of error in fractional equilibration: interannual climate variability; a hiatus in 20th century warming; and uncertainty in τ itself.

First, if we assume L'_{eq}, is still described by a linear trend but allow for a spread in L' due to variability, the spread in fractional equilibration is $\frac{L' \pm \sigma_L}{L'_{eq}}$. For the synthetic glaciers,

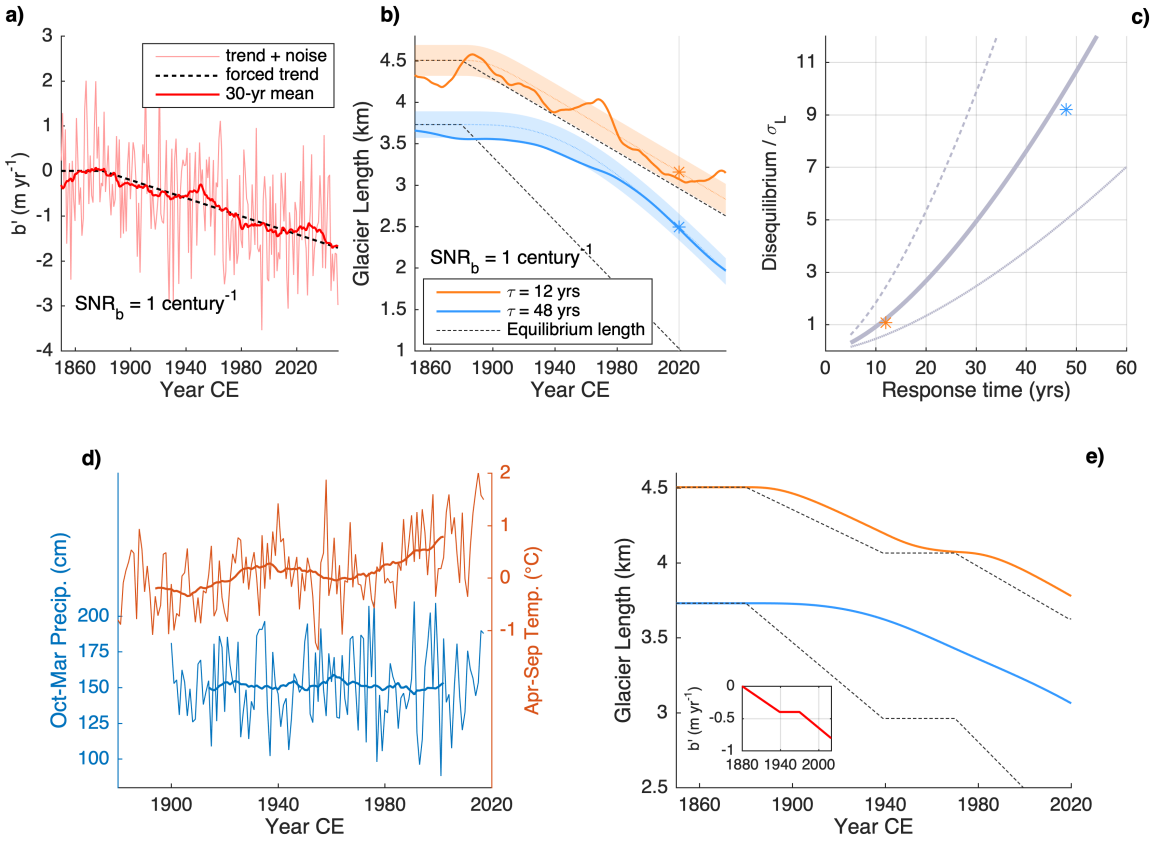

Figure 4.4: a) A synthetic mass balance forcing of a linear trend starting in 1880 (dashed line) plus white-noise anomalies. The trend has a signal-to-noise ratio (SNR_b) of 1 after one century. The bold red line shows the 30-year running mean. b) Length responses to (a) for glaciers with τ = 12 yrs (orange) and 48 yrs (blue). Shaded regions correspond to $\pm 1\sigma_L$ bounds around the response to the trend. Dashed black lines show equilibrium response (without variability). c) The relationship between disequilibrium and σ_L in the limit $t \gg \tau$. The solid line is for SNR_b = 1 century^{-1}, and stars correspond to the 2020 glacier states in (b). Dashed lines show relationship for SNR_b = 0.5 and 2 century^{-1}. d) Melt-season temperature from Rohde et al. (2013) and April–September precipitation from Matsuura and Willmott (2018) for the northwest slope of the Cascades ($\sim$ 121° W, 48.5° N). 30-year running means are shown with bold lines. e) Length responses of the idealized glaciers to a mass balance trend with a 30-year hiatus (inset). Dashed lines show the equilibrium response

fig. 4.5a shows this spread (shaded bounds), as well as L'/L'_{eq} for the particular realization of noise in Fig 4.4a–b. σ_L swamps $\frac{L' \pm \sigma_L}{L'_{eq}}$ early on, when L' and L'_{eq} are small. As expected from Fig. 4.4, the uncertainty in *current* fractional equilibration is greater for short response times, because forced disequilibrium can be overwhelmed by natural terminus variations.

Next, Fig. 4.5b compares L'/L'_{eq} for the trend with a hiatus (solid lines) verses a linear trend (dashed lines). Fractional equilibration increases more rapidly during the hiatus (L'_{eq} stops changing), but tends back toward the linear case after a few decades. While the glacier with $\tau = 12$ yr nearly equilibrates during the hiatus, it regains its (small) level of forced disequilibrium quickly. The result for both glaciers is that, provided a hiatus was several decades ago, the effects on current fractional equilibration are small. L'/L'_{eq} is simply dominated by the total forcing and response since 1880.

Finally, uncertainty in τ leads to a persistent uncertainty in disequilibrium and fractional equilibration (Christian et al., 2018). Available observations suggest that for individual glaciers, a substantial range in τ should be considered. Even for those with direct observations, the ambiguity in defining a "characteristic" thickness implies a conservative a range from $\bar{h}$ to h_{max}, which is often a factor of 2 or more (Table 1). Errors in b_t may be similar without direct observations (especially for small b_t; Table 2). Thus, Figure 4.5c shows a very broad spread in τ of $\pm 50\%$ (i.e., a factor of 3 between upper and lower bounds). In contrast to errors from neglecting short-term fluctuations, uncertainty in τ is more consequential for long response times.

Fig. 4.5 shows three qualitatively different uncertainties associated with our approach to estimating the current equilibration of glaciers in the Cascades. These synthetic examples suggest that simplifying the external forcing to a linear trend is a reasonable approach for estimating the equilibration to the *total* anthropogenic forcing thus far. The caveat, of course, is that forced disequilibrium simply never emerges far from the noise for glaciers with very short response times (Fig. 4.4c). For glaciers with longer response times, the more serious issue for estimating disequilibrium with current climate is uncertainty in individual response times.

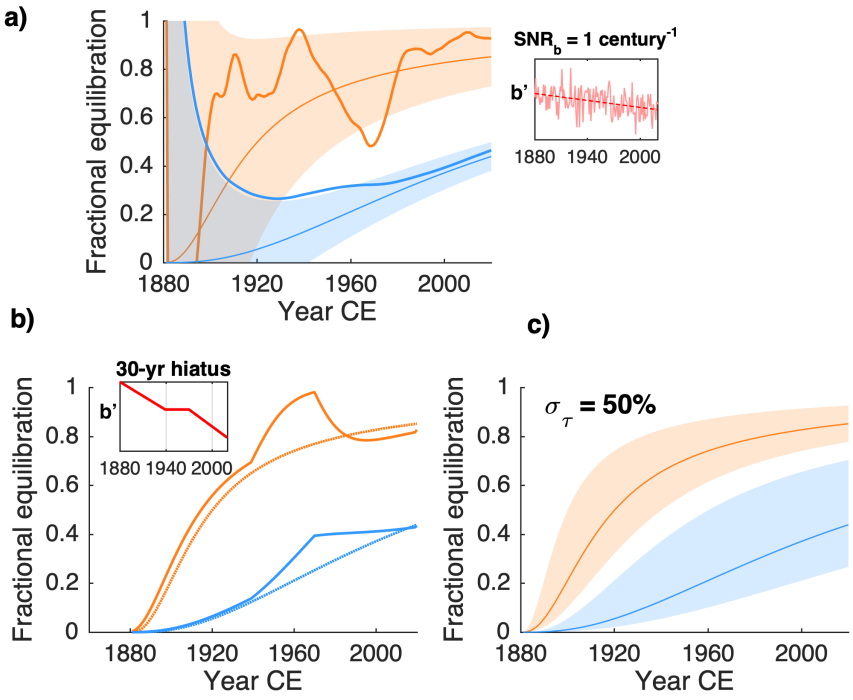

Figure 4.5: Errors in estimated fractional equilibration (L'/L'_{eq}) from three different sources. a) Climate variability drives natural glacier fluctuations, which temporarily drive a glacier towards or away from its long-term equilibrium length. Shaded bounds correspond to $\frac{L'\pm 1\sigma_L}{L'_{eq}}$ for glaciers with τ = 12 yr (orange) and 48 yr (blue). b) L'/L'_{eq} for the case with a forcing hiatus from 1940–1970. The difference compared to a linear forcing (dotted lines) is significant during the hiatus, but minimal after a few decades of resumed forcing. c) The spread in L'/L'_{eq} for a range of $\pm 50\%$ in τ. Uncertainty in the response time means persistent uncertainty in fractional equilibration.

4.6 Runoff changes

For a final analysis, we consider the role of response times in changes to melt-season glacier runoff, which is an important source of late-summer streamflow for some drainages in the Cascades (e.g., Riedel and Larrabee, 2016). Trends in total streamflow also depend on snowpack, prepitation, and other factors, but we focus on here on the glacier contribution. A common expectation is that climate warming causes glacier runoff to increase initially, and later decline as glacier area diminishes, leading to the concept of "peak runoff" in glacierized watersheds (e.g. Jansson et al., 2003). This phenomenon depends fundamentally on transient glacier dynamics. Recently, Carnahan et al. (2019) showed that, over a wide range of parameters, peak glacier runoff simulated with a numerical model occurred $\sim 1\tau$ after the onset of a climate trend. They estimated τ using a metric very similar to Eq. 4.1 (see Harrison et al., 2001). Their findings imply that a peak in runoff associated with the onset of anthropogenic warming in the late 19th century has long-since passed for glaciers in the Washington Cascades. However, as discussed above, the forcing has been noisy, and glacier retreat variable. Recent simulations show a complex picture of glacier runoff changes in the Pacific Northwest, both in time and between watersheds (Frans et al., 2018).

We do not address all aspects of these variations here, but we can illustrate some important considerations stemming from basic glacier dynamics. We consider a simple treatment of summer (i.e., melt-season) runoff Q_s, which we assume is equivalent to negative summer mass balance b_s, integrated over the glacier's surface area:

$$Q_s(t) = \int_0^{x=L(t)} -\bar{w}\ b_s(x,t)\ dx. \tag{4.10}$$

x is the coordinate from the glacier head ($x = 0$) to terminus ($x = L$), and $\bar{w}$ is the width, assumed constant for the sake of illustration. We assume a linear mass balance gradient along the glacier surface ($\frac{db_s}{dx}$), and spatially-uniform mass balance anomalies $b'_s(t)$. In this case, the integral at time t simplifies to the area $\bar{w}\ L(t)$ multiplied by the mean value of b_s

between 0 and $L(t)$. Then, the runoff *anomaly* is

$$Q'_s(t) = -\bar{w}\ L(t)\frac{1}{2}\Big(b'_s(0,t) + b'_s(L(t),t)\Big). \tag{4.11}$$

Two competing tendencies cause a peak in response to warming: increased melt per area via more negative $b'_s(t)$), and decreased area for melt as $\bar{w}\ L(t)$ drops. Because area loss occurs at the terminus where melt rates are highest, this is a strong negative tendency once retreat spins up. However, $L(t)$ lags $b_s(t)$ because of the stage of thickness change that must precede length changes (Roe and Baker, 2014). Thinning with little area loss thus allows runoff to peak after the onset of forcing, before diminishing as retreat accelerates. Equation 4.11 is a simple way to capture the role of glacier dynamics in runoff changes, provided that $L(t)$ accurately reflects the phase lag between forcing and response.

Figure 4.6a shows runoff for the idealized retreat and trend in b_s . Again, $L(t)$ is given by the RB14 model. Peaks are at 15 and 49 years, consistent with the Carnahan et al. (2019) finding of peaks at $t \sim \tau$. Because the slower glacier takes longer to "spin up" to rapid retreat, its runoff peak is delayed and higher. While the runoff from real glaciers will certainly also depend on the details of mass balance and geometry, increased melt and glacier recession are the first-order controls widely discussed in the literature. This approximation gives us a way to analyze the part of runoff change that is due to transient glacier dynamics, via $L(t)$.

How do these dynamics apply when the forcing isn't a linear trend? In Fig. 4.6b, we again consider an idealized hiatus from 1940–1970. Recall that both glaciers continue retreating during this period, but the fast glacier nearly equilibrates, while the slow glacier's disequilibrium remains substantial (Fig. 4.4d). When the forcing resumes, only the fast glacier has a second peak in runoff. Because the slow glacier's retreat is barely interrupted (Fig. 4.4d), the negative tendency on runoff remains large enough to dominate over increased melt, and there is no second peak in runoff as forcing resumes.

It is clear that τ affects the timing of peak runoff (Carnahan et al., 2019). While this basic response implies that a peak associated with the onset of anthropogenic warming has

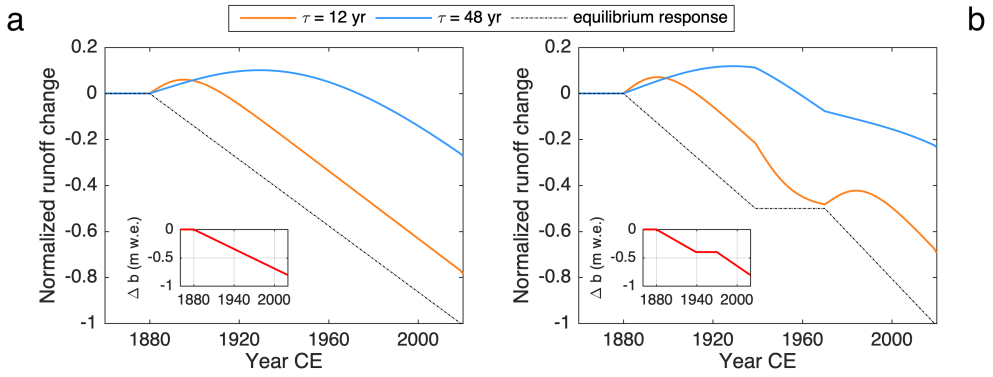

Figure 4.6: a) An idealized runoff curve for glaciers forced by a linear trend (inset). Runoff is normalized by the total change committed by the 2020 climate (dotted lines). Timing and peak of runoff depends on τ. (b) As for (a), but with a mid-century hiatus in forcing. Only the glacier with a short response time yields a second runoff peak when the trend resumes.

passed for glaciers in the Cascades, climate and glacier variability introduce the possibility of secondary peaks. Fig. 4.6b shows that τ also affects such secondary peaks, and suggests that we should not necessarily expect them for all glaciers - especially those that have retreated continuously over the industrial era.

Finally, it is worth noting that the committed retreat associated with glacier length disequilibrium (e.g., Fig 3d) means a committed loss of ablation area and thus of summer runoff. The dashed lines in 4.6a and b show the summer runoff associated with the equilibrium glacier length, illustrating the committed change as the forcing evolves. This, too, depends strongly on τ.

4.7 Summary and Discussion

We used geometric controls to estimate response times ($\tau = H/b_t$) for 383 glaciers in the Cascades. The scaling is based on robust assumptions: slope is a primary control on characteristic thickness (H), and total length is a primary control on mass balance near the terminus (b_t). Uncertainties are large for individual glaciers, but our main goal was to perform an overall survey of the region.

When calibrated to the few available thickness and mass-balance observations from the Cascades, the scaling yields a distribution of decadal-to-multidecadal response times (Fig. 2c), which is generally comparable to results for other mountain ranges (Haeberli and Hoelzle, 1995; Hoelzle et al., 2007; Zekollari et al., 2020). A result specific to the Cascades is that the largest glaciers, which reside on the major stratovolcanoes, tend to have very short response times ($\sim$ 10 years). This has been suggested previously based on observations of terminus behavior (Hubley, 1956; Harper, 1993; Pelto and Hedlund, 2001; Stevens et al., 2016). Our method for estimating τ frames this in terms of their steep slopes yielding thinner ice, and low termini yielding higher ablation rates.

Pelto and Hedlund (2001) estimated response times for 21 glaciers in the Cascades using multiple metrics including Eq. 4.1, although for most glaciers they took H as either 50 or 100 m depending on glacier shape. Our method offers an advance by taking advantage of RGI6 to estimate τ for more glaciers, and also applying the RB14 model to explore additional implications of these response times. However, our conclusions are qualitatively consistent with Pelto and Hedlund (2001), especially that different behaviors, linked to the response time, should be expected throughout the range.

Differentiating between fast and slow response times is important in the context of roughly a century of anthropogenic warming. We analyzed three issues where a typical range of response times implies markedly different interpretations for the fast and slow glaciers.

First, a glacier's disequilibrium with current climate, and its associated committed retreat, depends strongly on response time (Christian et al., 2018). We analyzed this for the Cascades using a fractional metric (Eq. 4.5), which is the ratio of the transient response (i.e., observed retreat) to the full equilibrium response to a climate trend. After $\sim$ 140 years of an anthropogenic forcing trend, there is a wide spread in this fractional equilibration amongst individual glaciers the Cascades (Fig. 3b). While uncertainties in τ are substantial, well-observed glaciers provide concrete examples of this disparity in disequilibrium between fast and slow glaciers. (Fig. 3d).

A glacier's response to natural climate variability is important context for this disequi-

librium, and also depends on the response time. After over a century of gradual forcing, the forced disequilibrium (i.e., that diven by a climate trend) of slower glaciers far outweighs fluctuations due to ongoing climate variability. For fast glaciers, noise-driven fluctuations can be similar in magnitude to long-term disequilibrium. Climate variability would thus be more important for interpreting the current state, or making near-term projections, of these fast glaciers. In the Cascades, this is an important consideration for the volcano glaciers.

We also considered an idealized hiatus in forcing. Whatever the ultimate source of multi-decadal variations in the forcing trend, the glacier response depends strongly on τ. The range of τ within the Cascades means that a steady-state or advance of one glacier does not necessarily mean a neighboring glacier is near steady state. This must be considered when initializing models any time after the onset of anthropogenic warming. Fortunately, simple considerations of the response time, as we have used here, could provide a first-order analysis when calibrating models.

Finally, a range of response times has implications for changes in glacier runoff. Based on the analyses of Carnahan et al. (2019), our estimates for τ imply that a peak associated with the onset of anthropogenic warming has passed for all glaciers in the Cascades. We applied a simple treatment of summer runoff to investigate the possibility of subsequent peaks following variations in forcing. Again, the response time plays a key role. Secondary peaks in runoff appear to require a response time short enough for the glacier to nearly equilibrate during an interruption in forcing. It follows that correctly accounting for the *disequilibrium* of slow glaciers during such a period would be important for capturing their ensuing runoff changes.

We might thus expect that multiple runoff peaks have occurred on faster glaciers in the Cascades over the industrial era, especially considering that some re-advanced in the mid 20th century. The simulations of Frans et al. (2018) do show rising runoff in several Cascades drainages after 1960. However, it is difficult to tell whether this reflects short glacier response times, because they initialized most glaciers assuming a steady state in the 1950s, and thus a peak in the following decades would be expected regardless of response time. A global-scale

study (Huss and Hock, 2018) estimated that peak glacier runoff in the Cascades' Skagit passed in the last few decades, but they began their analyses in 1980.

The concept of "peak runoff" in response to warming is physically robust, but quickly becomes nuanced when climate variability and a population of glaciers are considered. Our main point is that individual response times are almost certain to play a role. Given the onset of anthropogenic warming in the late 19th century (IPCC, 2013), an interesting question for future research would be whether peaks in glacier runoff in the late 20th Century (or later) reflect long glacier response times, secondary peaks associated with climate variability, model assumptions, or some other process.

These principles may be useful to apply to future variations in runoff, too. Decadal trends in future local climate are highly uncertain due to internal climate variability (e.g., Hawkins and Sutton 2009; Deser et al., 2012). However, better understanding the response times and disequilibrium of the glaciers contributing most to runoff may help characterize how volatile runoff will be in response to future variability.

Our analyses also point to some suggestions for future observations. Fractional uncertainty in τ has more consequential effects for large τ in terms of estimating the current state (Fig. 4.5). Thus, simple estimates like ours can be used to point to glaciers where new observations of thickness or mass balance might be most effective at reducing uncertainty in regional assessments. On the other hand, for some impacts such as runoff change, priority might simply be a function of glacier size. For large glaciers with short response times, as are found on the Cascade Volcanoes, constraining the patterns of mass balance and overall sensitivity might be more important for predicting future change.

A final point follows from the variable mass balance gradients observed in the Cascades (Table 2). Some of this variability could be related to small or atypical geometries and the maritime setting of the Cascades, but a range of gradients can be expected for unmeasured glaciers around the world. It is important to emphasize that the response time and length sensitivity are directly related to the mass balance gradient. This is built in to the geometric scaling we used to estimate τ, but also affects the response of numerical models that don't

rely on a stipulated response time. At the same time, equilibrium length and thickness are not highly sensitive to the mass balance gradient, provided the equilibrium line is correct. This point has been made before (Oerlemans, 2001), but is worth reemphasizing. In the context of tuning models, it follows that mass-balance gradients are not tightly constrained by matching glacier-wide mass balance an observed glacier geometry.

Progress has been made in estimating ice thicknesses around the world (e.g. Farinotti et al., 2019), but mass balance gradients are another important factor to consider for modeling large population of glaciers. Fortunately, existing observations indicate that a glacier's mass balance profile is fairly constant from year to year, despite any variability in glacier-wide balance (Oerlemans, 2001). Progress in constraining gradients on high-priority glaciers, and the heterogeneity within a region, might thus be possible from observations on a relatively short time frame. Additionally, advances in calculating geodetic changes from satellite data at sub-annual timescales (David Shean, personal communication) might also help constrain the patterns of mass balance, and thus important glacier response characteristics, across a region.

ACKNOWLEDGMENTS

JEC was supported by the NSF Graduate Research Fellowship Program (DGE-1256082), including a Graduate Research Internship at the USGS Washington Water Science Center in Tacoma, WA. JEC thanks Andrew Fountain for helpful perspective on Cascades inventories, and Shad O'Neel for welcoming and insightful conversation at the Alaska Climate Science Center. Jon Riedel and Mike Larrabee generously provided stake data for glaciers monitored by the National Park Service. We are grateful to many individuals from USGS, NPS, and Nichols College (MA) for their dedication to mass-balance monitoring in the Cascades.

BIBLIOGRAPHY

Baker, E. H., McNeil, C. J., Sass, L. C., Peitzsch, E. H., Whorton, E. N., Florentine, C. E., Clark, A. M., Miller, Z. S., Fagre, D. B., and O'Neel, S. (2019). USGS Benchmark Glacier Mass Balance and Project Data. Technical report, US Geological Survey, Alaska Science Center, AK, USA.

Bonan, D. B., Christian, J. E., and Christianson, K. (2019). Influence of North Atlantic climate variability on glacier mass balance in Norway, Sweden and Svalbard. *Journal of Glaciology*, 65(252):580–594.

Carnahan, E., Amundson, J. M., and Hood, E. (2019). Impact of glacier loss and vegetation succession on annual basin runoff. *Hydrol. Earth Syst. Sci*, 23:1667–1681.

Christian, J. E., Koutnik, M., and Roe, G. (2018). Committed retreat: controls on glacier disequilibrium in a warming climate. *Journal of Glaciology*, 64(246):675–688.

Christian, J. E., Siler, N., Koutnik, M., and Roe, G. (2016). Identifying dynamically induced variability in glacier mass-balance records. *Journal of Climate*, 29(24):8915–8929.

Cuffey, K. M. and Paterson, W. S. B. (2010). *The physics of glaciers, 4th Edition*. Academic Press.

Driedger, C. L. and Kennard, P. (1986a). Glacier volume estimation on Cascade volcanoes: an analysis and comparison with other methods. *Annals of Glaciology*, 8:59–64.

Driedger, C. L. and Kennard, P. M. (1986b). Ice volumes on Cascade volcanoes: Mount Rainier, Mount Hood, Three Sisters, and Mount Shasta. Technical report, US Geological Survey.

Farinotti, D., Huss, M., Fürst, J. J., Landmann, J., Machguth, H., Maussion, F., and Pandit, A. (2019). A consensus estimate for the ice thickness distribution of all glaciers on Earth. *Nature Geoscience*, 12(3):168–173.

Fountain, A. G. (1994). Borehole water-level variations and implications for the subglacial hydraulics of South Cascade Glacier, Washington State, USA. *Journal of Glaciology*, 40(135):293–304.

Fountain, A. G., Glenn, B., and Basagic IV, H. J. (2017). The geography of glaciers and perennial snowfields in the American West. *Arctic, Antarctic, and Alpine Research*, 49(3):391–410.

Frans, C., Istanbulluoglu, E., Lettenmaier, D. P., Fountain, A. G., and Riedel, J. (2018). Glacier recession and the response of summer streamflow in the Pacific Northwest United States, 1960–2099. *Water Resources Research*, 54(9):6202–6225.

Haeberli, W. and Hoelzle, M. (1995). Application of inventory data for estimating characteristics of and regional climate-change effects on mountain glaciers: a pilot study with the European Alps. *Annals of Glaciology*, 21:206–212.

Harper, J. T. (1992). *The Dynamic Response of Glacier Termini to Climatic Variation during the Period 1940-1990 on Mount Baker, Washington, USA*. PhD thesis, Western Washington University.

Harper, J. T. (1993). Glacier terminus fluctuations on Mount Baker, Washington, USA, 1940–1990, and climatic variations. *Arctic and Alpine Research*, 25(4):332–340.

Harrison, W., Elsberg, D., Echelmeyer, K., and Krimmel, R. (2001). On the characterization of glacier response by a single time-scale. *Journal of Glaciology*, 47(159):659–664.

Hegerl, G. C., Brönnimann, S., Schurer, A., and Cowan, T. (2018). The early 20th century warming: anomalies, causes, and consequences. *Wiley Interdisciplinary Reviews: Climate Change*, 9(4):e522.

Hodge, S. M. (1979). Direct Measurement of Basal Water Pressures: Progress and Problems. *Journal of Glaciology*, 23(89):309–319.

Hoelzle, M., Chinn, T., Stumm, D., Paul, F., Zemp, M., and Haeberli, W. (2007). The application of glacier inventory data for estimating past climate change effects on mountain glaciers: a comparison between the European Alps and the Southern Alps of New Zealand. *Global and Planetary Change*, 56(1-2):69–82.

Hubley, R. C. (1956). Glaciers of the Washington Cascade and Olympic Mountains; their present activity and its relation to local climatic trends. *Journal of Glaciology*, 2(19):669–674.

Huss, M. and Farinotti, D. (2012). Distributed ice thickness and volume of all glaciers around the globe. *Journal of Geophysical Research: Earth Surface*, 117(F4).

Huss, M. and Hock, R. (2018). Global-scale hydrological response to future glacier mass loss. *Nature Climate Change*, 8(2):135–140.

Huybers, K. and Roe, G. H. (2009). Spatial patterns of glaciers in response to spatial patterns in regional climate. *Journal of Climate*, 22(17):4606–4620.

IPCC (2013). Climate Change 2013: The Physical Science Basis. Contribution of Working Group I to the Fifth Assessment Report of the Intergovernmental Panel on Climate Change. Technical report, Cambridge.

Jansson, P., Hock, R., and Schneider, T. (2003). The concept of glacier storage: a review. *Journal of Hydrology*, 282(1-4):116–129.

Jóhannesson, T., Raymond, C., and Waddington, E. (1989). Time–scale for adjustment of glaciers to changes in mass balance. *Journal of Glaciology*, 35(121):355–369.

Leclercq, P. W., Oerlemans, J., Basagic, H. J., Bushueva, I., Cook, A., and Le Bris, R. (2014). A data set of worldwide glacier fluctuations. *The Cryosphere*, 8:659–672.

Leysinger Vieli, G.-M. and Gudmundsson, G. H. (2004). On estimating length fluctuations of glaciers caused by changes in climatic forcing. *Journal of Geophysical Research: Earth Surface*, 109(F1).

Lüthi, M. P., Bauder, A., and Funk, M. (2010). Volume change reconstruction of Swiss glaciers from length change data. *Journal of Geophysical Research: Earth Surface*, 115(F4).

Mantua, N. J., Hare, S. R., Zhang, Y., Wallace, J. M., and Francis, R. C. (1997). A Pacific interdecadal climate oscillation with impacts on salmon production. *Bulletin of the american Meteorological Society*, 78(6):1069–1080.

Marzeion, B., Kaser, G., Maussion, F., and Champollion, N. (2018). Limited influence of climate change mitigation on short-term glacier mass loss. *Nature Climate Change*, 8(4):305–308.

Matsuura, K. and Willmott, C. J. (2018). Terrestrial Precipitation: 1900-2017. Gridded Monthly Time Series. http://climate.geog.udel.edu/ climate/html_pages/Global2017/README.GlobalTsP2017.html. Accessed 25 Mar, 2020.

Meier, M. F. and Tangborn, W. V. (1965). Net budget and flow of South Cascade glacier, Washington. *Journal of Glaciology*, 5(41):547–566.

Meier, M. F., Tangborn, W. V., Mayo, L. R., and Post, A. (1971). Combined ice and water balances of Gulkana and Wolverine Glaciers, Alaska, and South Cascade Glacier, Washington, 1965 and 1966 hydrologic years. Technical report, US Geological Survey.

Menounos, B., Hugonnet, R., Shean, D., Gardner, A., Howat, I., Berthier, E., Pelto, B., Tennant, C., Shea, J., Noh, M.-J., et al. (2019). Heterogeneous changes in western North American glaciers linked to decadal variability in zonal wind strength. *Geophysical Research Letters*, 46(1):200–209.

Moore, P. L., Nelson, L. I., and Groth, T. M. (2019). Debris properties and mass-balance impacts on adjacent debris-covered glaciers, Mount Rainier, USA. *Arctic, Antarctic, and Alpine Research*, 51(1):70–83.

Moore, R., Fleming, S., Menounos, B., Wheate, R., Fountain, A., Stahl, K., Holm, K., and Jakob, M. (2009). Glacier change in western North America: influences on hydrology, geomorphic hazards and water quality. *Hydrological Processes: An International Journal*, 23(1):42–61.

Nye, J. (1952). The mechanics of glacier flow. *Journal of Glaciology*, 2(12):82–93.

Oerlemans, J. (2001). *Glaciers and climate change*. CRC Press.

Oerlemans, J. (2007). Estimating response times of Vadret da Morteratsch, Vadret da Palü, Briksdalsbreen and Nigardsbreen from their length records. *Journal of Glaciology*, 53(182):357–362.

Pelto, M. S. (2006). The current disequilibrium of North Cascade glaciers. *Hydrological Processes: An International Journal*, 20(4):769–779.

Pelto, M. S. and Hedlund, C. (2001). Terminus behavior and response time of North Cascade glaciers, Washington, USA. *Journal of Glaciology*, 47(158):497–506.

Rasmussen, L. (2009). South Cascade Glacier mass balance, 1935–2006. *Annals of Glaciology*, 50(50):215–220.

Rasmussen, L. and Conway, H. (2001). Estimating South Cascade Glacier (Washington, USA) mass balance from a distant radiosonde and comparison with Blue Glacier. *Journal of Glaciology*, 47(159):579–588.

RGI Consortium (2017). Randolph glacier inventory–a dataset of global glacier outlines: Version 6.0. Technical report, Global Land Ice Measurements from Space, Colorado, USA.

Riedel, J. and Larrabee, M. (2015). Mount Rainier National Park glacier mass balance monitoring annual report, water year 2011: North Coast and Cascades Network. Technical report, National Park Service, Fort Collins, CO, USA.

Riedel, J. and Larrabee, M. (2018). North Cascades National Park Complex glacier mass balance monitoring annual report, water year 2013: North Coast and Cascades Network. Technical report, National Park Service, Fort Collins, CO, USA.

Riedel, J. L. and Larrabee, M. A. (2016). Impact of recent glacial recession on summer streamflow in the Skagit River. *Northwest Science*, 90(1):5–22.

Roe, G. H. and Baker, M. B. (2014). Glacier response to climate perturbations: an accurate linear geometric model. *Journal of Glaciology*, 60(222):670–684.

Roe, G. H., Baker, M. B., and Herla, F. (2017). Centennial glacier retreat as categorical evidence of regional climate change. *Nature Geoscience*, 10(2):95–99.

Rohde, R., Muller, R., Jacobsen, R., Muller, E., Perlmutter, S., Rosenfeld, A., Wurtele, J., Groom, D., and Wickham, C. (2013). A New Estimate of the Average Earth Surface Land Temperature Spanning 1753 to 2011. *Geoinformatics & Geostatistics: An Overview*, 1(1):1–7.

Stevens, C., Conway, H., Kennard, P., Rasmussen, L., and Koutnik, M. (2016). Glacier Retreat, Outburst Floods, and Kinematic Waves: Nisqually Glacier Changes Related to Climate. http://depts.washington.edu/pnwcesu/reports/P12AC15072_Final_Report.pdf, accessed 21 Aug, 2020.

Tangborn, W. V., Fountain, A. G., and Sikonia, W. G. (1990). Effect of area distribution with altitude on glacier mass balance–a comparison of North and South Klawatti Glaciers, Washington State, USA. *Annals of Glaciology*, 14:278–282.

Zekollari, H., Fürst, J. J., and Huybrechts, P. (2014). Modelling the evolution of Vadret da Morteratsch, Switzerland, since the Little Ice Age and into the future. *Journal of Glaciology*, 60(224):1155–1168.

Zekollari, H., Huss, M., and Farinotti, D. (2020). On the imbalance and response time of glaciers in the European Alps. *Geophysical Research Letters*, 47(2):e2019GL085578.

Chapter 5

THE CONTRASTING RESPONSE OF OUTLET GLACIERS TO INTERIOR AND OCEAN FORCING

Chapter 5, in full, is a reprint of "The contrasting response of outlet glaciers to interior and ocean forcing" authored by J Christian, A Robel, C Proistosescu, G Roe, M Koutnik, and K Christianson, as it appears in *The Cryosphere*, 2020. The dissertation author was the primary investigator and author of this paper.

5.1 Abstract

The dynamics of marine-terminating outlet glaciers are of fundamental interest in glaciology, and affect mass loss from ice sheets in a warming climate. In this study, we analyze the response of outlet glaciers to different sources of climate forcing. We find that outlet glaciers have a characteristically different transient response to surface-mass-balance forcing applied over the interior than to oceanic forcing applied at the grounding line. A recently developed reduced model represents outlet glacier dynamics via two widely-separated response timescales: a fast response associated with grounding-zone dynamics, and a slow response of interior ice. The reduced model is shown to emulate the behavior of a more complex numerical model of ice flow. Together, these models demonstrate that ocean forcing first engages the fast, local response, and then the slow adjustment of interior ice, whereas surface-mass-balance forcing is dominated by the slow interior adjustment. We also demonstrate the importance of the timescales of stochastic forcing for assessing the natural variability of outlet glaciers, highlighting that decadal persistence in ocean variability can affect the behavior of outlet glaciers on centennial and longer timescales. Finally, we show that these transient responses have important implications for: attributing observed glacier changes to natural

or anthropogenic influences; the future change already committed by past forcing; and the impact of past climate changes on the preindustrial glacier state, against which current and future anthropogenic influences are assessed.

5.2 Introduction

Marine-terminating outlet glaciers drain large portions of the Greenland and Antarctic ice sheets, conveying ice from interior catchments to the ocean. Their dynamic response to a changing climate is a critical component of projections of sea-level rise (e.g., Aschwanden et al., 2019), and dramatic increases in discharge over recent decades have been observed in Greenland (e.g., Howat et al., 2008; Moon and Joughin, 2008; Moon et al., 2012) and Antarctica (e.g., Pritchard et al., 2009; Miles et al., 2013; Cook et al., 2016). Ocean forcing is thought to play a major role in observed change (e.g., Nick et al., 2009; Joughin et al., 2012a; Straneo and Heimbach, 2013; Jenkins et al., 2016). Increased melt and runoff driven by atmospheric warming is also a major component of mass loss in Greenland (e.g., Van Den Broeke et al., 2009).

Yet despite the clear signals of mass loss from the Greenland and Antarctic ice sheets (Shepherd et al., 2018), observed changes in terminus positions, velocities, and ice thickness vary widely among marine-terminating outlet glaciers, especially in Greenland (e.g., Moon et al., 2014; Csatho et al., 2014). This makes it difficult to establish consistent links between forcing and response, which are critical for projections of future glacier and ice sheet change. Some reasons for the heterogeneity in glacier change have become clearer. For example, localized features in bedrock and fjord geometry can control differences in terminus retreat (Catania et al., 2018) and inland dynamic thinning (Felikson et al., 2017) for individual glaciers. Additionally, regional variations may be associated with differences in surface melt and subglacial hydrology (Moon et al., 2014), or the ocean waters with which the glaciers are in contact (Straneo et al., 2012). However, catchment-specific factors continue to pose a challenge where observations are limited, as well as for ice-sheet-wide simulations. Further observations will continue to be critical, but this heterogeneity between outlet glaciers is also

a strong motivation to investigate general principles at the same time, which can be expected to apply to a wide range of settings.

In this study, we focus on a principle common to all outlet glaciers: climate forcing predominantly comes either from the atmosphere, via changes to the surface mass balance in the interior catchment, or from the ocean via changes to ice discharge at the marine margin. Our approach is to conduct idealized model experiments that isolate key physical principles of transient glacier responses to climate. We use a recently-developed reduced model (Robel et al., 2018) and an established numerical ice-flow model (Pollard and Deconto, 2012) as complementary tools. The reduced model yields simple physical and mathematical interpretations of the numerical model's response to forcing. Additionally, the reduced model can efficiently generate ensembles of responses for statistical analyses.

We will focus exclusively on stable geometries. The marine-ice-sheet instability (e.g., Weertman, 1974; Schoof, 2007a) is of course a critical consideration for some catchments, especially in West Antarctica. However, understanding how a physical system approaches, or fluctuates around, a long-term equilibrium is a core analytical approach. This requires that we start with stable systems, but the resulting insights can often be applied to unstable regimes (e.g., Robel et al., 2019). The following section describes experiments that illustrate the fundamental system dynamics, and establish the key differences between ocean and interior forcing. We then present three cases that illustrate the implications of these principles for interpreting observations and predicting the future behavior of outlet glaciers.

5.3 Part 1: Dynamical responses to ocean and interior forcing

5.3.1 A simple outlet glacier system

Before describing the dynamic models, it is useful to begin with the geometry and basic flux-balance arguments of the system we are investigating. We consider an idealized stable outlet glacier, a schematic of which is presented in Fig. 5.1a (see also Schoof, 2007a; Robel et al., 2018). Ice enters as snow accumulation over the interior surface, flows from the

interior towards the ocean on a forward-sloping (prograde) bed, and exits the system where it reaches flotation at the grounding line. Beyond this point, floating ice is assumed to calve into icebergs or melt due to contact with the ocean.

Ice flux across the grounding line (Q_g) has long been known to be a sensitive function of local ice thickness (e.g., Weertman, 1974; Thomas, 1979; Lingle, 1984; Schoof, 2007a). This function can be represented in general form as

$$Q_g = \Omega h_g^\beta, \tag{5.1}$$

where h_g is ice thickness at the grounding line, and Ω and β depend on ice dynamics near the grounding line. A floating ice shelf, tongue, or friction from valley sidewalls typically provides buttressing. This can be modeled explicitly, or analytically represented in Ω and β. Typically, $\beta \geqslant 1$, and this nonlinearity has been shown to depend on assumptions about the basal rheology near the grounding line (Schoof, 2007a; Tsai et al., 2015) and the characteristics of a buttressing ice shelf (Haseloff and Sergienko, 2018). h_g is simply determined by a flotation criterion: let $b(x)$ be the bed elevation relative to sea level (i.e., negative at the grounding line). Then, for a glacier of length L, h_g is

$$h_g(L) = -\frac{\rho_w}{\rho_i} b(L), \tag{5.2}$$

where ρ_w and ρ_i are the densities of seawater and ice, respectively.

In this study, we consider the grounding line the boundary of the outlet glacier system. That is, we consider floating ice a part of the boundary condition for the system's output flux (Q_g). In equilibrium, Q_g equals the surface mass balance integrated over the entire catchment (neglecting basal and englacial melt). Climate changes can perturb this flux balance in two distinct ways: the atmosphere can affect mass balance over the interior surface, or the ocean can modulate ice discharge at the grounding line (e.g., via a change in buttressing). In either case, Equations (5.1) and (5.2) reveal the basic system response to an imbalance: on a prograde bed, the terminus retreats into shallower water to decrease ice flux out of the system, or advances into deeper water to increase flux out of the system. The grounding-line

migration needed to restore equilibrium depends strongly on bed slope, and the degree of nonlinearity in Q_g (i.e., via β).

5.3.2 Flowline model

To simulate the dynamics of this outlet-glacier system, we begin with a 1-D (flowline) version of the ice-sheet model developed by Pollard and Deconto (2012; hereafter PD12). The evolution of local ice thickness h at a grid point reflects the balance of mass exchange at the surface and horizontal ice-flux divergence. Conservation of mass requires that

$$\frac{\partial h}{\partial t} = S - \frac{\partial(\bar{u}h)}{\partial x}, \tag{5.3}$$

where S is the local surface mass balance and $\bar{u}$ is depth-averaged horizontal ice velocity. The velocity profile has contributions from stretching, shear, and basal sliding, which are summarized as follows. In general, a sloping ice surface $\frac{\partial s}{\partial x}$ creates a driving stress,

$$\tau_d = \rho_i g h \frac{\partial s}{\partial x} \tag{5.4}$$

where ρ_i is ice density and g is acceleration due to gravity. Longitudinal stretching $\frac{\partial u}{\partial x}$ is represented by the shallow-shelf approximation, where stretching and basal drag τ_b balance driving stress:

$$\frac{\partial}{\partial x}\left(2hA^{-\frac{1}{n}}\left|\frac{\partial u}{\partial x}\right|^{\frac{1}{n-1}}\frac{\partial u}{\partial x}\right) - \tau_b = \tau_d. \tag{5.5}$$

We assume a typical power-law rheology, with coefficient A and exponent n (e.g., Glen, 1955). Internal shear deformation ($\frac{\partial u}{\partial z}$) is represented by the shallow-ice approximation. At a depth $h - z$, this is

$$\frac{\partial u}{\partial z} = 2A\tau_e^{n-1}\rho_i g(h-z)\frac{\partial s}{\partial x} \tag{5.6}$$

where $\tau_e^2 = (\frac{1}{2})\tau_{ij}\tau_{ij}$ is a scalar effective stress and τ_{ij} is the deviatoric stress tensor. Finally, sliding velocity is given by a Weertman-type power-law relationship

$$u_b = \left(\frac{\tau_b}{C}\right)^{\frac{1}{m}}, \tag{5.7}$$

where C is a friction coefficient and m is the sliding exponent. Here, m is the inverse of the flow exponent n, but note that this convention is flipped in some texts. The PD12 model uses a combination of the shallow-ice and shallow-shelf approximations to solve for $\frac{\partial u}{\partial z}$ and $\frac{\partial u}{\partial x}$, respectively. In this study, however, we use parameters that yield flow dominated by longitudinal stretching. We refer the reader to PD12 for further description of this hybridization.

A crucial simplification in the PD12 model is that flux across the grounding line is parameterized in the form of Equation (5.1). In PD12 and this study, Ω and β are taken from the analytical solution of Schoof (2007a):

$$\Omega = \left[A(\rho_i g)^{n+1} \Big(\Theta \big(1 - \frac{\rho_w}{\rho_i}\big) \Big)^n (4^n C)^{-1} \right]^{\frac{1}{m+1}} \tag{5.8}$$

$$\beta = \frac{m+n+3}{m+1}. \tag{5.9}$$

Θ is a buttressing factor between 0 and 1, and all other parameters are defined as above. The PD12 model calculates grounding line flux based on a thickness h_g that is linearly interpolated from the height above flotation of the last-grounded and first-floating grid cells, to the point where flotation is reached. The corresponding sub-grid grounding-line position is shown for all output from the PD12 model in this study. Although the PD12 model is typically run on coarse grids ($\mathcal{O} \sim$ 1–10 km) for continent-scale simulations over many millennia, we use a grid of 100 m to better resolve the details of grounding line variations. Finally, while the PD12 model does simulate a floating ice shelf, its dynamics are not important to our analyses as its buttressing effect is parameterized via Equation (5.8).

Figure 5.1b shows the steady-state profile for an idealized outlet glacier simulated with the flowline model. The domain begins at an ice divide and thus has a zero-flux lateral boundary condition. The bed is constant in time, and has an elevation of -100 m at the divide and constant prograde slope b_x of -2×10^{-3}. Surface mass balance S is 0.5 m yr^{-1} ice equivalent, assumed to be spatially uniform. Additional parameters are given in Table 1. The glacier has an equilibrium length (ice divide to grounding line) of $\sim$ 185 km, a

maximum thickness of $\sim$ 1580 m at the divide, and a thickness of $\sim$ 526 m at the grounding line. These scales are comparable to many outlet glacier catchments in Greenland, though direct comparisons are limited as the 1-D flowline cannot capture the flow convergence of many catchment geometries, and we emphasize that we are not simulating a particular outlet glacier. We discuss two additional geometries for comparison in Section 3.1.

5.3.3 Response to forcing

We begin by comparing the flowline model's response to forcing either from surface-mass-balance changes in the interior or ocean forcing at the terminus. In all model experiments throughout this study, "interior forcing" and "ocean forcing" will refer to perturbations applied in the following manner. Interior surface-mass-balance anomalies are assumed to be spatially uniform. We represent ocean forcing very simply by perturbing the grounding-line-flux coefficient, Ω. This broadly represents changes in the buttressing provided by an ice shelf or fjord walls, driven by anomalous melting or calving. In principle this could be targeted via Θ in Equation (5.8), and other analytical formulations for Ω explicitly represent a buttressing ice shelf (Haseloff and Sergienko, 2018). Perturbing these parameters might be more realistic, but we focus on Ω so that we can very generally represent flux perturbations, which may in reality result from a host of ice-ocean interactions. Our primary interest is in how glacier dynamics respond to each forcing type, and representing ocean forcing in this way makes comparison straightforward. For example, a fractional change in S (surface mass balance) constitutes a flux anomaly with the same initial magnitude as the same fractional change in Ω.

Figure 5.1c shows the length response to step forcings at time $t = 0$. The step is a 20% decrease in S or a 20% increase in Ω (i.e., more discharge for a given h_g), and in both cases, forces the terminus to retreat into shallower water to reduce the output flux. Note that the responses to changes in S and Ω do not converge to the same final length. The equilibrium sensitivities differ because of different nonlinearities in the input and output fluxes ($S \cdot L$ and Q_g) as the system state evolves. However, our main focus is the marked difference

between the initial responses to the step change, highlighted in the inset panel of Fig. 5.1c. Perturbing Ω results in a much faster initial retreat (blue curve) compared to perturbing S (orange curve), despite the larger equilibrium sensitivity to S. However, this faster retreat rate lasts only the first century or so, and accommodates only $\sim 25\%$ of the total equilibrium response. The remaining retreat occurs at a rate similar to that driven by a change in S, which is an asymptotic approach to equilibrium over several millennia. Thus, the length response to Ω forcing has both a "fast" and "slow" component, whereas S forcing primarily drives a slow response.

As an alternative to an impulse forcing, we also consider the glacier's response to stochastic variability in either Ω or S. We apply this variability as interannual white noise, which by definition has equal power at all frequencies and no interannual persistence. We apply the exact same white-noise time series as either Ω or S anomalies, but with opposite sign so that the corresponding ice-volume anomalies match. The anomaly time series (hereafter Ω' and S') are scaled to have standard deviations equal to 20% of the mean values ($\bar{\Omega}$ and $\bar{S}$). Figure 5.1d shows the resulting length responses. For both types of forcing, the glacier acts as a low-pass filter on the imposed climate anomalies, producing kilometer-scale fluctuations with clear persistence. However, the length anomalies driven by Ω' have much greater high-frequency content, and greater overall variance, than those driven by S'. The high-frequency response is perhaps intuitive, in that forcing applied at the grounding line has an immediate effect on grounding-line position. However, the response to Ω' also contains millennial-scale fluctuations onto which the faster variations are superimposed. These slow, wandering excursions are comparable to those driven by S', and, like the multi-millennial adjustment to step changes (Fig. 5.1c), suggest slow dynamics common to both responses.

Variability is intrinsic to climate, arising from the fundamentally chaotic nature of the natural system. The associated glacier fluctuations are a crucial part of characterizing glacier dynamics, and the implications have been extensively explored for mountain glaciers (e.g., Oerlemans, 2001; Roe, 2011; Roe et al., 2017), and more recently for marine-terminating outlet glaciers (Robel et al., 2018) and ice streams (Mantelli et al., 2016). Figure 5.1 suggests

Table 5.1: Parameters used for flowline and two-stage models. Values for A and C follow previous idealized case studies (Schoof, 2007a; Robel et al., 2018).

Parameter	Description	Value	Units
m	Sliding exponent	$\frac{1}{3}$	
C	Sliding coefficient	7.624×10^6	Pa $\mathrm{m}^{-\frac{1}{3}}$ $\mathrm{s}^{\frac{1}{3}}$
n	Deformation exponent	3	
A	Deformation coefficient	4.22×10^{-25}	Pa^{-3} s^{-1}
Θ	Buttressing factor	0.7	
ρ_w	Seawater density	1028	kg m^{-3}
ρ_i	Ice density	917	kg m^{-3}
$\bar{S}$	Surface mass balance	0.5	m yr^{-1}
b_0	Bed elev. at divide	-100	m
b_x	Bed slope	-2×10^{-3}	

a new and intriguing complication for outlet glaciers: the timescale and magnitude of glacier fluctuations depend on whether the climate variability comes in the form of surface mass balance or ocean anomalies. Additionally, the response to step changes (Fig. 1c) suggests that the type of forcing is also relevant for the response to non-stationary climate changes. In the next section, we investigate these contrasting responses using a recently developed reduced model.

5.3.4 The two-stage model

Robel, Roe, and Haseloff (2018; hereafter RRH) developed a simple model for marine-terminating outlet glacier dynamics, derived from ice-flux conservation and constrained by large-scale glacier geometry. RRH showed that this model could accurately emulate a more complex numerical model on the multidecadal and longer timescales on which most glacier variance occurs. A full description and derivation can be found in RRH, but a summary of

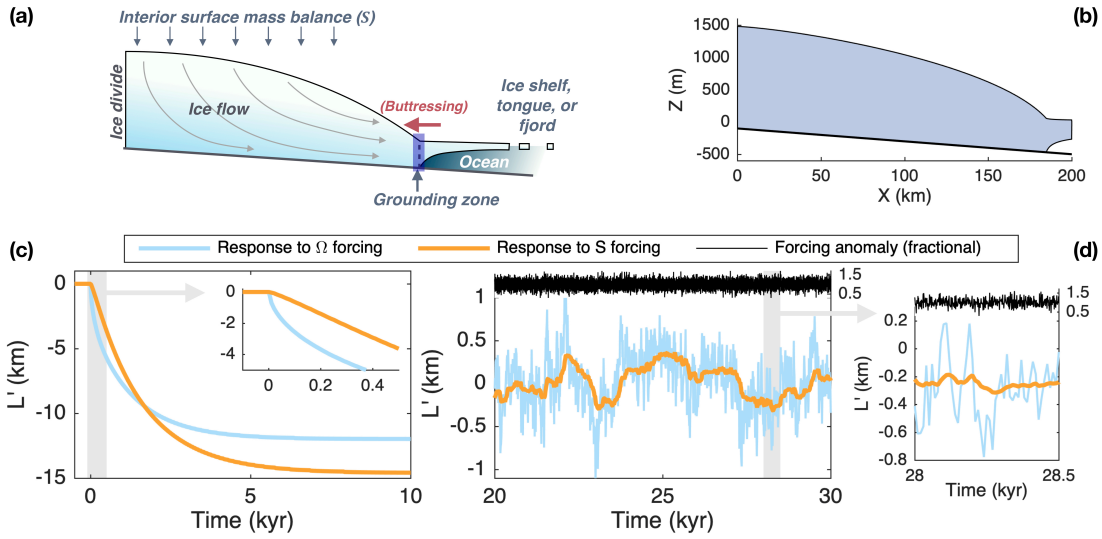

Figure 5.1: Model schematic and responses to ocean forcing (via Ω) and interior forcing (via S). **(a)** An idealized marine-terminating glacier system. **(b)** Initial steady-state profile simulated by the flowline model. **(c)** Length responses to 20% step increase in Ω (blue) and 20% step decrease in S (orange) at $t = 0$. Inset panel zooms into the first 0.5 kyr of response. Note the difference in initial retreat rates depending on the type of forcing. **(d)** Length responses to white-noise interannual variability in Ω or S. Right panel shows a 0.5 kyr segment in more detail. Anomalies (black) have a standard deviation of 20% of the mean value, and have opposite signs for Ω and S so that length anomalies are correlated for comparison. The response to ocean forcing (blue) contains much more high-frequency content than the response to interior forcing (orange).

the model follows.

The RRH model reduces the outlet glacier to a system with two degrees of freedom: L, the length from ice divide to grounding line; and H, the characteristic interior ice thickness (Fig. 5.2a). The glacier can be conceptualized as a small grounding-zone reservoir with a length $l_{gz} \ll L$ and thickness h_g, coupled to a large interior reservoir with thickness H and length $L - l_{gz}$. The geometry is further described by a bed topography with constant average slope b_x. Recall that the ice thickness at the grounding line, h_g, is a state-dependent quantity, set entirely by L and $b(x)$ (see Eq. 5.2).

The model dynamics are derived by balancing ice fluxes through these linked reservoirs (Fig. 5.2a). Ice thus enters the system via an accumulation flux $S \cdot L$, flows via an interior flux Q to the grounding zone, and leaves the system as a flux across the grounding line Q_g. A steady state of H and L is one which balances these three fluxes. L ultimately controls the system's input and output fluxes by setting the total catchment area for accumulation, and by controlling Q_g via h_g (Eqs. 5.1 and 5.2). Interior dynamic ice flux has the form

$$Q = \left(\frac{\rho_i g}{C}\right)^n \frac{H^\alpha}{L^\gamma}, \tag{5.10}$$

where α and γ can vary depending on the particular processes controlling interior flow. We use $\alpha = 2n + 1 = 7$ and $\gamma = n = 3$, consistent with deformation dominated by longitudinal stretching (RRH).

Two coupled equations capture the transient adjustment of the two degrees of freedom, H and L, as they relax towards a steady state that balances all three fluxes:

$$\frac{dH}{dt} = S - \frac{Q}{L} - \frac{H}{h_g L}(Q - Q_g) \tag{5.11}$$

$$\frac{dL}{dt} = \frac{1}{h_g}(Q - Q_g). \tag{5.12}$$

Because achieving steady state requires adjustment of both H and L, we refer to this model as the "two-stage model", following RRH. We discuss the operation of these stages further in Section 2.6. Note that Equation (5.10) captures the nonlinear dependence of ice

flux on driving stress (e.g., Eqs. 5.4–5.6) and ice thickness, and that the first two terms of Equation (5.11) resemble the continuity equation that governs ice thickness in the flowline model (Eq. 5.3). The two-stage model makes significant simplifications, but stems from the same physical principles as the flowline model, and most other contemporary ice-sheet models (see RRH for further discussion).

RRH also linearized these equations for fluctuations H' and L' about a steady state, $\bar{H}$ and $\bar{L}$. The linear model yields analytical expressions for a number of important quantities, including two widely separated characteristic response timescales. With some simplifications detailed in RRH, the fast and slow response timescales (τ_F and τ_S, respectively) are

$$\tau_F = \frac{\bar{h_g}}{\bar{S}}(\alpha + \gamma + 1 - s_T)^{-1} \tag{5.13}$$

$$\tau_S = \frac{\bar{H}}{\bar{S} s_T \alpha}(\alpha + \gamma + 1 - s_T), \tag{5.14}$$

where $s_T = 1 + \frac{\rho_w}{\rho_i}\frac{\beta \bar{b_x} \bar{L}}{\bar{h_g}}$ is a parameter describing the stability of glacier response based on its geometry and grounding-line dynamics (via β). Both response times contain a characteristic thickness divided by mass balance rate $\bar{S}$, reminiscent of the canonical mountain glacier response time (Jóhannesson et al., 1989). τ_F is controlled by h_g, and thus the volume of the system's small grounding-zone reservoir, whereas τ_S relates to the volume of the interior reservoir via $\bar{H}$. For scales typical of outlet glaciers, τ_F is on the order of decades to centuries, whereas τ_S is on the order of millennia. Thus, the two-stage model approximates the outlet-glacier system as linked interior- and grounding-zone reservoirs with distinct timescales.

Here we generalize the RRH linearization to simultaneously include perturbations to interior surface mass balance (S') and grounding-line flux (Q_g'; proportional to Ω'). The linearized equations take the form of a two-dimensional dynamical system with two forcing terms:

$$\frac{\partial}{\partial t}\begin{bmatrix} H' \\ L' \end{bmatrix} = \begin{bmatrix} A_H & A_L \\ B_H & B_L \end{bmatrix}\begin{bmatrix} H' \\ L' \end{bmatrix} + \begin{bmatrix} \bar{L}^{-1}\left(\frac{\bar{H}}{\bar{h_g}} - 1\right) \\ \bar{h_g}^{-1} \end{bmatrix} {Q_g}' + \begin{bmatrix} 1 \\ 0 \end{bmatrix} S'. \tag{5.15}$$

A_H, A_L, B_H, and B_L are shorthand for the couplings between length, thickness, and flux changes, which are given in the appendix. This linear system is readily discretized, and can

be cast as a two-dimensional autoregressive process (e.g., Box et al., 2008), which we also present in the appendix.

5.3.5 Model comparison

RRH showed that the two-stage model emulated the response of a flowline model forced with surface mass balance anomalies. Their flowline model (described in Schoof, 2007b; Robel et al., 2014) used a stress-based, as opposed to flux-based, grounding-line condition, but was otherwise dynamically similar to the PD12 model. Here, we use the PD12 model and extend the comparison to grounding-line flux perturbations. Although the two-stage model output includes H, we focus our comparison on L anomalies, which are more directly comparable between models. H is a more heuristic variable in the two-stage model; however, it does govern the evolution of interior fluxes, which we discuss in the next section. Both models use the parameters given in Table 1, for which Equations (5.13) and (5.14) give response times of ~ 76 and ~ 2000 years, respectively.

Figure 5.2 shows output from both models in response to step and stochastic forcings. Fig. 5.2b shows the grounding line retreat following a 20% increase in Ω (blues) and 20% decrease in S (orange/brown). For clarity, only the linearized two-stage output is shown. Note that the nonlinear two-stage model is constrained to have the same equilibrium response as the flowline model by Equation (5.1). The linear and nonlinear responses match almost exactly for the stochastic fluctuations, but disagree somewhat for the step changes. However, the disagreement is not severe, suggesting that we can reasonably use the linearized model and its response times as analytical tools. Importantly, the two-stage model captures the faster initial response to forcing at the grounding line, with a slightly more pronounced slope break in the first few hundred years.

Figure 5.2c shows a 5 kyr sample of 100 kyr of length fluctuations driven by white-noise forcing in S' and Ω'. Again, anomalies have no interannual persistence, are identical except for a sign reversal between Ω' and S', and have a standard deviation of 20% of $\bar{\Omega}$ or $\bar{S}$. The two-stage and flowline models agree closely for both types of forcing, although the two-

stage model slightly underestimates the magnitude of high-frequency fluctuations. Figure 5.2d shows the autocorrelation function of each length time series. This is a measure of the persistence of anomalies, and reveals the memory within a dynamical system. For forcing from Ω', the autocorrelation drops off rapidly to approximately 0.4 after a couple of centuries, corresponding to the fast response time. However, it then requires several millennia to drop below ~ 0.1, indicating the persistent influence of the slow timescale. For S' forcing, the autocorrelation is dominated by the slow timescale. The power spectra of length fluctuations are shown in Fig. 5.2e. Because white-noise forcing has a flat power spectrum, the shapes of the response spectra reveal the glacier's filtering properties. The glacier is a strong low-pass filter for both forcing types, but damps high frequencies even more for S' forcing. The two-stage model underestimates the high-frequency response of the flowline model, but agreement is very good at the lower frequencies that contain the majority of the variance. Critically, both models capture the clear split between the spectra of Ω'- and S'-driven anomalies at frequencies around 10^{-2} to 10^{-3} yr^{-1}, where the models agree quite well.

5.3.6 Interpretations

The two-stage model's agreement with the flowline model suggests that it captures the essential dynamics responsible for the contrasting transient responses to interior and grounding-line flux anomalies. At this point, it is useful to discuss some of the interpretations enabled by this reduced model.

The linearized two-stage model (Eq. 5.15) is a dynamical system with two eigenmodes, which, for the stable geometries considered here, are exponentially decaying functions with characteristic times τ_F and τ_S (the eigenvalues being τ_F^{-1} and τ_S^{-1}). The responses of the system's two degrees of freedom (H' and L') are linear combinations of these "fast" and "slow" eigenmodes. However, the two forcing types, Ω' and S', project onto each mode with different relative weights. Forcing via S' projects almost entirely onto the slow mode. For forcing in Ω', the fast mode makes a substantial contribution on multi-decadal to centennial timescales. However, the slow mode still dominates the equilibrium response to an impulse,

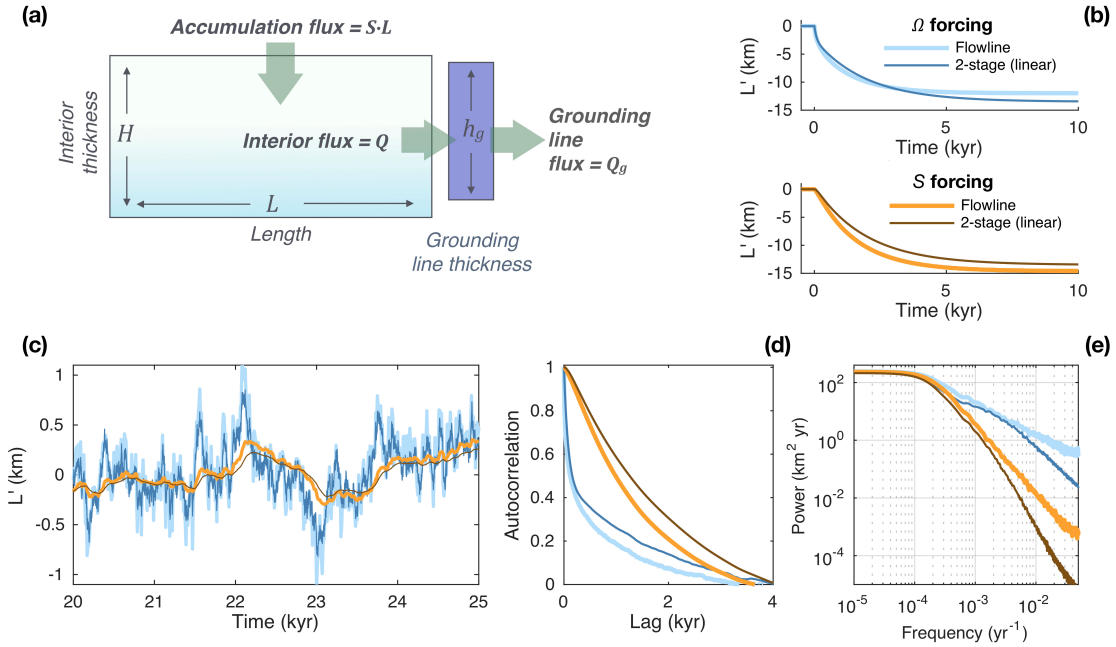

Figure 5.2: Comparing the transient response of flowline and two-stage models to ocean forcing (via Ω) and interior forcing (via S). **(a)** Schematic of the two-stage model. **(b)** Flowline and linearized two-stage model length responses to step changes in Ω (blues) and S (orange/brown). The thinner lines show the two-stage output. **(c)** Length anomalies in response to white-noise forcing in Ω (blues) and S (orange/brown). As in Figure 1, anomalies have standard deviation of 20% of the mean value and have opposite signs. 5 kyr of the 100 kyr model runs are shown. **(d)** Autocorrelation function for the stochastic length fluctuations shown in **(c)**. **(e)** Power spectral density for the stochastic length fluctuations, which is estimated throughout this study via Welch's method with windows of 1/16 the time series length, and 50% overlap. Note the clear split between fluctuations driven by Ω' (blues) and S' (orange/brown) at millennial and shorter timescales. This split is robust across models. The flowline model has more high-frequency power for both types of forcing, but note that the spectral power is orders-of-magnitude lower at such high frequencies.

as well as the power spectrum of stochastic fluctuations.

These modes can also be conceptualized as a two-stage low-pass filter on any forcing time series (e.g., Fig. 5.2e), and the type of forcing determines the order in which they are applied. Forcing over the interior (S') is first filtered by the slow mode, and the fast mode then operates on interior flux anomalies whose high-frequency content has already been strongly damped; there is little additional filtering to do. In contrast, if forcing is applied at the grounding line (Q'_g via Ω'), the fast mode responds to unfiltered anomalies and the grounding-line position exhibits a fast initial response before engaging the slow mode in the interior. Figures 5.1 and 5.2 suggest that the response to S' could be reasonably approximated by the adjustment of a single multi-millennial mode. However, we stress that the response to Ω' is *not* simply the response of a single multi-decadal mode, because the grounding zone is coupled to the slower, but ultimately more sensitive interior reservoir.

While these mathematical interpretations may seem abstract, it is helpful to remember that the two-stage model was derived from mass conservation, and that the linear response times (eigenmodes) reflect the large-scale glacier geometry. Because a glacier is a Stokes (i.e., non-inertial) fluid driven by potential-energy gradients, the large-scale glacier geometry must reflect the aggregate dynamics by which the system seeks flux balance. This relationship between geometry and dynamics is another way to interpret why Ω' and S' forcings project differently onto the fast and slow modes: these flux imbalances have different geometries, and thus the geometry and dynamics of the transient responses must also be distinct.

To help illustrate this, Fig. 5.3 tracks the evolution of fluxes following step changes in S and Ω. Five fluxes are shown for the flowline model: over the interior surface ($S \cdot L$), across the grounding line (Q_g), and at conceptual flux gates located 5, 25, and 50 km up-glacier of the grounding line (Fig. 5.3a). For the nonlinear two-stage model, $S \cdot L$, Q, and Q_g are shown (Fig. 5.3b). In all cases, flux anomalies are normalized by their final (equilibrium) change. A change in surface mass balance has an immediate, spatially distributed tendency on interior thickness, which slowly alters driving stresses and thus fluxes throughout the interior. Anomalous ice flux arrives at the grounding zone, driving advance or retreat, which

then modifies Q_g according to Equation (5.1). Most of the disequilibrium during the transient response is between surface mass balance and interior fluxes, while Q_g can quickly keep pace with flux anomalies from the interior. In the two-stage model, Q_g keeps up on the fast timescale. In contrast, a perturbation to Q_g (here, via Ω) is highly localized and first creates a large disequilibrium between Q_g and interior flux. The increase in Q_g causes the grounding zone to drain, drawing in ice from the interior, which transfers the disequilibrium from Q and Q_g, to Q and $S \cdot L$. Both models capture this transfer, and the flowline model flux gates show that it gradually propagates up from the grounding zone. The transient peak in fluxes is similar to a kinematic wave propagating from the terminus, which reaches well into the interior within a few multiples of τ_F. The ensuing drawdown of the interior reservoir (the slow mode in the two-stage model) brings interior fluxes back down, and again, Q_g must follow via grounding line retreat.

Although the flowline model captures a more realistic and spatially distributed response, the two-stage model contains enough geometric information to emulate the basic sequence of flux anomalies. Note that more discretized interior reservoirs could be added to the two-stage model, which would eventually approach the form of the flowline model. However, a single reservoir could not capture the essential transient response. The distinct stages of the response to a perturbation in Q_g, borne out in both models, show that a two-mode framework is useful for understanding the response to forcing applied at the grounding zone.

5.3.7 Persistence in variability

In the previous sections, we imposed stochastic variability with a flat power spectrum (i.e., white noise) because it allowed us to identify the influence of forcing type and model physics across all relevant frequencies. In reality, surface-mass-balance and ocean variability may exhibit different power spectra. Climate variables associated with the atmosphere (such as surface mass balance) often have little interannual memory (e.g., Medwedeff and Roe, 2017), but the ocean's thermal inertia can introduce persistence (e.g., Hasselmann, 1976). While the comparisons above show that interior and ocean forcing elicit different glacier responses

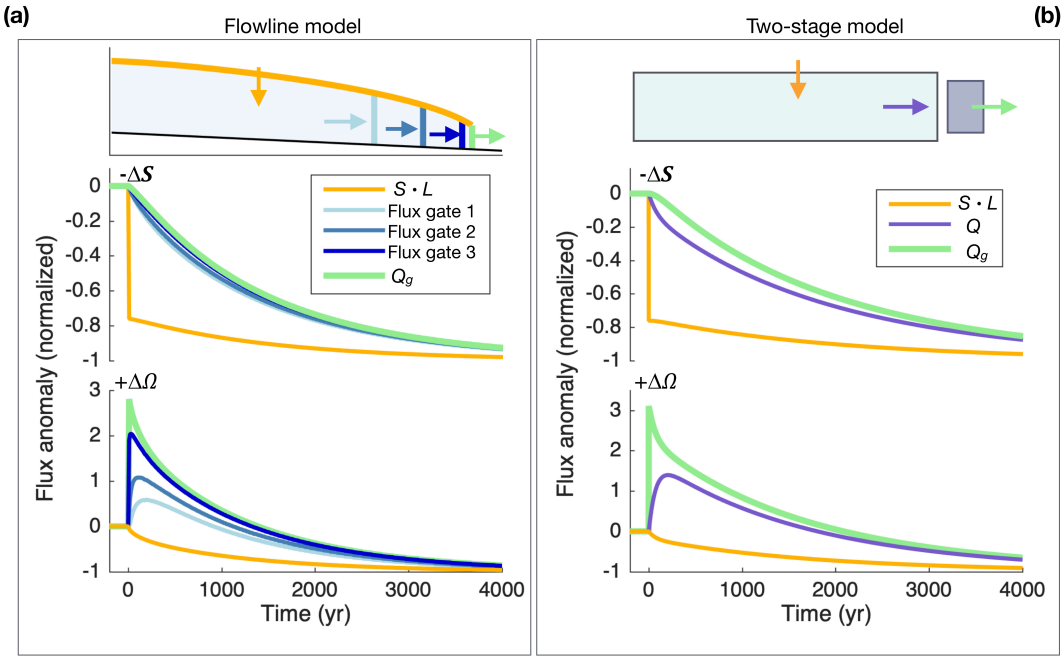

Figure 5.3: Flux changes following interior vs. ocean forcing. (a) Flowline model flux anomalies to perturbations in S and Ω. The schematic (top) shows the flux gates considered. Below, normalized flux responses to the perturbations are shown for each flux gate. (b) as for (a), but for the two-stage model, which has three flux variables. The two-stage model's interior flux variable (Q) captures the basic tendencies of interior fluxes in the flowline model. In both cases, the response to a perturbation in Ω clearly shows the two-timescale nature of outlet glacier dynamics.

due to the distinct geometries of the respective flux anomalies, we must also consider the possibility of climatic persistence in order to fully characterize an outlet glacier's response to natural climate variability. Roe and Baker (2016) showed that persistence in surface mass balance variability amplified the length fluctuations of mountain glaciers; we can expect similar principles to be especially relevant to outlet glaciers if they are sensitive to decade-scale ocean variability.

We consider four types of synthetic forcing with different persistence characteristics: (1) white noise; (2) and (3) first-order autoregressive (AR-1) processes with persistence timescales τ_{AR1} of 4 and 20 yr, respectively; and (4) power-law persistence. These are all plausible models for the sort of persistence that may affect outlet-glacier forcing. For example, an AR-1 process with a 4 yr memory is characteristic of sea-surface temperature anomalies in the North Atlantic (e.g., Deser et al., 2003), while the 20 yr timescale would better correspond to subsurface anomalies (e.g., Gwyther et al., 2018; Jenkins et al., 2018). Additionally, the continuum of surface-temperature variability from interannual to multimillenial timescales has been described with a power-law spectrum (e.g. Huybers and Curry, 2006).

We generate time series following Percival et al. (2001) and Roe and Baker (2016), first defining the desired spectral properties in frequency space, and then applying the same set of random phases to each case so that the resulting anomalies are correlated in the time domain. The power spectrum of a discrete AR-1 process as a function of frequency f, is

$$P_r = P_0\big(1 + r^2 - 2r\cos(2\pi\Delta t f)\big)^{-1}, \tag{5.16}$$

where P_0 scales the total variance and r is the auto-correlation at a lag of Δt (here, 1 yr). The memory timescale of the process is related to r by $\tau_{AR1} = \frac{\Delta t}{1-r}$. Power-law noise has a spectrum defined by

$$P_\nu = P_0\Big(\frac{f_0}{f}\Big)^\nu, \tag{5.17}$$

where f_0 is the highest sampled frequency. The power increases continually out to low frequencies, where ν is the slope of the spectrum in log-log space. We use $\nu = 0.5$, consistent

with $\nu \sim 0.5$ to 1 identified by Huybers and Curry (2006) in a large collection of paleoclimate records.

We normalize the forcing time series so that they all have the same variance. This ensures that, for a given choice of S' or Ω' forcing, differences in glacier response are due only to differences in persistence. Figure 5.4a shows 200 yr samples of the 10^5 yr synthetic forcing time series, and Fig. 5.4c shows their power spectra. The AR-1 processes (red, maroon) have clear persistence in the time domain. The low-frequency content of power-law noise (blue) is hard to discern at short timescales, but the spectra show that it has similar power to the AR-1 processes at millennial timescales (and, again, identical total variance). Power-law variability is thus difficult to constrain from century-scale instrumental records alone (e.g., Percival et al., 2001). At a certain point, the spectrum of climate variability runs into timescales where paleoclimate reconstructions, rather than synthetic noise or instrumental observations, would be a more relevant choice for understanding natural glacier variability; we will return to this point in Section 3.3.

Figure 5.4b shows 10^3 yr samples of the resulting length responses for the two-stage model. The effects of persistence are dramatic: for both S' or Ω' forcing, 4 yr AR-1 persistence more than doubles σ_L compared to length fluctuations driven by white-noise forcing, and both 20 yr AR-1 and power-law persistence cause a $\sim$ 5-to-6-fold increase in σ_L. This is consistent with the approximate proportionality between σ_L^2 and τ_{AR1} predicted by theory (see, e.g., Roe and Baker, 2016; Robel et al., 2019).

The power spectra of the forcings and responses show why persistence has such a strong effect. The response to white-noise forcing reveals the system's sensitivity across all timescales (Fig. 5.4d), because the input has equal power at all frequencies. The glacier response is set by its internal dynamics and the forcing type (S' or Ω'). Any forcing time series must be filtered by the same dynamics, and if the forcing has persistence, some of its spectral power is shifted toward lower frequencies where glacier sensitivity is higher. Thus, the shape of the response spectrum (Fig. 5.4e) reflects both the frequency content of the forcing (Fig. 5.4c), and the frequency dependence of the glacier dynamics, or, in other words, the spectral shape

of the glacier filter (Fig. 5.4d).

The practical takeaway is that persistence in climate forcing increases the total variance of length fluctuations. When combined with the finding that terminus-flux anomalies excite the fast mode of response more than surface-mass-balance anomalies, the implication is that ocean variability—which tends to have persistence—may drive much larger terminus fluctuations than surface-mass-balance variability.

Figures 1–3 demonstrate that marine-terminating outlet glaciers have different transient responses to interior and ocean forcing, because of how the fast and slow modes respond in each case. In the next sections, we examine the consequences for three key issues: the committed response to forcing, the attribution of an observed change, and a glacier's memory of past climate changes. The relative roles of ocean and interior forcing will, of course, vary widely among individual glaciers. Rather than conducting simulations of specific settings, we will use our simplified model framework to outline the general implications and assess how the combination of fast and slow dynamics applies to each question.

5.4 Part 2: Implications

5.4.1 Committed Change

Any system with a non-zero response time will lag applied forcing. "Committed change" refers to the total response such a system would need to undergo to attain equilibrium with the current level of forcing. In the context of a warming climate, committed change is an important lower bound on future change that is independent of future emissions scenarios. It has long been recognized that surface temperatures lag CO_2 forcing due to the ocean's thermal inertia (e.g., Hansen et al., 1985; Wigley and Schlesinger, 1985). In turn, other aspects of the climate system respond to warming with their own lags, including mountain glaciers (e.g., Christian et al., 2018) and global sea level (e.g., Meehl et al., 2005; Levermann et al., 2013). Industrial-era climate forcing began in the 19th century (e.g., IPCC, 2013; Abram et al., 2016), and so the millennial response times (i.e., Eq. 5.14) of outlet glaciers

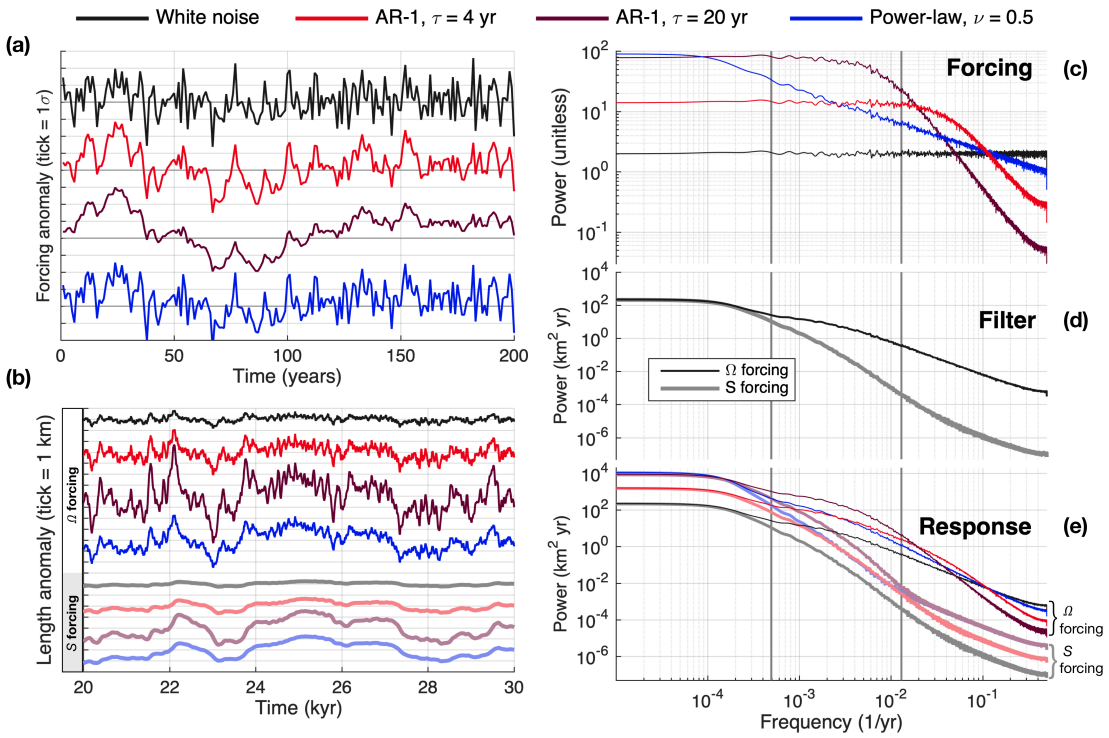

Figure 5.4: The effect of climatic persistence on glacier fluctuations. **(a)** Segments of synthetic anomalies with different levels of persistence: white noise (no persistence; black); red noise with $\tau_{AR1} = 4$ yr (red) and $\tau_{AR1} = 20$ yr (maroon); and power-law noise with $\nu = 0.5$ (blue). Time series shown are dimensionless and offset for clarity, with vertical ticks of 1σ. **(b)** The glacier-length variations generated by the two-stage model, when the synthetic anomalies are applied as Ω' (dark lines) and S' (pastel lines). Time series are again offset, with vertical ticks of 1 km. **(c)** Power spectra of the synthetic climate forcings. For reference, vertical lines correspond to $\frac{1}{\tau_F}$ and $\frac{1}{\tau_S}$. **(d)** Spectra of the glacier's response to white noise, which illustrates the glacier's sensitivity as a function of frequency, and thus its temporal filtering properties. This depends on whether forcing is applied as Ω' (black) or S' (gray). **(e)** Spectra of glacier response to Ω' (dark lines) or S' (pastel lines). Responses depend on the spectra of the forcing and the glacier's filtering properties. Forcing with persistence has more power at low frequencies where glacier sensitivity is highest, increasing the overall glacier variance.

imply a severe disequilibrium with current climate and a large committed change, even with no additional forcing.

To illustrate the current committed change of outlet glaciers, we use the two-stage model and follow the framework of Christian et al. (2018), using idealized glacier geometries and forcings. Disequilibrium, and thus committed retreat, is defined in reference to an "instantaneous equilibrium" response, which is the state at which the glacier would be in equilibrium with climate at any given time. This is governed largely by the bed geometry and climate forcing. An idealized geometry (e.g., uniform bed slope and width) makes for a simple equilibrium response, but the physical principle of course also holds for more complex systems. For an idealized outlet glacier, the instantaneous equilibrium is the grounding-line position (L) that yields $Q_g = S \cdot L$.

We consider ramp forcing scenarios where S decreases, or Ω increases, by 30% from 1880 to 2020 CE. The forcing is fixed at 2020, and the glacier is allowed to relax towards a new equilibrium. Figure 5.5 shows the responses of three glaciers with varied response times: (1) $\tau_F, \tau_S \sim (76, 2000)$ yr; (2) $\tau_F, \tau_S \sim (56, 1200)$ yr; and (3) $\tau_F, \tau_S \sim (140, 4600)$ yr. The parameters for each glacier are provided in Table 2. Dashed lines show the instantaneous equilibrium responses, which indicate the total committed response at any given time.

The most basic result is that, in all cases, the transient response as of 2020 is a small fraction ($\sim$ 1–23%) of the instantaneous equilibrium response. The disequilibrium for S forcing is particularly severe, as pointed out previously by RRH. Although changes in surface mass balance are already a major component of overall mass loss in some settings, basic glacier dynamics require that S anomalies also have an impact on the grounding-line position, which is, as yet, essentially unrealized. Perturbations in Ω elicit a faster response over the industrial era, but Fig. 5.5a–c shows that both types of forcing have a long-term commitment associated with the slow drawdown of interior ice.

The "slow response" (interior thinning $\rightarrow$ reduced interior fluxes $\rightarrow$ grounding-line retreat) comprises the majority of the response to S forcing, but it is important to remember that it is also the second stage of the response to ocean forcing, and it dictates the total

committed change. Following recent observed increases in ice discharge, Price et al. (2011) and Goldberg et al. (2015) examined the committed responses of several outlet glaciers in Greenland and Antarctica, respectively. These studies found substantial "dynamic" commitments associated with thinning and elevated fluxes, although they focused on near-term sea-level rise and did not project past 2100. Our flux-balance perspective is a complementary view of committed change, and shows that dynamic thinning necessarily drives additional retreat on long timescales as a consequence of reduced interior fluxes. The slow equilibration of the interior would thus be a critical part of determining the total commitment due to ocean forcing, especially if the long-term retreat moves the terminus to more- or less-stable slopes.

The slow mode also means that there can be large uncertainties in committed change if the magnitude of forcing is uncertain. Figure 5.5d shows the response to a trend in Ω, ranging from a 20–40% increase from the initial value. As of 2020, the differences in observed retreat are small, but diverge as the system approaches equilibrium over subsequent millennia. In other words, the slow response limits how "wrong" short-term simulations might be due to errors in the assumed forcing, but makes no such constraints on the committed change. The same principle also applies to uncertainty in the outlet glacier's length sensitivity: note that glaciers 1 and 2 have nearly identical responses on centennial timescales, but different equilibrium sensitivities. Similar arguments have been made for uncertainty in radiative forcing and equilibrium climate sensitivity (Armour and Roe, 2011).

5.4.2 The emergence and detectability of forced responses

We now turn to the topic of attributing outlet glacier retreats to natural or anthropogenic forcing. The attribution of an observed change to a particular cause (i.e., an external forcing) can be a challenge because of factors specific to individual glaciers, such as complexities in bed geometry, regional climate, or the local collection of ice-ocean interactions. It can also be a challenge because of factors intrinsic to the transient ice dynamics, which affect the amount of the forced response that can be expressed over a given time. We focus here on

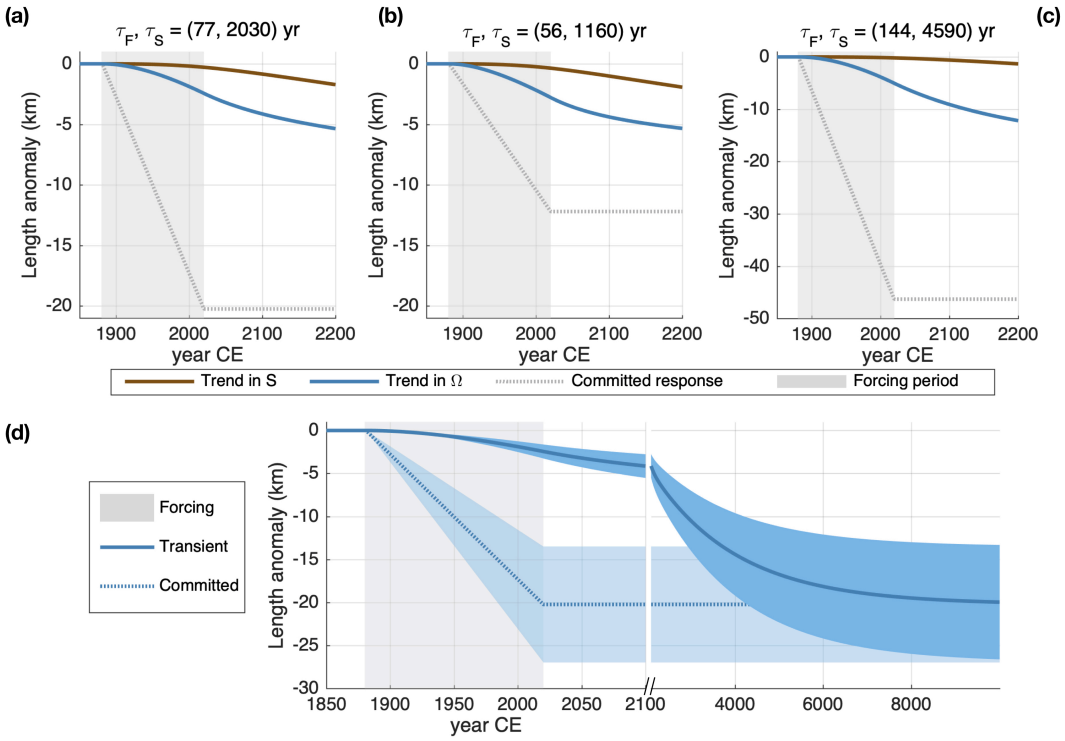

Figure 5.5: Glacier responses to idealized climate forcing over the industrial era. **(a)** Responses for glacier 1 (see Table 2). A 30% change in S (brown) or Ω (blue) is realized as a linear trend from 1880–2020 CE. Dotted lines show the grounding-line position that would balance accumulation and grounding-line fluxes. **(b)** As for **(a)**, but for glacier 2, which has faster response times and smaller equilibrium sensitivity. **(c)** As for **(a)** and **(b)**, for glacier 3, which has slower response times and greater equilibrium sensitivity. **(d)** The range of responses of glacier 1 due to an uncertain forcing, idealized as a trend in Ω reaching a 20–40% change by 2020. The slow transient response means a small range in absolute length change in the modern era, but uncertainty in the forcing projects directly onto the committed equilibrium response. Note the break in the time-axis scale at 2100.

Table 5.2: Parameters varied between three idealized glaciers (top) and the resulting steady-state values (bottom). The steady state is calculated by the nonlinear two-stage model, and the linearized response times are given by Equations (5.13) and (5.14).

Parameter	Description	Units	Glacier 1	Glacier 2	Glacier 3
$\bar{S}$	Surface mass balance	m yr^{-1}	0.5	0.6	0.3
Θ	Buttressing factor		0.7	0.75	0.6
b_0	Bed elev. at divide	m	-100	$+150$	$+100$
b_x	Bed slope		-2×10^{-3}	-3×10^{-3}	-1×10^{-3}
Steady-state value					
$\bar{H}$	Interior thickness	m	1413	1569	2814
$\bar{L}$	Length	km	185	212	700
h_g	Grounding line thickness	m	526	545	673
τ_F	Fast response time	yr	77	56	144
τ_S	Slow response time	yr	2030	1160	4590

this latter set, and in particular on the contrasting implications of ocean vs. interior forcing.

Attribution is often framed in terms of the signal-to-noise ratio (SNR) of an observed trend. For a variable x, the SNR is often defined as $\frac{\Delta x}{\sigma_x}$, where Δx is the change estimated by a linear fit and σ_x is the standard deviation of the residuals. For glacier retreat (or changes in any analogous system), this depends on the SNR of the relevant forcing variable (e.g., surface temperature, ocean heat content, etc.), and also on the memory timescale over which the glacier integrates anomalies in that variable. A glacier's memory damps its response to high-frequency noise, but the tradeoff is that it also delays its response to a persistent trend (see Fig. 5.5). Roe et al. (2017) showed that mountain glaciers exemplify this concept and moreover, that their multidecadal response times are optimal for damping interannual climate variability while responding sensitively to centennial trends, thereby producing an amplified SNR.

For outlet glaciers, however, two types of forcing (ocean and interior) and much longer response times are at play. To understand how these factors interact on the timescales of historical anthropogenic forcing, we consider three idealized scenarios of stationary variability plus a trend (Fig. 5.6a). Cases 1 and 2 have variability with no interannual persistence (i.e., white noise) in S and Ω, respectively. Case 3 has multidecadal variability in Ω, generated by an AR-1 process with a memory timescale of 20 yr (see Section 2.7). To compare glacier responses, we standardize the forcing scenarios by their SNR: In each case, a linear trend begins in 1880 CE (negative in S for case 1, positive in Ω for 2 and 3). We stipulate that the trend reaches a 20% departure from the mean by 2020 CE, and continues thereafter at the same rate. The stationary variability again has $\sigma = 20\%$ of the initial mean. Thus, the imposed trends in climate forcing all have a SNR that reaches 1 by 2020.

Figure 5.6b shows the resulting grounding line anomalies of the test glacier described in Section 2, generated with the two-stage model. In all cases, the simulation was initialized in the year 0 CE. For reference, responses without variability are also shown (thin lines), as well as responses with variability but no trend. Shading indicates the 1σ and 2σ bounds of grounding-line fluctuations, determined from 10^7 yr simulations of stationary variability.

In case 1, noisy surface mass balance drives small length fluctuations, but the very slow response to the trend in S means that the forced response is slow to emerge from the noise; it remains within $2\sigma_L$ until the late 21st century. In contrast, the faster response to a trend in Ω exceeds $5\sigma_L$ by 2020, for case 2 (interannual variability). The multidecadal fast response time thus acts to amplify the climate trend's SNR roughly by a factor of 5, consistent with the findings of Roe et al. (2017) for mountain glaciers. However, because persistence amplifies natural glacier variability (Section 2.7), the multidecadal variability in case 3 inflates the envelope of natural glacier fluctuations such that the forced response is again hard to detect on centennial timescales. The forced response is roughly $1\sigma_L$ by 2020, meaning that glacier dynamics no longer improve upon the SNR of the forcing. Thus, a multidecadal fast timescale does not necessarily amplify the SNR of a climate trend, if a glacier is subjected to multidecadal ocean variability.

These idealized cases are useful for understanding factors that affect the detectability of a length trend, but they also demonstrate that the SNR may be a problematic metric in a practical sense. Because most of the natural glacier variability is expressed at very low frequencies, σ_L (i.e., the noise) is undersampled by direct observations, which cover only several decades for most outlet glaciers. Additionally, slow natural excursions could dominate the baseline against which a trend is measured. For example, in case 3, the *initial* length anomaly due to random variability is greater in magnitude in 1880 than the forced component of the retreat from 1880–2020 (i.e., the difference between orange and blue lines).

An alternative approach is to evaluate an observed ΔL against the distribution of natural trends that occur over the same interval of time as the observation. This incorporates information about the rate and persistence of natural length fluctuations. The simplicity of the two-stage model allows us to generate large synthetic ensembles of random fluctuations for a range of glacier parameters and forcing scenarios. We develop distributions of naturally-forced trends as follows: If Δt_{obs} is the length of a hypothetical observational period, we draw the last Δt_{obs} years from model runs of 10^4 years, each of which are forced with stationary noise and no trend. For each realization, ΔL_{null} is the trend in grounding-line position over the observational period. We find ΔL_{null} for 10^4 independent simulations for each type of variability, yielding distributions of ΔL_{null} for a given Δt_{obs}. The resulting distributions are shown in Fig. 5.6c, for Δt_{obs} of 50, 100, 250, and 500 years.

For variability in S, the distribution of ΔL_{null} is narrow for short Δt_{obs} due to the strong damping of high frequencies, but widens as Δt_{obs} increases. In other words, large fluctuations are possible, but ice dynamics constrain them to be slow. As expected, Ω variability increases the likelihood of observing larger trends on centennial timescales, and the effects of persistence are once again dramatic: a 1 km retreat in 50 yr is very rare with no persistence (99th percentile), but fairly commonplace with multidecadal variability (70th percentile).

As Δt_{obs} increases out to 500 years, the distributions of ΔL_{null} do not widen as much for variability in Ω as for variability in S. This suggests that centennial timescales (i.e., a few

multiples of τ_F) are nearly optimal for sampling large, persistent trends driven by stochastic Ω variability alone (note that in the limit of $\Delta t_{obs} \gg \tau_S$, the distributions would narrow back to zero). This raises the importance of the fast mode for attributing changes in the time frame of one-to-two centuries of anthropogenic climate forcing.

The widely-separated dynamical timescales characteristic of outlet glaciers pose a unique challenge for understanding their modern changes. The slow mode means that the overall variance (i.e., σ_L^2) must be considered, as stochastic variability over the last millennia may be important for the preindustrial state. Yet if the glacier is sensitive to variability at the terminus, the fast mode enables shorter-term fluctuations that may obscure the early response to anthropogenic forcing, especially if the variability has significant persistence. The sensitivity of grounding line flux to ocean variability and large calving events, and the associated timescales, will thus be critical for attribution studies. Finally, it should be borne in mind that these detection challenges arise from slow dynamics, and not from low sensitivity. As is clear from Fig. 5.5, only a small fraction of the committed response is available for attribution studies today.

5.4.3 Inherited conditions

We have thus far considered outlet-glacier fluctuations due to stationary interannual-to-multidecadal climate variability. However, long response times also imply some memory of climate variations throughout the Holocene. Ice-sheet models are often "spun up" using paleoclimate proxy data precisely for this reason (e.g., Bindschadler et al., 2013). However, these strategies do not always reproduce the same modern ice extent (e.g., Goelzer et al., 2018), and the simulated ice-sheet history can depend strongly on the choice of proxy and its implementation in the model (e.g., Nielsen et al., 2018; Buizert et al., 2018). Here, we compare outlet glacier responses to ocean versus interior forcing over the Holocene as an additional factor for the modern state. We focus on climate anomalies that are well-documented in the Northern Hemisphere, but similar considerations would apply to Antarctic outlet glaciers.

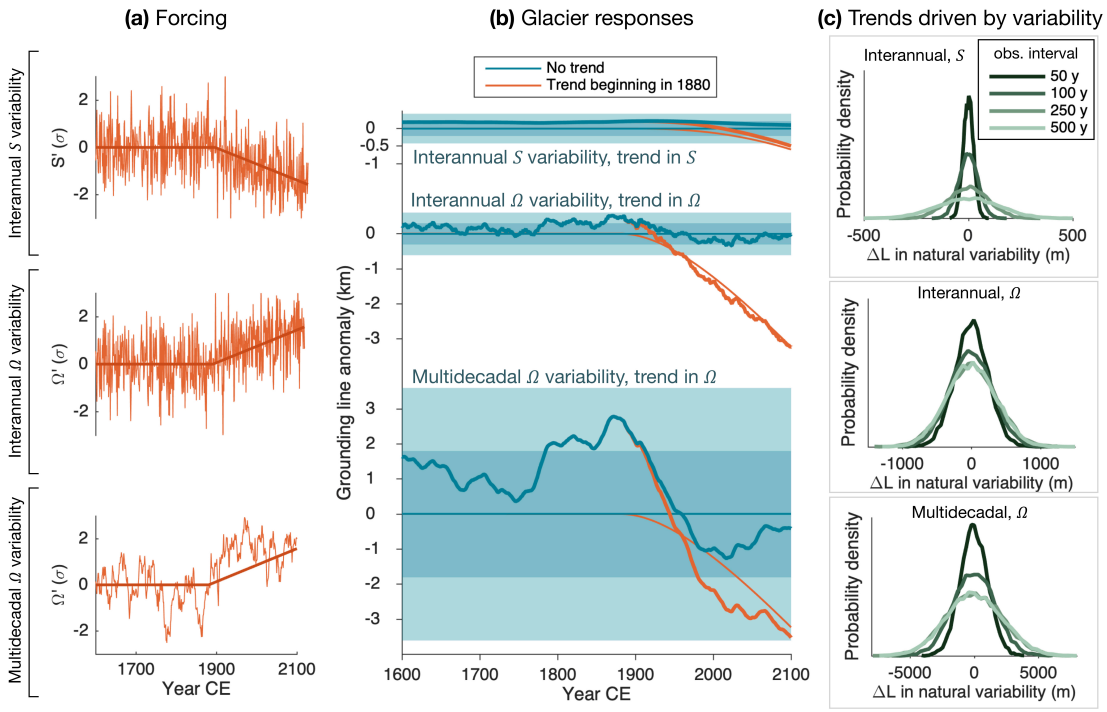

Figure 5.6: Detecting the response to a climate trend in the presence of natural variability. Three types of natural variability are considered in each panel. The top row corresponds to interannual variability in S; middle row to interannual variability in Ω; and bottom row to multidecadal variability (τ_{AR1} = 20 yr) in Ω. **(a)** The idealized climate trends (plus variability) beginning in 1880. In all cases, the linear trend reaches a SNR of 1 by 2020. **(b)** Grounding-line responses to each idealized trend. Shaded regions are the $1\sigma_L$ and $2\sigma_L$ bounds for each type of noise. The orange lines indicate when the trend has been applied. Thinner lines show the grounding-line response without variability. **(c)** Probability density functions for grounding-line trends driven by each type of natural variability, but no external forcing, over time periods from 50–500 years. Note the different length scales in each case. Trends on the order of km century^{-1} are extremely unlikely to occur due to variability in S alone (top), but commonplace if the glacier is sensitive to multidecadal variability in Ω (bottom).

First, we consider a climate scenario with idealized representations of three events: a deglacial warming at 11 kya, a Little Ice Age (LIA) cool period from 1450 to 1850 CE, and an anthropogenic warming trend from 1880 to 2100 CE. The deglacial and LIA transitions are smoothed by error functions of 500 yr and 50 yr widths, respectively. The magnitudes of deglacial, LIA, and anthropogenic events have a ratio of 10:1:4, and the intervening Holocene climate is assumed constant. We scale forcings linearly to the climate anomalies, where warming corresponds to negative S' or positive Ω'. Obviously, different combinations of these forcings could be expected in reality. Rather than choosing a particular combination, we examine each in isolation and normalize the glacier responses. These experiments thus serve as limiting cases to illustrate the relative influences of ocean and interior forcing over different timescales. This scenario is designed to explore two practical points: (1) the glacier's memory of large, long-ago events compared to smaller, more recent events; and (2) the glacier's relative memory of past ocean vs. interior forcing.

We use the two-stage model, linearized with respect to the Holocene climate with parameters for glacier 1 (See Table 2; $\tau_F, \tau_S \sim 76, 2000$ yrs). The advantage of using the linear model here is that it has uniform sensitivity to fractional perturbations in S and Ω. This allows us to more clearly distinguish the signatures of fast and slow dynamics; the tradeoff is that it ignores nonlinearities that are surely a factor for very large climate changes. Accurate simulations over such transitions would depend not only on nonlinearities in ice dynamics, but also on spatial information (e.g., bed topography) that is simplified in reduced models. Nevertheless, the linear model is a straightforward tool for demonstrating consequences of having both fast and slow dynamics. Focus should be directed toward the responses to the idealized LIA, for which the linearization is more valid. Including the deglaciation signal primarily serves to account for residual, albeit faint, disequilibrium implied by millennial response times.

Figure 5.7a shows the idealized climate (top) and two-stage model responses. Anomalies are shown relative to the mid-Holocene and normalized to the large deglacial transition. Figure 5.7b shows 1000 to 2000 CE in more detail, including a scenario with no anthropogenic

warming (dashed). For reference, the length at which the glacier would be in equilibrium with the LIA climate is also plotted (gray). For both forcings, the grounding-line retreat due to the deglacial signal is nearly complete by the onset of the LIA. However, the LIA advance is $\sim 2\times$ greater for forcing in Ω, because it can engage the fast mode to a greater degree. Yet, even forcing in Ω yields a muted response: the transient response only reaches $\sim 35\%$ equilibration before the period ends. The slow mode, which takes up the majority of the response for both forcing types, barely feels our 400 yr LIA before it is reversed. This is worth bearing in mind whenever the duration of glacier excursions and climate anomalies are less than τ_S, because the system never achieves equilibrium. This would be an issue particularly if such events are used to tune glacier sensitivity in models.

The idealized LIA is a much more discrete "event" than is supported by paleoclimate records, and ignores other variations in the Holocene. Thus, we also consider the response to a more realistic forcing time series. Again, this is not a reconstruction of actual terminus changes, but it is useful to see how glacier memory integrates the continuum of variations found in paleoclimate records. We use a time series of temperatures for Disko Bay, Greenland, from the regional reconstruction of Buizert et al. (2018) (Fig. 5.7c–d). The forcings are scaled as above, and normalized to 1880 CE.

The glacier responses in Fig. 5.7d show the same essential behavior as the more idealized case in Fig. 5.7b. Even with a more subtle LIA, the terminus response is much more pronounced if it is driven by Ω anomalies that engage the fast response. It is worth noting, though, that most of the glacier disequilibrium in the 1800s is due to cooling over the previous millennia, to which the slow mode responds with a pronounced lag. Thus, the preindustrial state of an outlet glacier may depend significantly both on LIA and longer-term ocean cooling, via its two distinct response timescales.

5.5 Summary and discussion

Marine-terminating outlet glaciers are sensitive to two fundamental types of forcing: changes in surface mass balance, which are distributed over a large interior catchment; and changes

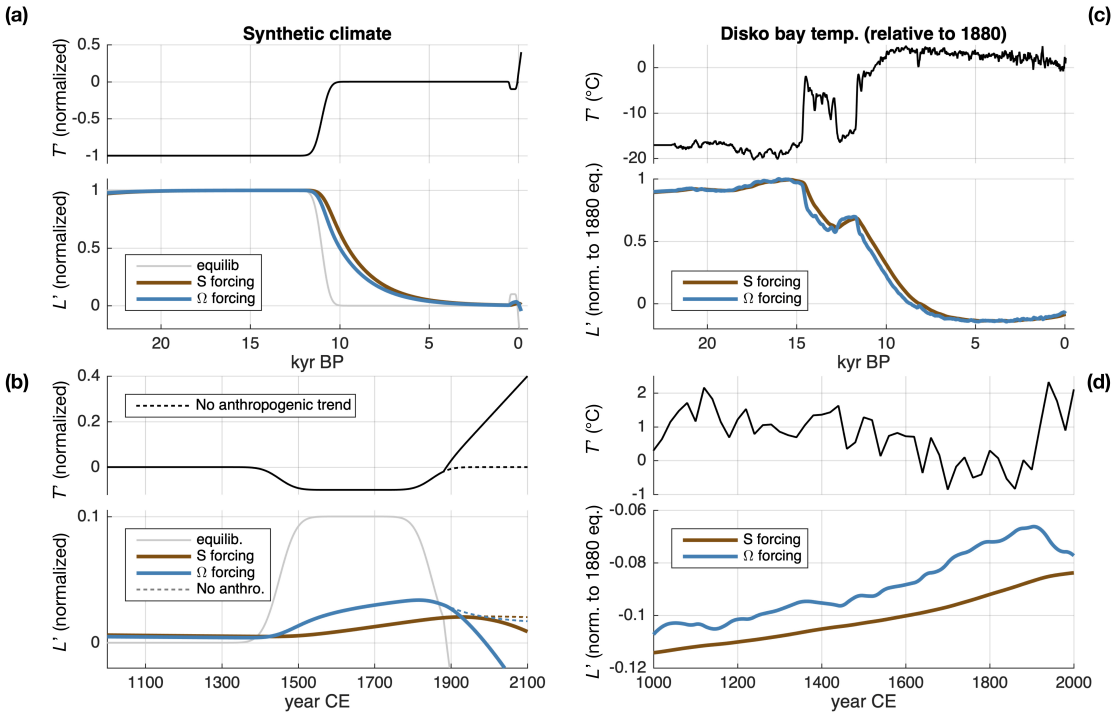

Figure 5.7: Response to long-term climate variations. **(a)** An idealized climate scenario representing the last deglaciation, Little Ice Age (LIA), and anthropogenic forcing (black line). Normalized length responses of the linear model are shown for forcing applied via S (brown) and Ω (blue). The length at which the glacier would remain in equilibrium with climate is shown for reference (gray). **(b)** As for **(a)**, but zoomed into the last 1000 yr. Ω forcing produces a much larger response on multi-century timescales, but the glacier does not reach equilibrium with the LIA in either case. **(c)** A more realistic forcing time series, based on reconstructed atmospheric temperatures for Disko Bay (black line; Buizert et al., 2018). Normalized length responses are again shown for both forcing types, which yield similar responses on multimillennial timescales. **(d)** As for **(c)**, but zoomed into the last 1000 yr. Again, the LIA is expressed to a greater degree through ocean forcing. Note also the long-term advance driven by gradual cooling over the last several millennia.

in their flux at the grounding line, which are typically driven by the ocean. We have used two models of different complexity to explore and contrast the dynamic responses to these two categories of forcing. Our key findings are as follows:

1. Ocean forcing (via the grounding-line flux coefficient, Ω) and interior surface-mass-balance forcing elicit fundamentally different transient grounding-line responses (Figs. 5.1 and 5.2). The response to ocean forcing is characterized by a fast initial grounding-line migration, followed by a second, much slower stage of adjustment. In contrast, the response to interior forcing is dominated by slow grounding-line migration, with very strong damping at short timescales.

2. The two-stage model (Robel et al., 2018) captures the evolution of flux anomalies that gives rise to these two contrasting dynamic responses (Fig. 5.3). This lends further confidence to the two-mode interpretation of outlet glacier dynamics: a fast mode associated with adjustment of the grounding zone, and a slow mode associated with the interior reservoir. We have shown here that ocean forcing projects onto both modes, while interior forcing projects almost entirely onto the slow mode.

3. Persistence in stochastic climate forcing amplifies natural grounding-line fluctuations (Fig. 5.4). Increased persistence means more of the variance in the forcing occurs at low frequencies, where the glacier is ultimately more sensitive. In particular, multidecadal ocean variability can drive large fluctuations on multidecadal to millennial timescales. Understanding the magnitude and persistence of ocean forcing is thus critical for attributing observed terminus changes and detecting the response to anthropogenic forcing (Fig. 5.6).

4. Despite contrasting responses on short timescales, slow (i.e., millennial) dynamics dominate the full system response for both types of forcing. This implies a large committed response (Fig. 5.5), as well as a memory of past climate fluctuations (Fig. 5.7), for both types of forcing. The slow response of interior ice and the attendant consequences

have been explored in a number of previous studies (e.g., Nye, 1960; Levermann et al., 2013; Robel et al., 2018); the results presented here demonstrate how a slow response is fundamental to ocean forcing as well.

Given the rapid observed changes linked to ocean forcing in the past few decades, it is useful to discuss points (3) and (4) further. Increases in discharge from Greenland outlet glaciers have been linked to regional climate variability and warming of the subpolar North Atlantic (Straneo and Heimbach, 2013). Records for a smaller selection of glaciers extend up to a century (Andresen et al., 2012; Bjørk et al., 2012) and futher indicate sensitivity to regional oceanic forcing on relatively short timescales. Evidence for the response to decadal variability is strong in Antarctica, too (e.g., Jenkins et al., 2016, 2018). In sum, the capacity for outlet-glacier grounding lines to react quickly to changes at the terminus is quite clear from the observational record.

Our results show that climate and glacier fluctuations over the historical record also have a longer-timescale context. The widely-separated glacier response timescales mean that fast fluctuations are essentially superimposed on millennial fluctuations. This is clear even in the flowline model, which does not make an explicit approximation of only two timescales (e.g., Fig. 5.1d). Slow fluctuations are difficult to resolve in observational records, but the practical point is that short periods of terminus "stabilization", or fluctuations about a *short-term* mean state do not necessarily preclude a large disequilibrium between fluxes near the grounding line and fluxes from the interior. This disequilibrium should be reflected in ice-thickness and velocity profiles, and has been noted for some systems whose retreat or discharge rates have leveled off, including Jakobshavn Isbrae (e.g., Joughin et al., 2012b; Khazendar et al., 2019) and Pine Island Glacier (e.g., Christianson et al., 2016). Careful modeling might integrate such observations with climate reconstructions to inform attribution studies or model initialization. Wherever the forcing history is uncertain, multiple realizations of past variability should be considered, and we again emphasize that the persistence of this variability is a critical parameter.

A number of simplifying assumptions throughout our study warrant some discussion. First of all, we have assumed a constant, prograde bed slope. In reality, variations in bed topography can have a strong effect on retreat rates and sensitivity, both at the terminus (Catania et al., 2018) and in the interior (Felikson et al., 2017). The effect of these variations on the fast and slow modes remains to be investigated. Felikson et al. (2017) showed that bedrock knick-points may serve as barriers to rapid inland thinning following forcing at the terminus. Depending on where the knickpoint is, this could mean that the dimensions of the effective interior reservoir is different for ocean vs. interior forcing, potentially changing the relevant response timescales.

A related issue is the instability associated with retrograde slopes (e.g., Weertman, 1974; Schoof, 2007a). In an unstable configuration, the linearized timescales diverge, but RRH showed that fast and slow tendencies still govern the rates of unstable retreat. More recently, Robel et al. (2019) showed that instability magnifies variability in transient retreat rate due to internal climate variability. Together, these points suggest that instability might also magnify the difference between retreats initiated by interior and grounding-line flux anomalies.

Another simplification is that we have focused on spatially-uniform interior forcings, whereas in reality, surface-mass-balance anomalies are likely to be greater near the marine margin. We conducted several experiments with the flowline model in which S anomalies were concentrated towards the grounding line, and also amplified to produce the same volume anomalies. This enhanced the high-frequency length response, although there was still a clear difference from the transient response to Ω forcing. Compared to a uniform S anomaly, a step change in S concentrated on the lower half of the glacier (with doubled magnitude) nearly doubles the grounding-line response after 100 yr, while the 100 yr response following a step in Ω is 4 times greater. For white-noise forcing, σ_L increases $\sim 12\%$ if S anomalies are concentrated in the same way, but increases $> 50\%$ if applied as Ω anomalies. Thus, the temporal distinction between interior and ocean forcing will depend on the spatial pattern of mass balance, but it would likely take extremely large and concentrated anomalies to match the fast response of Ω forcing. We expect that the distinction would also depend on the

horizontal catchment geometry: convergence would amplify the effects of anomalies from the deep interior, even if they are smaller in magnitude. Further experiments with 2-D geometries would help to clarify these potentially competing effects. We have also neglected orographic and surface-elevation feedbacks, which would depend on the spatial pattern of thinning, and may thus affect fast and slow responses differently. These would provide another interesting avenue for future analyses.

Finally, we chose to impose ocean forcing via the grounding-line-flux coefficient, which adjusts the parameterized relationship between ice thickness and grounding-line flux. This allowed us to compare flux perturbations in a very general way, but it would be more realistic to directly force a dynamic ice shelf or to perturb calving processes. The analytical flux conditions of Haseloff and Sergienko (2018) could be an intermediate route, and would be feasible for models that parameterize grounding-line flux. RRH showed that these conditions can introduce nonlinear sensitivity to perturbations in a buttressing ice shelf, and thus another key difference between glacier responses to interior and ocean forcing. For example, this nonlinearity would skew the distribution of fluctuations driven by natural ocean variability, changing the thresholds for trend detection (i.e., Fig. 5.6).

Previous studies have employed a variety of forcing strategies for glaciers without buttressing ice shelves. Some have directly perturbed stresses at the grounding line (e.g., Nick et al., 2009; Price et al., 2011), while others have implemented forcing via frontal melt rates (e.g., Morlighem et al., 2016; Aschwanden et al., 2019). Another approach is to impose terminus retreat based on observations, and then allow up-glacier ice thickness and flux to evolve. This approach has been used to isolate the effects bed topography on inland thinning (Felikson, 2018).

Regardless of how forcing is implemented, our analyses show that the coupling between grounding-zone and interior dynamics is a key part of an outlet glacier's response to ocean forcing. In particular, increased discharge is what eventually precipitates the slow (but large) second stage of grounding-line retreat. Our idealized ocean forcing has limitations, of course, but the mechanism for a second stage of retreat is physically robust: elevated

interior fluxes must eventually fall as the interior drains, creating a tendency towards further grounding line retreat (Fig. 5.3). The actual retreat could be modulated depending on the bed topography through which the grounding line migrates, and this would be yet another factor to investigate with more realistic geometries.

At the ice-sheet scale, ocean forcing must often be simplified considerably, and the optimal strategy remains to be determined. The Ice Sheet Model Intercomparison Project for CMIP6 (ISMIP6; Nowicki et al., 2016) defines several experimental protocols for use across various ice sheet models. The ISMIP6 ocean-forcing parameterizations for Greenland were recently established, based on an empirical study of a large collection of terminus observations and regional climate data (Slater et al., 2019, 2020). They proposed two strategies: one in which length change is imposed directly as a function of climate forcing ("retreat implementation"), and one in which submarine melt rates are prescribed ("melt implementation"). Both leave the evolution of ice flux up to the ice sheet model, but the retreat implementation does not allow interior ice dynamics to feed back into the terminus position. The results presented here suggest that, because the timescale of interior dynamics is much longer than the observational records used to calibrate the imposed retreats, the retreat implementation would project less long-term terminus retreat compared with the melt implementation.

The impact that the choice of parameterization would have on projections of near-term sea level rise is not immediately clear, however. Slater et al. (2020) note that these parameterizations are intended primarily for 21st century projections. In a scenario with severe warming, the fast response to progressive forcing might plausibly outweigh the contribution of the slow mode over this period. On the other hand, in a scenario of climate stabilization, the two approaches could yield more disparate results. Under the retreat implementation, the terminus stabilizes if the climate stabilizes (Slater et al., 2019), whereas under the melt implementation, it could in principle continue retreating due to disequilibrium between interior and grounding-zone fluxes (much like in Fig. 5.5). In such a case, the choice of parameterization would affect the difference between responses to low versus high emissions scenarios (e.g., RCP 2.6 vs. 8.5). The principles from our idealized experiments suggest that

a fixed versus free terminus would yield a different partition between fast and slow glacier responses, but further experimentation is needed to investigate this. Although much attention is directed toward sea-level rise by 2100, longer-timescale comparisons within in the ISMIP6 framework, both with idealized and comprehensive models, may also prove illuminating.

Understanding the timescales of glacier dynamics is a long-standing pursuit in glaciology (e.g., Nye, 1960; Jóhannesson et al., 1989; Oerlemans, 2001; Roe and Baker, 2014; Robel et al., 2018). Here, we have explored for marine-terminating outlet glaciers how these timescales manifest under different types of forcing. Interpreting observations and making useful projections will always depend partly on characteristics that are unique to each outlet glacier, and on processes that remain to be investigated further. However, the basic constraints of flux conservation and large-scale geometry will always apply, and, as we have shown here, are enough on their own to yield consequential differences in glacier response. Obviously, there are many intermediate levels of complexity between the models we have used here and those used for detailed simulations and projections. Alongside the need for more-comprehensive glacier and ice-sheet projections in a warming climate, there also remains the need to improve understanding by analyzing model experiments positioned throughout this hierarchy of model complexity (e.g., Held, 2005). Reduced models and experiments with idealized glacier geometries, in which the fundamentals are laid bare, can thus serve as a useful foundation for the needed analyses.

5.6 Appendix: Linearized two-stage model

Here we present the linearized two-stage model in more detail, and derive a discrete autoregressive form. Again, a full model derivation can be found in RRH; we start here from the linearized equations with perturbations in Q_g and S:

$$\frac{\partial H'}{\partial t} = A_H H' + A_L L' + \frac{1}{\bar{L}}\left(\frac{\bar{H}}{\bar{h}_g} - 1\right) Q'_g + S' \tag{5.18}$$

$$\frac{\partial L'}{\partial t} = B_H H' + B_L L' - \frac{1}{\bar{h}_g} Q'_g. \tag{5.19}$$

A_H, A_L, B_H, and B_L are the linear couplings between length and thickness anomalies:

$$A_H(\bar{H},\bar{L}) = -\bar{Q}_g\alpha(\bar{h_g}\bar{L})^{-1} \tag{5.20}$$

$$A_L(\bar{H},\bar{L}) = \bar{Q}_g\bar{L}^{-2}\big[1+\gamma\bar{H}\bar{h_g}^{-1}+\beta\lambda b_x\bar{L}\bar{h_g}^{-1}(1-\bar{H}\bar{h_g}^{-1})\big] \tag{5.21}$$

$$B_H(\bar{H},\bar{L}) = \bar{Q}_g\alpha(\bar{H}\bar{h_g})^{-1} \tag{5.22}$$

$$B_L(\bar{H},\bar{L}) = \bar{Q}_g\bar{h_g}^{-1}(\beta\lambda b_x\bar{h_g}^{-1}-\gamma\bar{L}^{-1}), \tag{5.23}$$

where $\lambda = \frac{\rho_w}{\rho_i}$. For numerical implementation, Equations (5.18) and (5.19) can be discretized using a backward-Euler method, where Δt is the timestep between glacier states $[i]$ and $[i-1]$:

$$\frac{H'_{[i]}-H'_{[i-1]}}{\Delta t} = A_H H'_{[i]} + A_L L'_{[i]} + \frac{1}{\bar{L}}\left(\frac{\bar{H}}{\bar{h_g}}-1\right)Q'_{g[i]} + S'_{[i]} \tag{5.24}$$

$$\frac{L'_{[i]}-L'_{[i-1]}}{\Delta t} = B_H H'_{[i]} + B_L L'_{[i]} - \frac{1}{\bar{h_g}}Q'_{g[i]}. \tag{5.25}$$

Solving for $H_{[i]}$ and $L_{[i]}$ gives

$$H'_{[i]} = \frac{1}{1-A_H\Delta t}\left[A_L\Delta t L'_{[i]} + H'_{[i-1]} + \frac{1}{\bar{L}}\left(\frac{\bar{H}}{\bar{h_g}}-1\right)\Delta t Q'_{g[i]} + \Delta t S'_{[i]}\right] \tag{5.26}$$

$$L'_{[i]} = \frac{1}{1-B_L\Delta t}\left[B_H\Delta t H'_{[i]} + L'_{[i-1]} + \frac{1}{\bar{h_g}}\Delta t Q'_{g[i]}\right], \tag{5.27}$$

which are still semi-implicit in terms of the current state $[i]$. However, we can substitute Equation (5.27) for the $L'_{[i]}$ term in Equation (5.26), and vice versa for $H_{[i]}$. Solving again for $H_{[i]}$ and $L_{[i]}$, we arrive at explicit expressions that depend on only the past state and current forcing. This takes the form of a two-dimensional autoregressive process (e.g., Box et al., 2008) with two forcing terms. For compactness, we redefine several parameter combinations at this point. Let $\epsilon = (1-B_L\Delta t)^{-1}$, $\eta = (1-A_H\Delta t)^{-1}$, and $\kappa = (1-\eta\epsilon A_L B_H\Delta t^2)^{-1}$. Then,

$$\begin{bmatrix} H'_{[i]} \\ L'_{[i]} \end{bmatrix} = \mathbf{C}\begin{bmatrix} H'_{[i-1]} \\ L'_{[i-1]} \end{bmatrix} + \vec{d}Q'_{g[i]} + \vec{e}S'_{[i]} \tag{5.28}$$

where the autoregressive coefficients are contained in the matrix $\mathbf{C}$ and vectors $\vec{d}$ and $\vec{e}$:

$$\mathbf{C} = \kappa \begin{bmatrix} \eta & \epsilon\eta A_L \Delta t \\ \epsilon\eta B_H \Delta t & \epsilon \end{bmatrix} \tag{5.29}$$

$$\vec{d} = \kappa\Delta t \begin{bmatrix} \eta\Big(\bar{L}^{-1}\big(\frac{\bar{H}}{\bar{h}_g} - 1\big) - \epsilon A_L {h_g}^{-1}\Delta t\Big) \\ \epsilon\Big(B_H \bar{L}^{-1}\big(\frac{\bar{H}}{\bar{h}_g} - 1\big)\Delta t - \bar{h_g}^{-1}\Big) \end{bmatrix} \tag{5.30}$$

$$\vec{e} = \kappa\eta\Delta t \begin{bmatrix} 1 \\ \epsilon B_H \Delta t \end{bmatrix}. \tag{5.31}$$

$$\tag{5.32}$$

This form lends iteslf to a straightforward solution algorithm, given steady-state glacier parameters and forcing time series as inputs. Note that for the ocean forcing used in this study, Q'_g is proportional to Ω', but other relationships could easily be implemented.

Code used for the analyses in this study is available as a public repository at https://github.com/johnerich/outlet-glac-forcing. Output from the flowline model is available upon request.

ACKNOWLEDGMENTS

We are very grateful to David Pollard (Penn State Univ.) for model code and a generous introduction to using the flowline model. We also thank Ginny Catania, Fiamma Straneo, and Donald Slater for insightful conversations on outlet glacier dynamics. Finally, we thank Martin Lüthi and an anonymous reviewer for comments that helped clarify the manuscript, and the editor Olivier Gagliardini. JEC was supported by the NSF Graduate Research Fellowship Program (DGE-1256082).

BIBLIOGRAPHY

Abram, N. J., McGregor, H. V., Tierney, J. E., Evans, M. N., McKay, N. P., Kaufman, D. S., Thirumalai, K., Martrat, B., Goosse, H., Phipps, S. J., Steig, E. J., Kilbourne, K. H., Saenger, C. P., Zinke, J., Leduc, G., Addison, J. A., Mortyn, P. G., Seidenkrantz, M. S., Sicre, M. A., Selvaraj, K., Filipsson, H. L., Neukom, R., Gergis, J., Curran, M. A., and Von Gunten, L. (2016). Early onset of industrial-era warming across the oceans and continents. *Nature*, 536(7617):411–418.

Andresen, C. S., Straneo, F., Ribergaard, M. H., Bjørk, A. A., Andersen, T. J., Kuijpers, A., Nørgaard-Pedersen, N., Kjær, K. H., Schjøth, F., Weckström, K., and Ahlstrøm, A. P. (2012). Rapid response of Helheim Glacier in Greenland to climate variability over the past century. *Nat. Geosci.*, 5(1):37–41.

Armour, K. C. and Roe, G. H. (2011). Climate commitment in an uncertain world. *Geophys. Res. Lett.*, 38(1).

Aschwanden, A., Fahnestock, M. A., Truffer, M., Brinkerhoff, D. J., Hock, R., Khroulev, C., Mottram, R., and Abbas Khan, S. (2019). Contribution of the Greenland Ice Sheet to sea level over the next millennium. *Sci. Adv.*, 5(6):eaav9396.

Bindschadler, R. A., Nowicki, S., Abe-OUCHI, A., Aschwanden, A., Choi, H., Fastook, J., Granzow, G., Greve, R., Gutowski, G., Herzfeld, U., Jackson, C., Johnson, J., Khroulev, C., Levermann, A., Lipscomb, W. H., Martin, M. A., Morlighem, M., Parizek, B. R., Pollard, D., Price, S. F., Ren, D., Saito, F., Sato, T., Seddik, H., Seroussi, H., Takahashi, K., Walker, R., and Wang, W. L. (2013). Ice-sheet model sensitivities to environmental forcing and their use in projecting future sea level (the SeaRISE project). *J. Glaciol.*, 59(214):195–224.

Bjørk, A. A., Kjær, K. H., Korsgaard, N. J., Khan, S. A., Kjeldsen, K. K., Andresen, C. S., Box, J. E., Larsen, N. K., and Funder, S. (2012). An aerial view of 80 years of climate-related glacier fluctuations in southeast Greenland. *Nat. Geosci.*, 5(6):427–432.

Box, G. E. P., Jenkins, G. M., and Reinsel, G. C. (2008). *Time series analysis : forecasting and control*. John Wiley.

Buizert, C., Keisling, B. A., Box, J. E., He, F., Carlson, A. E., Sinclair, G., and DeConto, R. M. (2018). Greenland-Wide Seasonal Temperatures During the Last Deglaciation. *Geophys. Res. Lett.*, 45(4):1905–1914.

Catania, G. A., Stearns, L. A., Sutherland, D. A., Fried, M. J., Bartholomaus, T. C., Morlighem, M., Shroyer, E., and Nash, J. (2018). Geometric Controls on Tidewater Glacier Retreat in Central Western Greenland. *J. Geophys. Res. Earth Surf.*, 123(8):2024–2038.

Christian, J. E., Koutnik, M., and Roe, G. (2018). Committed retreat: Controls on glacier disequilibrium in a warming climate. *J. Glaciol.*, 64(246):675–688.

Christianson, K., Bushuk, M., Dutrieux, P., Parizek, B. R., Joughin, I. R., Alley, R. B., Shean, D. E., Abrahamsen, E. P., Anandakrishnan, S., Heywood, K. J., Kim, T. W., Lee, S. H., Nicholls, K., Stanton, T., Truffer, M., Webber, B. G., Jenkins, A., Jacobs, S., Bindschadler, R., and Holland, D. M. (2016). Sensitivity of Pine Island Glacier to observed ocean forcing. *Geophys. Res. Lett.*, 43(20):10,817–10,825.

Cook, A. J., Holland, P. R., Meredith, M. P., Murray, T., Luckman, A., and Vaughan, D. G. (2016). Ocean forcing of glacier retreat in the western Antarctic Peninsula. *Science*, 353(6296):283–286.

Csatho, B. M., Schenka, A. F., Van Der Veen, C. J., Babonis, G., Duncan, K., Rezvanbehbahani, S., Van Den Broeke, M. R., Simonsen, S. B., Nagarajan, S., and Van Angelen, J. H. (2014). Laser altimetry reveals complex pattern of Greenland Ice Sheet dynamics. *Proc. Nat. Acad. Sci. USA*, 111(52):18478–18483.

Deser, C., Alexander, M. A., and Timlin, M. S. (2003). Understanding the Persistence of Sea Surface Temperature Anomalies in Midlatitudes. *J. Clim.*, 16(1):57–72.

Felikson, D. (2018). *Geometric controls on the inland extent of dynamic thinning for Greenland Ice Sheet outlet glaciers*. Phd thesis, University of Texas, Austin.

Felikson, D., Bartholomaus, T. C., Catania, G. A., Korsgaard, N. J., Kjær, K. H., Morlighem, M., Noël, B., Van Den Broeke, M., Stearns, L. A., Shroyer, E. L., Sutherland, D. A., and Nash, J. D. (2017). Inland thinning on the Greenland ice sheet controlled by outlet glacier geometry. *Nat. Geosci.*, 10(5):366–369.

Glen, J. W. (1955). The creep of polycrystalline ice. *Proc. R. Soc. London. Ser. A. Math. Phys. Sci.*, 228(1175):519–538.

Goelzer, H., Nowicki, S., Edwards, T., Beckley, M., Abe-Ouchi, A., Aschwanden, A., Calov, R., Gagliardini, O., Gillet-Chaulet, F., Golledge, N. R., Gregory, J., Greve, R., Humbert, A., Huybrechts, P., Kennedy, J. H., Larour, E., Lipscomb, W. H., Le clec'h, S., Lee, V., Morlighem, M., Pattyn, F., Payne, A. J., Rodehacke, C., Rückamp, M., Saito, F., Schlegel, N., Seroussi, H., Shepherd, A., Sun, S., van de Wal, R., and Ziemen, F. A. (2018). Design and results of the ice sheet model initialisation experiments initMIP-Greenland: an ISMIP6 intercomparison. *The Cryosphere*, 12(4):1433–1460.

Goldberg, D. N., Heimbach, P., Joughin, I., and Smith, B. (2015). Committed retreat of Smith, Pope, and Kohler Glaciers over the next 30 years inferred by transient model calibration. *The Cryosphere*, 9(6):2429–2446.

Gwyther, D. E., O'Kane, T. J., Galton-Fenzi, B. K., Monselesan, D. P., and Greenbaum, J. S. (2018). Intrinsic processes drive variability in basal melting of the Totten Glacier Ice Shelf. *Nat. Commun.*, 9(1).

Hansen, J., Russell, G., Lacis, A., Fung, I., Rind, D., and Stone, P. (1985). Climate response times: Dependence on climate sensitivity and ocean mixing. *Science*, 229(4716):857–859.

Haseloff, M. and Sergienko, O. V. (2018). The effect of buttressing on grounding line dynamics. *J. Glaciol.*, 64(245):417–431.

Hasselmann, K. (1976). Stochastic climate models Part I. Theory. *Tellus*, 28(6):473–485.

Held, I. M. (2005). The gap between simulation and understanding in climate modeling. *Bull. Amer. Meteorol. Soc.*, 86(11):1609–1614.

Howat, I. M., Joughin, I., Fahnestock, M., Smith, B. E., and Scambos, T. A. (2008). Synchronous retreat and acceleration of southeast Greenland outlet glaciers 2000-06: Ice dynamics and coupling to climate. *J. Glaciol.*, 54(187):646–660.

Huybers, P. and Curry, W. (2006). Links between annual, Milankovitch and continuum temperature variability. *Nature*, 441(7091):329–332.

IPCC (2013). Climate Change 2013: The Physical Science Basis. Contribution of Working Group I to the Fifth Assessment Report of the Intergovernmental Panel on Climate Change. Technical report, Cambridge.

Jenkins, A., Dutrieux, P., Jacobs, S., Steig, E. J., Gudmundsson, G. H., Smith, J., and Heywood, K. J. (2016). Decadal ocean forcing and Antarctic Ice Sheet response: lessons from the Amundsen Sea. *Oceanography*, 29(4):106–117.

Jenkins, A., Shoosmith, D., Dutrieux, P., Jacobs, S., Kim, T. W., Lee, S. H., Ha, H. K., and Stammerjohn, S. (2018). West Antarctic Ice Sheet retreat in the Amundsen Sea driven by decadal oceanic variability. *Nat. Geosci.*, 11(10):733–738.

Jóhannesson, T., Raymond, C., and Waddington, E. (1989). Time–Scale for Adjustment of Glaciers to Changes in Mass Balance. *J. Glaciol.*, 35(121):355–369.

Joughin, I., Alley, R. B., and Holland, D. M. (2012a). Ice-sheet response to oceanic forcing. *Science*, 338(6111):1172–1176.

Joughin, I., Smith, B. E., Howat, I. M., Floricioiu, D., Alley, R. B., Truffer, M., and Fahnestock, M. (2012b). Seasonal to decadal scale variations in the surface velocity of Jakobshavn Isbrae, Greenland: Observation and model-based analysis. *J. Geophys. Res. Earth Surf.*, 117(F2).

Khazendar, A., Fenty, I. G., Carroll, D., Gardner, A., Lee, C. M., Fukumori, I., Wang, O., Zhang, H., Seroussi, H., Moller, D., Noël, B. P., van den Broeke, M. R., Dinardo, S., and Willis, J. (2019). Interruption of two decades of Jakobshavn Isbrae acceleration and thinning as regional ocean cools. *Nat. Geosci.*, 12(4):277–283.

Levermann, A., Clark, P. U., Marzeion, B., Milne, G. A., Pollard, D., Radic, V., and Robinson, A. (2013). The multimillennial sea-level commitment of global warming. *Proc. Nat. Acad. Sci. USA*, 110(34):13745–13750.

Lingle, C. S. (1984). A numerical model of interactions between a polar ice stream and the ocean: Application to ice stream E, West Antarctica. *J. Geophys. Res.*, 89(C3):3523.

Mantelli, E., Bertagni, M. B., and Ridolfi, L. (2016). Stochastic ice stream dynamics. *Proc. Nat. Acad. Sci. USA*, 113(32):E4594–E4600.

Medwedeff, W. G. and Roe, G. H. (2017). Trends and variability in the global dataset of glacier mass balance. *Clim. Dynam.*, 48(9-10):3085–3097.

Meehl, G. A., Washington, W. M., Collins, W. D., Arblaster, J. M., Hu, A., Buja, L. E., Strand, W. G., and Teng, H. (2005). How much more global warming and sea level rise? *Science*, 307(5716):1769–1772.

Miles, B. W., Stokes, C. R., Vieli, A., and Cox, N. J. (2013). Rapid, climate-driven changes in outlet glaciers on the Pacific coast of East Antarctica. *Nature*, 500(7464):563–566.

Moon, T. and Joughin, I. (2008). Changes in ice front position on Greenland's outlet glaciers from 1992 to 2007. *J. Geophys. Res.*, 113(F2):F02022.

Moon, T., Joughin, I., Smith, B., and Howat, I. (2012). 21st-century evolution of Greenland outlet glacier velocities. *Science*, 336(6081):576–578.

Moon, T., Joughin, I., Smith, B., Van Den Broeke, M. R., Van De Berg, W. J., Noël, B., and Usher, M. (2014). Distinct patterns of seasonal Greenland glacier velocity. *Geophys. Res. Lett.*, 41(20):7209–7216.

Morlighem, M., Bondzio, J., Seroussi, H., Rignot, E., Larour, E., Humbert, A., and Rebuffi, S. (2016). Modeling of Store Gletscher's calving dynamics, West Greenland, in response to ocean thermal forcing. *Geophys. Res. Lett.*, 43(6):2659–2666.

Nick, F. M., Vieli, A., Howat, I. M., and Joughin, I. (2009). Large-scale changes in Greenland outlet glacier dynamics triggered at the terminus. *Nat. Geosci.*, 2(2):110–114.

Nielsen, L. T., Adalgeirsdóttir, G., Gkinis, V., Nuterman, R., and Hvidberg, C. S. (2018). The effect of a Holocene climatic optimum on the evolution of the Greenland ice sheet during the last 10 kyr. *J. Glaciol.*, 64(245):477–488.

Nowicki, S. M., Payne, A., Larour, E., Seroussi, H., Goelzer, H., Lipscomb, W., Gregory, J., Abe-Ouchi, A., and Shepherd, A. (2016). Ice Sheet Model Intercomparison Project (ISMIP6) contribution to CMIP6. *Geosci. Model Dev.*, 9(12):4521–4545.

Nye, J. F. (1960). The response of glaciers and ice-sheets to seasonal and climatic changes. *Proc. R. Soc. London. Ser. A. Math. Phys. Sci.*, 256(1287):559–584.

Oerlemans, J. J. (2001). *Glaciers and climate change*. A.A. Balkema Publishers.

Percival, D. B., Overland, J. E., and Mofjeld, H. O. (2001). Interpretation of North Pacific Variability as a Short-and Long-Memory Process. *J. Clim.*, 14(24):4545–4559.

Pollard, D. and Deconto, R. M. (2012). Description of a hybrid ice sheet-shelf model, and application to Antarctica. *Geosci. Model Dev.*, 5(5):1273–1295.

Price, S. F., Payne, A. J., Howat, I. M., and Smith, B. E. (2011). Committed sea-level rise for the next century from Greenland ice sheet dynamics during the past decade. *Proc. Nat. Acad. Sci. USA*, 108(22):8978–8983.

Pritchard, H. D., Arthern, R. J., Vaughan, D. G., and Edwards, L. A. (2009). Extensive dynamic thinning on the margins of the Greenland and Antarctic ice sheets. *Nature*, 461(7266):971–975.

Robel, A. A., Roe, G. H., and Haseloff, M. (2018). Response of Marine-Terminating Glaciers to Forcing: Time Scales, Sensitivities, Instabilities, and Stochastic Dynamics. *J. Geophys. Res. Earth Surf.*, 123(9):2205–2227.

Robel, A. A., Schoof, C., and Tziperman, E. (2014). Rapid grounding line migration induced by internal ice stream variability. *J. Geophys. Res. Earth Surf.*, 119(11):2430–2447.

Robel, A. A., Seroussi, H., and Roe, G. H. (2019). Marine ice sheet instability amplifies and skews uncertainty in projections of future sea-level rise. *Proc. Nat. Acad. Sci. USA*, 116(30):14887–14892.

Roe, G. H. (2011). What do glaciers tell us about climate variability and climate change? *J. Glaciol.*, 57(203):567–578.

Roe, G. H. and Baker, M. B. (2014). Glacier response to climate perturbations: An accurate linear geometric model. *J. Glaciol.*, 60(222):670–684.

Roe, G. H. and Baker, M. B. (2016). The response of glaciers to climatic persistence. *J. Glaciol.*, 62(233):440–450.

Roe, G. H., Baker, M. B., and Herla, F. (2017). Centennial glacier retreat as categorical evidence of regional climate change. *Nat. Geosci.*, 10(2):95–99.

Schoof, C. (2007a). Ice sheet grounding line dynamics: Steady states, stability, and hysteresis. *J. Geophys. Res. Earth Surf.*, 112(3).

Schoof, C. (2007b). Marine ice-sheet dynamics. Part 1. The case of rapid sliding. *J. Fluid Mech.*, 573:27–55.

Shepherd, A., Ivins, E., Rignot, E., Smith, B., Van Den Broeke, M., Velicogna, I., Whitehouse, P., Briggs, K., Joughin, I., Krinner, G., Nowicki, S., Payne, T., Scambos, T., Schlegel, N., Geruo, A., Agosta, C., Ahlstrøm, A., Babonis, G., Barletta, V., Blazquez, A., Bonin, J., Csatho, B., Cullather, R., Felikson, D., Fettweis, X., Forsberg, R., Gallee, H., Gardner, A., Gilbert, L., Groh, A., Gunter, B., Hanna, E., Harig, C., Helm, V., Horvath, A., Horwath, M., Khan, S., Kjeldsen, K. K., Konrad, H., Langen, P., Lecavalier, B., Loomis, B., Luthcke, S., McMillan, M., Melini, D., Mernild, S., Mohajerani, Y., Moore, P., Mouginot, J., Moyano, G., Muir, A., Nagler, T., Nield, G., Nilsson, J., Noel, B., Otosaka, I., Pattle, M. E., Peltier, W. R., Pie, N., Rietbroek, R., Rott, H., Sandberg-Sørensen, L., Sasgen, I., Save, H., Scheuchl, B., Schrama, E., Schröder, L., Seo, K. W., Simonsen, S., Slater, T., Spada, G., Sutterley, T., Talpe, M., Tarasov, L., Van De Berg, W. J., Van Der Wal, W., Van Wessem, M., Vishwakarma, B. D., Wiese, D., and Wouters, B. (2018). Mass balance of the Antarctic Ice Sheet from 1992 to 2017. *Nature*, 558(7709):219–222.

Slater, D. A., Felikson, D., Straneo, F., Goelzer, H., Little, C. M., Morlighem, M., Fettweis, X., and Nowicki, S. (2020). Twenty-first century ocean forcing of the Greenland ice sheet for modelling of sea level contribution. *The Cryosphere*, 14(3):985–1008.

Slater, D. A., Straneo, F., Felikson, D., Little, C. M., Goelzer, H., Fettweis, X., and Holte, J. (2019). Estimating Greenland tidewater glacier retreat driven by submarine melting. *The Cryosphere*, 13(9):2489–2509.

Straneo, F. and Heimbach, P. (2013). North Atlantic warming and the retreat of Greenland's outlet glaciers. *Nature*, 504(7478):36–43.

Straneo, F., Sutherland, D. A., Holland, D., Gladish, C., Hamilton, G. S., Johnson, H. L., Rignot, E., Xu, Y., and Koppes, M. (2012). Characteristics of ocean waters reaching greenland's glaciers. *Ann. Glaciol.*, 53(60):202–210.

Thomas, R. H. (1979). The Dynamics of Marine Ice Sheets. *J. Glaciol.*, 24(90):167–177.

Tsai, V. C., Stewart, A. L., and Thompson, A. F. (2015). Marine ice-sheet profiles and stability under Coulomb basal conditions. *J. Glaciol.*, 61(226):205–215.

Van Den Broeke, M., Bamber, J., Ettema, J., Rignot, E., Schrama, E., Van Berg, W. J. D., Van Meijgaard, E., Velicogna, I., and Wouters, B. (2009). Partitioning recent Greenland mass loss. *Science*, 326(5955):984–986.

Weertman, J. (1974). Stability of the Junction of an Ice Sheet and an Ice Shelf. *J. Glaciol.*, 13(67):3–11.

Wigley, T. M. L. and Schlesinger, M. E. (1985). Analytical solution for the effect of increasing CO2 on global mean temperature. *Nature*, 315(6021):649–652.

Chapter 6

CONCLUSIONS AND OUTLOOK

6.1 Synthesis and Conclusions

Within the overall focus on glacier changes over time, the studies in this dissertation trace a progression of timescales: Chapter 2 focused on interannual variability and decadal trends in mass balance; Chapters 3 and 4 focused on multidecadal response times in the context of centennial warming trends; and Chapter 5 dealt with the interaction of multi-decadal and millennial dynamics. The shorter timescales in Chapter 2 are related to its focus on mass balance, which directly reflects the influence of short-term atmospheric variability. Chapters 3–5 focused more on the dynamic responses of glaciers, which operate on decadal to millennial timescales, depending on the setting and geometry. These studies extended previous insights that glacier geometry strongly controls transient ice dynamics. Together, Chapters 3–5 show how these principles apply across the cryosphere, from small mountain glaciers to major outlet glaciers.

This comparison is not intended to isolate glaciers into discrete silos in the frequency domain based on their response times. On the contrary, the larger lesson is that processes on a broad continuum of timescales affect the interactions of glaciers and climate. Interpreting temporal observations or making projections of glacier change ultimately means analyzing a timeseries or generating one. And in order to reach reliable conclusions in either case, one must think not only on the timescale of the record or projection in question, but also on shorter and longer timescales. My analyses adapted recently-developed tools and models in a way that can help us incorporate these shorter and longer timescales into our thinking. For example, a multi-decade memory dictates how a mountain glacier responds to short-term variability in mass balance (i.e., the variability explored in Ch 2), as well as the century-scale

anthropogenic warming trend. Chapters 3 and 4 show that the balance of these drivers varies between glaciers, but can be understood through a few key parameters.

Investigating marine-terminating glaciers requires considering an even wider range of timescales, due to the coupling of multidecadal and multi-millennial ice dynamics. As demonstrated in Chapter 5, the "fast" elements of outlet glacier dynamics can already be responding to observed climate variability and trends, but the very slow dynamics of interior ice require that we also consider how a multi-decade record of observations, or a future projection, is also a response to long-term climate history.

My hope is that this work contributes a framework of questions about geometry, climate setting and history, and glacier memory, that can be adapted to given glacier(s) of interest.

6.2 Outlook for future research

The basic principles of climate variability and glacier memory leave much territory yet to explore. The outcomes of my research indicate several directions for future research. A major, encompassing challenge in glacier and ice sheet modeling is scaling up model experiments and simulations to broader spatial and temporal scales. For mountain glaciers, there is a growing effort to simulate large populations of individual glaciers for sea-level-rise or hydrological projections, and a number of global-scale models have now been introduced (e.g., Hock et al., 2019, and references therein). Among these models there is a wide variety of approaches for representing glacier dynamics, mass balance, and extrapolating constraints from the relatively small fraction of glaciers with direct observations. Chapter 4 of this dissertation highlighted some of the basic challenges for accurately simulating the transient response for a wide range of glaciers within a population. However, the principles investigated here could also be used to evaluate the implications of different model assumptions, and help correct inconsistencies. For example, a model's initial condition, by construction, implicitly incorporates the prior climate history and the glacier's disequilibrium (or lack thereof). This assumption directly affects the modeled glacier evolution. The analyses in Chapters 3 and 4 provide a framework for evaluating and differentiating the disequilibrium of individual

glaciers, which could be used to refine the initial conditions that the models must impose on a broad population of glaciers. As these global models begin to incorporate more realistic ice dynamics (e.g. Maussion et al., 2019; Zekollari et al., 2019), there are more elements of the glacier state, and differences between glaciers, that must be incorporated to give accurate results. I hope that the analyses here may inform a productive dialogue between theoretical understanding and the applied challenge of modeling hundreds of thousands of glaciers. Challenges related to scale are also abundant in ice-sheet modeling, due to the large number of outlet glaciers that drain ice sheets, and the disparity between observational timescales and ice-sheet-response timescales. It is thus important to understand where to add detail to a model experiment so as to maximize the additional insight or realism gained in the results. A natural next step from my work on outlet glaciers is to compare the large-scale geometric lens I used with the smaller geometric variations known to be important for the observed behavior of individual outlet glaciers (e.g., Catania et al., 2018). Gradually adding geometric complexity to model experiments, and identifying ensuing changes to the transient response, would be a straightforward way to approach this.

Additionally, we know that internal climate variability poses challenges for understanding observed or projected changes, especially on relatively short timescales. The presence of geometric instabilities for outlet glaciers (e.g., retrograde slopes or overdeepenings in fjords) introduces an additional challenge in the presence of climate variability. Instabilities amplify uncertainties in the rate of future retreat (e.g., Robel et al., 2019), and also make it difficult to attribute an observed retreat to natural or anthropogenic causes. Our understanding of past and future changes depends on a balance between uncertainties in climate forcing and variability, and the constraints on glacier evolution we can identify based on glacier geometry. Idealized experiments showing which parameters affect this balance could yield another contribution to linking local and large-scale processes.

Modelers always face a tradeoff between the spatio-temporal scope of an experiment, and the details that it can resolve. Assimilating detailed oceanographic and geophysical observations into models is an active research frontier. Continental-scale ice-sheet models

are also beginning to resolve individual outlet glaciers over long timescales (e.g., Aschwanden et al., 2019), though simplifications are still necessary. Simultaneous progress on both of these fronts is important and necessary, though it will likely maintain a gap between the processes that models represent in detailed, local-scale simulations, versus at the scale of the whole ice sheet and on millennial timescales. Basic computational constraints exist when expanding the scale of simulations, and designing ever-more complex experiments also challenges our ability to understand all aspects of the model results. It remains to be seen whether improved observations and modeling tools will narrow or widen the gaps between local- and large-scale modeling, but I expect that we will continue to need analytical bridges between developments on both fronts. Idealized experiments using a combination of simple and complex models can be one such bridge for building understanding.

BIBLIOGRAPHY

Aschwanden, A., Fahnestock, M. A., Truffer, M., Brinkerhoff, D. J., Hock, R., Khroulev, C., Mottram, R., and Abbas Khan, S. (2019). Contribution of the Greenland Ice Sheet to sea level over the next millennium. *Sci. Adv.*, 5(6):eaav9396.

Catania, G. A., Stearns, L. A., Sutherland, D. A., Fried, M. J., Bartholomaus, T. C., Morlighem, M., Shroyer, E., and Nash, J. (2018). Geometric Controls on Tidewater Glacier Retreat in Central Western Greenland. *J. Geophys. Res. Earth Surf.*, 123(8):2024–2038.

Hock, R., Bliss, A., Marzeion, B. E., Giesen, R. H., Hirabayashi, Y., Huss, M., Radic, V., and Slangen, A. B. (2019). GlacierMIP-A model intercomparison of global-scale glacier mass-balance models and projections. *Journal of Glaciology*, 65(251):453–467.

Maussion, F., Butenko, A., Champollion, N., Dusch, M., Eis, J., Fourteau, K., Gregor, P., Jarosch, A. H., Landmann, J., Oesterle, F., Recinos, B., Rothenpieler, T., Vlug, A., Wild, C. T., and Marzeion, B. (2019). The Open Global Glacier Model (OGGM) v1.1. *Geoscientific Model Development*, 12(3):909–931.

Robel, A. A., Seroussi, H., and Roe, G. H. (2019). Marine ice sheet instability amplifies and skews uncertainty in projections of future sea-level rise. *Proc. Nat. Acad. Sci. USA*, 116(30):14887–14892.

Zekollari, H., Huss, M., and Farinotti, D. (2019). Modelling the future evolution of glaciers in the European Alps under the EURO-CORDEX RCM ensemble. *Cryosphere*, 13(4):1125–1146.